UNIVERSIDAD DE MURCIA

FACULTAD DE MEDICINA

ABERRACIONES EN LENTES OFTÁLMICAS DE POTENCIA PROGRESIVA Y SU IMPACTO EN LA CALIDAD VISUAL

Trabajo presentado por:

Eloy Ángel Villegas Ruiz

para aspirar al grado de Doctor por la Universidad de Murcia.

Posgrado en Ciencias de la Visión. Facultad de Medicina.
Laboratorio de Óptica. Departamento de Física.
Universidad de Murcia.

Murcia, 29 de septiembre de 2009

D. Pablo Artal Soriano, Catedrático de Universidad del Área de Óptica en el Departamento de Física, AUTORIZA:

La presentación de la tesis doctoral titulada “Aberraciones en lentes oftálmicas de potencia progresiva y su impacto en la calidad visual”, realizada por D. Eloy Ángel Villegas Ruiz bajo mi inmediata dirección y supervisión, en el Departamento de Física, y que presenta para la obtención del grado de Doctor por la Universidad de Murcia.

Murcia, 29 de septiembre de 2009

La Comisión General de Doctorado de la Universidad de Murcia ha autorizado la redacción de la presente tesis doctoral en inglés, según resolución en su sesión del 13 de marzo de 2009. Según la normativa vigente de la Universidad de Murcia, en caso de que se autorice la redacción en una lengua distinta del castellano, la tesis deberá contener un resumen de la misma en castellano. Este resumen deberá tener una extensión mínima de 2000 palabras y deberá ser encuadernado como parte de la tesis. El índice y los datos de la portada de la tesis deberán estar en castellano.

.

ÍNDICE

RESUMEN

Introducción

El sistema acomodativo del ojo humano permite enfocar objetos a diferentes distancias. Según la teoría de Helmholtz, para enforcar objetos cercanos, el músculo ciliar se contrae y las fibras axiales de la zónula se relajan produciendo un aumento del espesor y de la curvatura de las superficies del cristalino, principalmente de la anterior. En personas emétropes o amétropes corregidas, este mecanismo permite ver nítidamente tanto de lejos como de cerca hasta aproximadamente entre los 40 y 45 años, cuando el máximo poder acomodativo no permite ver confortablemente a distancias cercanas.

Las soluciones para corregir esta deficiencia óptica pasan por diferentes alternativas, todas ellas dirigidas a aumentar la potencia del ojo en visión cercana. En el terreno de la cirugía ocular, se practican diferentes técnicas, como la cirugía refractiva multifocal. En personas con cataratas, al reemplazar el cristalino por lentes intraoculares, se puede optar por diferentes opciones, como monovisión, lentes mulltifocales, y últimamente también se está experimentando con lentes acomodativas que aprovechan el mecanismo de contracción-relajación residual del músculo ciliar para desplazar la lente hacia delante en visión cercana. Con lentes de contacto, también se puede optar por la monovisión o lentes multifocales. Sin embargo, estas técnicas no son exitosas en un número importante de pacientes, debido a la dificultad del sistema neuronal para anular la visión de un ojo, o bien eliminar las imágenes desenfocadas que se superponen a la nítida. La opción tradicional, y la que menos rechazos genera, son las lentes oftálmicas monofocales en gafas con la potencia adecuada para ver cómodamente de cerca. Desde hace más de dos siglos, las lentes bifocales en gafas es otra opción muy recurrida y con buenos resultados de adaptación, aunque a partir de los 55 años no cubren la visión a distancia intermedia. La alternativa son lentes trifocales que apenas se utilizan en Europa por razones estéticas y por los continuos saltos de imagen que se producen en los límites de las zonas de visión.

Finalmente, la alternativa que más ha crecido en las últimas décadas son las lentes de potencia progresiva. Estas lentes para gafas proporcionan una visión continua a todas las distancias debido a un cambio progresivo de potencia desde la zona superior, que se utiliza para visión de lejos, hasta la zona inferior, que se usa para visión de cerca, dejando la zona de progresión de potencia para distancias intermedias. La empresa francesa Essel comercializó en 1959 la primera lente progresiva con éxito comercial. Como bien dictaminó Minkwitz (1963), es imposible producir una superficie con potencia esférica progresiva sin generar astigmatismo residual y distorsión. De hecho, en superficies progresivas simples, el astigmatismo residual crece del centro a la periferia el doble de rápido que la progresión de potencia, degradando la calidad visual en las zonas excéntricas. Para analizar la calidad

óptica de las lentes progresivas se utilizan tres representaciones convencionales: líneas de isocilindro, líneas de isopotencia y el perfil de potencia. La primera y la segunda nos permiten evaluar la distribución de astigmatismo y la distribución de potencia respectivamente, y la última nos muestra la progresión de potencia en la línea umbilical de progresión. El astigmatismo residual periférico es mayor cuanto mayor es la adición (potencia esférica añadida a la refracción de lejos para ver de cerca) o cuanto menor es la longitud de progresión de potencia. Hoy en día las máquinas de control numérico, permiten fabricar cualquier diseño teórico. Sin embargo, el astigmatismo sigue siendo un handicap para los diseñadores. Existen diseños "duros", en los que las zonas de lejos y cerca son amplias, pero el astigmatismo residual crece muy rápidamente hacia la periferia, y otros "suaves", en los que el astigmatismo crece más lentamente en detrimento de la anchura de las zonas de lejos y cerca. Por lo que respecta a la evaluación óptica de las lentes progresivas, se han usado diferentes técnicas como la interferometría, deflectometría "Moiré" o frontofocómetros, que permiten medir las lentes aisladas sin tener en cuenta el ojo. Si bien el astigmatismo residual en diferentes zonas de las lentes progresivas se ha medido en algunos estudios anteriores, por lo que respecta a las aberraciones de alto orden no hemos encontrado en la bibliografía medidas experimentales. En relación a la evaluación visual de las lentes progresivas, los estudios anteriores confirman la disminución de la agudeza visual (AV) en zonas excéntricas, aunque para las tareas diarias no supone un inconveniente en la mayoría de casos. De hecho, entre un 10 y un 15% de los usuarios de lentes progresivas pueden tener problemas de adaptación debido a diferentes factores: astigmatismo, distorsión, movimientos de ojos-cabeza, errores de desenfoque y quizá también por las aberraciones de alto orden.

Objetivos

El primer objetivo de este trabajo es medir las aberraciones espacialmente resueltas en lentes progresivas, tanto aisladas como combinadas con el ojo. Para ello desarrollaremos un sistema con un sensor Hartmann-Shack (HS), que por su robustez y precisión se está utilizando durante los últimos años para medir y caracterizar las propiedades ópticas oculares. A continuación, analizaremos el posible acople de las aberraciones de la lente y las del ojo. También compararemos las aberraciones de las lentes con las de los ojos présbitas. Al sistema se le incorporará un brazo extra que nos permitirá medir la AV (de alto y bajo contraste) a través de diferentes zonas de las lentes progresivas bajo condiciones ópticas controladas, y así estimar el impacto de las aberraciones en la calidad visual. Se correlacionarán distintos parámetros ópticos (tanto de la lentes aisladas como combinadas con los ojos) con la AV, para así poder establecer la

métrica óptica que mejor predice el comportamiento visual. Además, adaptaremos lentes progresivas a personas présbitas y mediremos la posible adaptación a las aberraciones. Con el fin de establecer diferencias entre los distintos diseños actuales, se medirán las aberraciones en tres lentes progresivas de última generación de tres casas comerciales diferentes.

Métodos

El sistema experimental desarrollado utiliza un láser He-He de 543 nm, que una vez que se refleja en la retina sale fuera del ojo hacia la lente progresiva, pasa por un compensador de prismas y después por un sistema Badal (para corregir desenfoque) y llega finalmente al sensor HS, formado por una matriz de microlentes (distancia focal 40 mm y apertura 0.6 mm) y una cámara CCD. Para medir solo las lentes, se sustituye el ojo por un espejo que dirige el haz de luz hacia la superficie posterior de la lente. Todas las medidas se realizan replicando la posición y la inclinación de la lente con respecto al ojo para reproducir las condiciones reales de visión. A partir de las imágenes de puntos proporcionadas por el sensor HS, se obtienen las aberraciones de onda expresadas en polinomios de Zernike hasta quinto orden. Se calcula el RMS (*root mean square*) de la aberración de onda, la PSF (*point-spread function*) y la razón de Strehl, como el cociente del valor máximo de la PSF con y sin aberraciones.

Entre el sistema Badal y el sensor se monta el brazo auxiliar para las medidas de AV, que se realizan utilizando la letra E en negro sobre fondo verde para poder correlacionar con las medidas ópticas. La AV se mide con un test de elección forzada a partir del cual se obtiene un ajuste sigmoidal del porcentaje de aciertos en función del tamaño de letra. El valor de AV corresponde con el tamaño que proporciona un 75% de aciertos. Las medidas de AV decimal (1/MAR) se obtienen con pupila dilatada con tropicamida y se usan pupilas artificiales de 3.0 y 4.5 mm de diámetro, y la letra E con contraste 100% y 15%.

Resultados

Aberraciones de onda en lentes progresivas: aisladas e *in situ*

Inicialmente se midieron las aberraciones de una lente Varilux Comfort (Essilor International, Francia), con potencia cero en la zona de lejos y una adición de 2 D. En un principio, la lente se evalúo aislada (sin ojo) en 21 zonas a lo largo del pasillo de progresión y zonas aledañas usadas a menudo en condiciones normales de visión. Para 4.5 mm de pupila, el RMS total (sin desenfoque), es de 0.1 μm en las zonas centrales de visión de lejos y cerca, en el pasillo de progresión oscila entre 0.1 y 0.2 μm, y en las zonas periféricas

a 3 y 6 mm desde el centro del pasillo aumenta a 0.6 y 0.9 μm respectivamente. Sin considerar el astigmatismo, el RMS oscila entre 0.03 y 0.06 μm, siendo mayor en las zonas del pasillo donde la progresión de potencia es mayor. Estos valores corresponden principalmente a los coeficientes de tercer orden (coma y *trefoil*), siendo el resto, incluida la aberración esférica, despreciables. Por lo que respecta a la razón de Strehl, en las zonas de lejos y cerca es alrededor de 0.5, bajando a 0.2 en el pasillo debido al aumento de coma, *trefoil* y astigmatismo, cayendo a valores por debajo de 0.1 en las zonas periféricas debido al aumento del astigmatismo. Las PSFs en las zonas de lejos y cerca son muy "puntuales", en las zonas del pasillo tienen forma comática hacia abajo modificada por el *trefoil*, y en las periféricas predomina la forma del círculo de mínima confusión del astigmatismo con mayor intensidad abajo debido al coma. Al comparar las aberraciones de tercer orden de la lente con las típicas en ojos présbitas, los valores son del mismo orden, alrededor de 0.05 μm; sin embargo, la aberración esférica ocular es ligeramente positiva mientras que en la lente es prácticamente cero.

Por otra parte, al medir las aberraciones de las lentes progresivas en seis zonas relevantes delante de dos ojos de personas diferentes, los valores de las aberraciones son muy parecidos a cuando se suman directamente, por lo que la distancia de vértice entre la lente y el ojo no influye demasiado en el acople de las aberraciones entre lente y ojo.

Impacto de las aberraciones de las lentes progresivas en la agudeza visual

A través de seis zonas de la lente progresiva Varilux Comfort, se midió la AV en tres ojos jóvenes (25-30 años) con astigmatismo reducido y desenfoque corregido. En promedio, la AV (para pupila de 4.5 mm y contraste 100%) en las zonas del pasillo son parecidas con y sin lente progresiva, entre 1.2 y 1.4, en zonas a 3 mm del pasillo, la AV cae a 1.0, y a 6 mm es de 0.7. Al disminuir el tamaño pupilar y el contraste las diferencias entre las zonas son menores, por ejemplo con pupila de 3.0 mm y 15% de contraste se pasa de AV promedio en el pasillo de 0.7 a 0.5 en la zona a 6 mm de excentricidad.

Agudeza visual y parámetros ópticos

Al correlacionar los distintos parámetros ópticos con la AV, obtenemos que la mejor predicción la proporciona el logaritmo de parámetros que evalúan la PSF de la imagen sobre la retina (por ejemplo el logaritmo neperiano de la razón de Strehl).

Adaptación neuronal a las aberraciones de las lentes progresivas

Por lo que respecta al estudio de la adaptación a las aberraciones de las lentes progresivas, hicimos un seguimiento durante el primer día (justo antes de la dispensación de las gafas, y después de 2 y 7 horas) y la primera semana (a los 2, 5 y 7 días) en cuatro sujetos présbitas (entre 43 y 51 años) a las que se les adaptó la lente progresiva Varilux Panamic (Essilor). Se midió la AV (contraste 100%) en tres zonas, una en el centro del pasillo, otra a 3 mm hacia el lado nasal y la otra a 6 mm hacia el lado temporal. El valor promedio de AV de los tres sujetos cuyas lentes tenían una adición entre 2.0 y 2.25 D, fue de 1.0 en el pasillo, de 0.8 a 3 mm hacia el lado nasal y de 0.6 a 6 mm hacia el lado temporal, siendo el valor de astigmatismo en la lente aproximadamente 0.15, 0.80 y 1.70 D respectivamente. Aunque en el transcurso de las primeras horas y días encontramos una ligera mejoría en la AV a través de las zonas excéntricas, estos cambios están por debajo de los errores experimentales, y por lo tanto no se pueden considerar significativos.

Comparación óptica entre lentes progresivas de última generación

En la comparación de tres lentes progresivas de distintas casas comerciales, encontramos en todas ellas valores parecidos de coma y *trefoil*, pero distinta distribución de la aberración astigmática. En una de ellas se prioriza la calidad óptica periférica, en otra la visión binocular (menos aberraciones en zona temporal) y en la tercera la visión central. Sin embargo, si se suman los valores de astigmatismo de todas las zonas medidas, el valor es muy parecido.

Conclusiones

Hemos desarrollado un sistema para medir las aberraciones en diferentes zonas de cualquier lente oftálmica, tanto aislada como delante del ojo. En el presente trabajo este sistema se ha utilizado para medir lentes progresivas replicando condiciones normales de visión.

Además del astigmatismo que aumenta periféricamente, también hemos encontrado pequeños valores de aberraciones de tercer orden, coma y *trefoil*, que disminuyen ligeramente conforme nos alejamos de la línea umbilical de progresión de potencia.

La calidad óptica de los ojos mirando a través de una lente progresiva se puede predecir con bastante exactitud sumando las aberraciones de la lente y el ojo. Este acople entre las aberraciones de la lente y las del ojo pueden cambiar significativamente la calidad óptica de los dos elementos por separado. De hecho, en las lentes progresivas aisladas la

calidad óptica disminuye rápidamente hacia la periferia, mientras que cuando se acoplan las aberraciones oculares el cambio es más suave. Esto supone que la caída de AV en zonas excéntricas sea menor de lo que se podría prever suponiendo únicamente el deterioro óptico de las lentes progresivas.

Los pequeños valores de coma y *trefoil* presentes en las lentes progresivas unidos a los pequeños diámetros pupilares característicos de personas présbitas, producen un bajo deterioro de la calidad de imagen retiniana, lo que conlleva a que estas aberraciones tengan poco impacto en la AV. Esto supone que en la zona del pasillo de progresión, donde el coma y el *trefoil* tienen valores parecidos al astigmatismo, la AV no difiere de la obtenida en ausencia de lente.

El logaritmo de métricas sobre la PSF de la imagen retiniana del sistema lente con ojo son las que mejor predicen la AV con alto contraste. Esto sugiere que las prestaciones visuales de las lentes progresivas se podrían mejorar si los diseños se personalizaran según las aberraciones oculares de cada persona, utilizando parámetros como el logaritmo del volumen de la PSF o el de la Razón de Strehl.

Estudios anteriores han demostrado la existencia de la adaptación a la distorsión, inclusive en el caso de las lentes progresivas, y también la adaptación a cambios estables en las aberraciones oculares. Sin embargo, nuestros resultados muestran una ligera mejoría, pero no significativa, en la AV al mirar por zonas periféricas de las lentes progresivas durante la primera semana de adaptación. Es decir, parece ser que el sistema visual tiene dificultad para adaptarse a los múltiples patrones de aberración, uno por cada dirección de mirada, a los que está expuesto el ojo, al menos durante la primera semana.

Por lo que respecta a las diferencias entre los diseños de última generación que se comercializan, el valor global de aberraciones es parecido, pero distribuidas de forma diferente dependiendo de la filosofía del diseño. Las aberraciones de las lentes progresivas se comportan como un colchón de agua, donde el agua es el astigmatismo que se puede mover pero no eliminar.

AGRADECIMIENTOS

To them who fought to be alive
but death was the end of the fight

LLegado este momento, son muchas las personas a las que les tengo que agradecer su ayuda, colaboración y compañerismo. Esta tesis se ha realizado en el Laboratorio de Óptica de la Universidad de Murcia que dirige Pablo Artal. A él le agradezco su confianza y el continuo apoyo que ha mostrado para que de una forma u otra, incluso en un país o en otro, pudiera presentar mi tesis doctoral. Pero sobre todo a Pablo debo agradecerle la perseverancia en la búsqueda de ideas y recursos con los que seguir avanzando en aspectos desconocidos de la Óptica Visual.

Ha sido un lujo haber podido contar con las críticas y sugerencias de un experto en lentes progresivas como es Ralf Blendowske (Alemania). A él le debo el desarrollo del modelo analítico para describir las aberraciones de las lentes progresivas, que muestro en un apéndice de este trabajo.

No me olvido de mis comienzos en el campo de la investigación en Óptica en la Universidad de Alicante, donde Felipe Mateos y especialmente Antonio Fimia me dieron la oportunidad de involucrarme en su grupo. Mención especial para Luis Carretero, que fue mi guía y maestro durante dos años. A Conchi González por ser la “liebre” en mi carrera docente e investigadora.

Con Conchi y Juanma Bueno compartí mi primer despacho en la Universidad de Murcia, y a ellos debo agradecer el compañerismo, la disposición y el buen ambiente del que disfrutamos durante aquellos años. Desde entonces Juanma sigue siendo ese buen compañero, siempre presto a echarte una mano. Tras la partida de Conchi, su lugar lo ocupó Antonio Benito, que desde el principio se empeño en culminar nuestras aspiraciones doctorales. Compañero desde entonces, su afán de mejora repercute directamente en la del resto del grupo. Colega y vecino de laboratorio, E. Joshua Fernández siempre estuvo presto a ayudarme en los problemas que tuve con mi sistema. A él y a Silvestre Manzanera agradecer además su disponibilidad para participar como sujetos en los experimentos de

esta tesis. A Silvestre, que siempre te echa una mano en lo que haga falta, agradecerle la programación del test de agudeza visual. Pedro Prieto siempre dispuesto a solucionarme cualquier problema, que por físico se me escapa. A Pedro y a todos los informáticos e ingenieros que forman o han formado parte del grupo (Nicolás, Juan Luis, Diego, Luis) por el desarrollo del CAMWIN, software que nos permite la adquisición y procesado de las imágenes de Hartmann-Shack de forma rápida y sencilla. Esther Berrio, compañera desde hace años, además de ser la alegría de la huerta, está dispuesta a comprometerse con retos que pocos están dispuestos a abordar. La competencia y disposición de Encarna Alcón y Carmen Cánovas hacen que los proyectos de envergadura sean más llevaderos. Los comentarios animosos del "Doctor" Alejandro Mira siempre se agradecen. Astrid Duque, informática para todo, es imprescindible. Los trabajos de Guillermo Pérez y Juan Tabernero (no se me olvida ni South Beach, ni Le Café de Paris en las Olas Blvd.) enriquecen a quien está alrededor, como es mi caso. A todos los que he nombrado hasta ahora y al resto del grupo, que se ha incorporado más recientemente (Emilio Gualda, Linda Lundström, Christina Schwarz, Luis Blanco y Bart Jaeken) agradeceros el buen ambiente que se respira en el laboratorio.

A Diego Ayala, ex-miembro reciente del grupo, por su espontaneidad, y su profesionalidad como ingeniero informático. A Antonio Guirao y Fernando Vargas por sus importantes aportaciones durante los años que formaron parte del laboratorio.

Agradecer también a Chris Hull y a John Barbur, de la City University de Londres, la posibilidad de haber podido presentar mi tesis en el Reino Unido, si no se hubieran producido los cambios legales en España, para la adaptación al Espacio Europeo de Educación Euperior, que han permitido presentar esta tesis en la Universidad de Murcia.

Dejo constancia de mi agradecimiento a las personas présbitas que actuaron como sujetos en una parte importante de este trabajo: Santiago Pina, Miguel Ortuño, Lucía Sevilla, y el propio Pablo Artal.

He de agradecer la financiación de algunas partes de esta tesis por las siguientes instituciones y empresas:

- Ministerio de Educación y Ciencia (proyectos FIS2004-2153, FIS2007-64765).
- Fundación Séneca, Region de Murcia (Proyecto Grupos de excelencia 04524/GERM/06).
- Essilor International, Francia; y Essilor España

Quiero dar las gracias a mi familia, por estar ahí. A mis hijos de cuatro años, que en innumerables ocasiones han interrumpido la escritura de esta tesis, como por ejemplo acaba de hacer Yago “arréglame el *Spiderman*” o hace un rato Claudia “mira que zapatillas de mora más bonitas”. A mi esposa, Mari Carmen, que siempre me da el soporte emocional que necesito y me apoya sin paliativos. A mis padres, Ángel y Vicenta, que me inculcaron “el que quiere puede”, pero sin perder la perspectiva de lo que es la vida.

UNIVERSIDAD DE MURCIA

FACULTAD DE MEDICINA

WAVE ABERRATIONS IN OPHTHALMIC PROGRESSIVE POWER LENSES AND IMPACT ON VISUAL QUALITY

Eloy Ángel Villegas Ruiz

2009

CONTENTS:

Chapter 1

INTRODUCTION

1. 1 OPTICAL SYSTEM OF THE HUMAN EYE

The visual system permits humans to detect and interpret information from visible light reaching the eye. In the first part of this system, the optics of the eye focuses the light onto a light-sensitive membrane, the retina. The optical system of the eye is formed by two lenses, cornea and crystalline lens, and a diaphragm called iris. In the retina, the photoreceptors cells, rods and cones, are directly sensitive to light, and a complex processing produces action potentials in retinal ganglion cells whose axons form the optic nerve. The neural signals are sent out the optical nerve through the optic chiasm to the lateral geniculate nucleus and then to the back of the brain, specifically to V1 Primary visual cortex. The fovea is the responsible of the central sharp vision. It has a diameter of about 1 mm with high concentration of cones [Kaufman and Alm 2003(a)]

The main parts of the eye are shown in figure 1. The cornea has a high refractive power, around 42 D in average, and the crystalline lens has around 22 D to focus far objects. However, in young people, this lens can increase its power above 30 D to focus objects at near distances. The diameter of iris aperture (pupil) varies between 1 and 10 mm depending on illumination conditions, but in older people, pupil sizes larger than 5 mm are not common. The aqueous and vitreous humours fill the spaces between cornea and lens, and between lens and retina, respectively [Le Grand 1964].

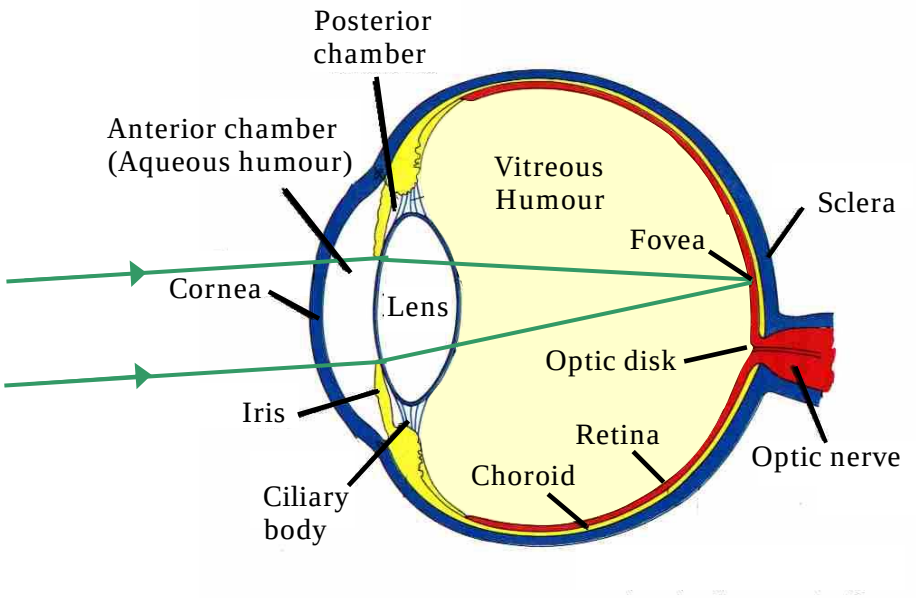

Figure 1. Parts of the human eye.
(*Image published in Kimber DC, Gray CE, Stackpole CE. Anatomy and Physiology, 1966, MacMilar Co, NY, pg 335)*

When a collimated beam, from a far object, is focused in the retina, the eye is emmetropic. But if the beam is focused in front of retina, the eye is myopic and if it is focused behind, the eye is hyperopic. In addition to these refractive errors, the human eyes also have other optical defects called high order aberrations which have been widely studied in the last years.

1.2 PRESBYOPIA AND ITS CORRECTION

1.2.1 Accommodation and presbyopia

Accommodation is the dynamic ability of the human eye to change its power to focus objects at varying distances. This mechanism is due to the change of shape of the crystalline lens. The accommodative system of the eye consists of the ciliary body, the ciliary muscle, the zonular fibers, the lens capsule and the crystalline lens (figure 2). Our present understanding of the mechanism of accommodation is based on the theory of Helmholtz. When the eye accommodates, the ciliary muscle contracts and the ciliary body moves forward and toward the axis of the eye. This tension is translated to the peripheral zonular fibers. However, the tension on the axial zonular fibers is reduced and the lens capsule molds crystalline lens into a more spherical form. The lens thickness increases, lens diameter decreases and the curvature radii, specially that of the anterior surface, decrease. This results in an increase of the positive power of the lens [Kaufman and Alm 2003(b), Atchison 1995]. Figure 3 is a simple diagram of this accommodative mechanism.

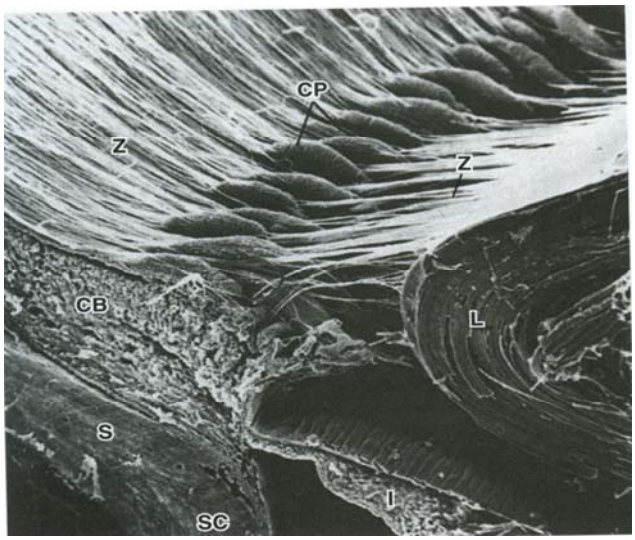

Figure 2. Scanning electron micrograph (SEM) of the accommodative apparatus of a cynomolgus monkey eye. Z, zonular fibers; L, crystalline lens; CP, ciliary processes; CB, ciliary body; S, sclera; SC Schelmm's canal.
(*Image published in [Kaufman and Alm 2003(b)] from Rohen JW: Invest Ophthalmol Vis Sci 1979; 18:137).*

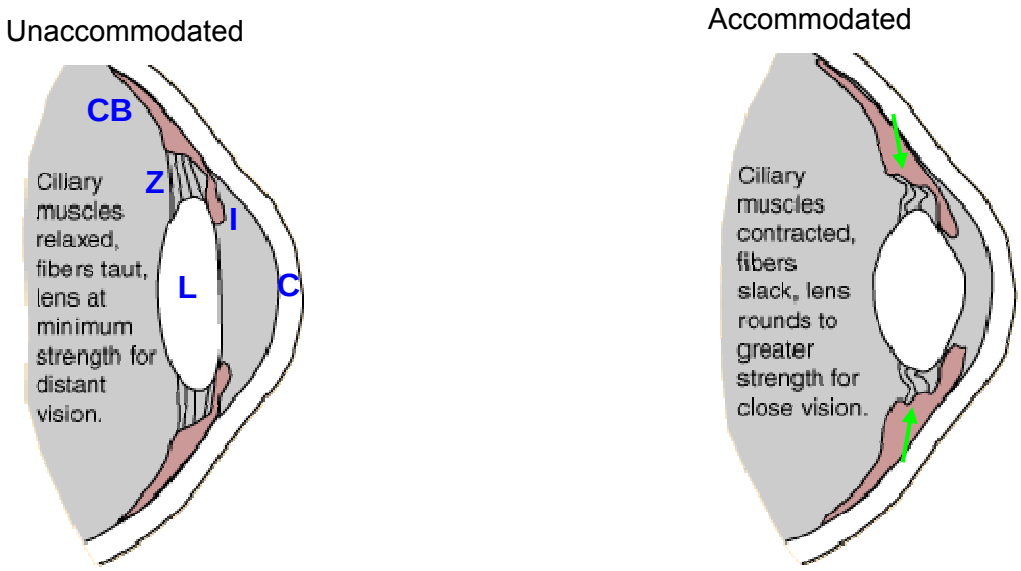

Figure 3. Helmholtz accommodative mechanism. Z, zonular fibers; L, crystalline lens; CB, ciliary body; I, iris; C, cornea.
(Picture obtained from HyperPhysics (©C.R. Nave, 2006), Georgia State University)

Presbyopia is the age-related loss of the ability to accommodate. Duane (figure 4) found that presbyopia starts early in life. But emmetropes (or people corrected for far vision) start to feel the symptoms of this visual degradation from between age 40 and 45 years, because of the maximum accommodation doesn't give enough positive power to see comfortably at close distances. Nowadays, it is not yet clear the factors that cause the presbyopia. The main theories deal with the lenticular sclerosis and the altered geometry of the lens/zonular relationships due the increased growth of the lens [Kaufman and Alm 2003(b)].

Figure 4. Range of accommodative amplitude as a function of age obtained by Duane (1912).

1.2.2 Surgical solutions

Apart from ophthalmic lenses for spectacles and contact lenses which will be treated in particular points, in the following, I describe briefly the current corrections of presbyopia using surgery [Murphy 2003] on the cornea and implanting intraocular lenses.

– Cornea surgery

Conductive keratoplasty consists of creating a ring of application spots around the periphery of the cornea using a hair-thin probe into the stroma to release radiofrequency. It shrinks the peripheral tissue and increases the curvature of the central cornea. This technique creates monovision, because it is only applied in the non-dominant eye which will be used for near vision. The main problem is a progressive amount of regression that can be interpreted as the natural progression of presbyopia or even the progression of hyperopia.

The other possibility with the cornea is the *multifocal ablation (presbyLASIK)*. This technique has the same problems that the multifocal contact and intraocular lenses, and moreover the ablation is not reversal. Until now, this solution is not giving good results. Indeed, it is not still clear the better zones of the ablation for near and far vision [Kent 2005].

– Intraocular lenses

Posterior chamber intraocular lenses (IOLs) are the artificial lenses that replace the eye's natural lens that is removed during cataract surgery. Standard IOLs are monofocal, and so have the adequate power for one distance only.

Multifocal IOLs are an option for pseudophakic eyes. There are three type of lenses [Fuerst 2006, Lavin 2001]: zonal refractive, diffractive and combinations. The first type consists of concentric changes in curvature. Diffractive IOLs have concentric edge junctions producing different focal points for distance and near distances. The last alternative is the combination of refractive and diffractive zones in one IOL, for instance, a central diffractive zone for both near and distance foci and a peripheral refractive zone for distance vision [Fuerst 2006]. Figure 5 shows an example of these type of lenses, with the diffractive rings in detail. In general, the users of recent designs of multifocal IOLs can achieve acceptable near vision VA [Chiam *et al.* 2007, Vingolo *et al.* 2007], 0.5 or better, but these lenses with different foci present some disadvantages [Vingolo *et al.* 2007, Fuerst 2006] such as glare and haloes, low contrast sensitivity, limited vision for some viewing distances and visual limitations due to uncorrected astigmatism higher than 0.5D. In addition, small pupil sizes and the common decentrations produced in the lens implantation reduce the optical and visual performance of this type of lenses [Hayashi *et al.* 2001].

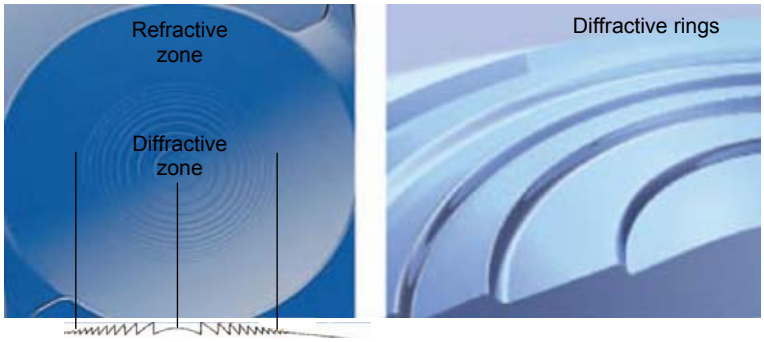

Figure 5. Alcon's ReStor Apodized Diffractive/Refractive IOL.
(Images published in [Fuerst 2006])

Several studies have demonstrated that the remaining constriction and relaxation of zonules changes posterior capsule tension and moves the IOL along the anterior–posterior axis. In the accommodation state, the lens is moved from posterior to anterior position. In teenagers with congenital cataracts operated, the average shift is around 0.42 mm, and for this value of lens movement the apparent accommodation ranges between 1 and 6 D depending on the subject [Lesiewska-Junk and Kaluzny 2000]. Figure 6 shows an example of an accommodative IOL (CrystaLens, model AT-50) with grooved hinges in the plates to make easier the lens movement. In older pseudophakic subjects using this accommodative lens [Marchini *et al.* 2004], the lens shift is also less than 0.5 mm, and most of them reach an accommodation amplitude between 0.5 and 1.5 D. Preliminary clinical results have shown that in most implanted eyes with this type of lenses, the near visual acuity ranges between 0.7-0.4 in decimal scale. In some people, these values of visual acuity permit to perform daily activities without glasses, but they can not see sharply in near vision for precision activities such as reading. On the other hand, calculations in model eyes [Hunter *et al. 2006*] show that a forward movement of 0.5 mm can only produce a positive change in power between 0.25 and 1 D. The rest of apparent accommodation could be due to the larger focus depth in presbyopic eyes due to senile myosis. Some authors have suggested the implication of third order aberrations of the cornea in the increase of apparent accommodation of pseudophakic eyes [Oshika *et al. 2002*]. Furthermore, these accommodative lenses are still controversial, since experiments in humans with accommodation estimated with pilocarpine reported a counterproductive backward shift of the AT-45 IOL [Koeppl *et al.* 2005].

Recently, in order to increase the power change, some companies have developed dual-element IOLs which consist of either two positive lenses or a combination of a plus and a minus lens. Clinical trials [Ossma *et al.* 2007] with one of this type of lenses show a range of accommodation from 1.00 to 5.00 D and a range between 1.00 and 2.50 D in a control group with monofocal IOL. The intraocular system of figure 7 consist of two lenses, the

posterior minus lens stays fixed at the posterior capsular bag and the anterior positive lens moves forward, allowing near vision.

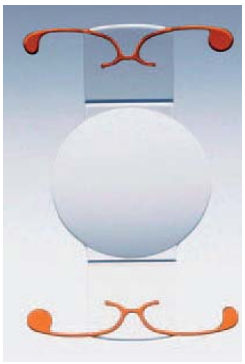

Figure 6. Accommodative IOL: CrystaLens (model AT-50) from Eyeonics (Aliso Viejo, California, USA) *(Images published in [Doane and Jackson 2007] by Courtesy of EyeOnics.)*

Figure 7. Dual optic accommodating IOL: Visiogen Synchrony from Visiogen Inc. of Irvine (California, USA). *(Images published in [Doane and Jackson 2007] by Courtesy of Visiogen)*

Other techniques to restore the accommodation in pseudophakic eyes consist of filling the capsular bag with soft gel-like materials [Doane and Jackson 2007]. In a particular design, the lens material is pressed through the natural pupil decreasing the anterior radius of the lens. In primates, this lens has produced an enormous accommodation around 40 D.

The accommodating and multifocal IOLs are designed supposing that patients achieve emmetropia for distance vision. However, at present, precise IOL distance power selection is a problem unsolved due to inaccurate preoperative measurements, postoperative corneal astigmatism or unstable axial position of the IOL. So, around half the patients implanted with IOLs may have residual refractive error higher than 0.5 D and they would need spectacles for optimal distance vision [Brandser *et al.*1997, Olsen 2007]. In the near future, this problem could be solved using light-adjustable IOLs [Schwartz *et al.* 2003, Sandstedt *et al.* 2006] whose refractive power can be modified after cataract surgery illuminating the lens with UV light.

1.2.3 Contact lenses

An alternative solution for presbyopia without need of surgery is multifocal contact lenses. As in IOL, the contact lenses (CL) for presbyopes have multiple powers positioned within the pupil to focus near or distance objects suppressing the most blurred images. The majority of designs available are based on changes of curvature [Bennett 2008] which can be aspheric or concentric. Figure 8 shows examples of the gradual change of power in aspheric design and annular zones in concentric design. The choice of the central zone for near or distance vision is still a controversial issue and both options are commercialized. Although some clinical reports claim high success rates (around 75%), these type of corrections have some disadvantages such as the intersubject variability of pupil sizes that is the base of the lens performance, limitations in visual quality due to the decentrations, and the lack of stability in astigmatic corrections.

Similar to bifocal lenses for spectacles, the translating CLs have two vertical zones where the near prescription is on the bottom (figure 8). When patient looks down, the lens remains supported by his lower lid, so he uses the lower portion of the lens. But, these lenses cannot be used for intermediate-range visual tasks such as computer work [DeFranco 2008].

Figure 8. Examples of different designs of multifocal contact lenses
(Images published in this web site: www.allaboutvision.com)

1.2.4 Monovision

Monovision is another option to avoid the use of spectacles. It consists of wearing near correction in one eye and distance correction in the other eye. This technique can be applied in corneal refractive surgery (such as LASIK), in cataract surgery and with contact lenses. A major problem with monovision is a reduction in stereopsis. An adaptation period is recommended to see independently with each eye.

1.3 OPHTHALMIC LENSES

In this section, different options for correcting presbyopia using ophthalmic lenses are revised.

1.3.1 Reading glasses

The use of spectacles with monofocal lenses for near work is the simplest solution for presbyopes. Reading glasses give patients a clearer and wider near visual field than any other option, without an adaptation period. However, if the subject needs eyeglasses for correcting distance vision, he must use different spectacles for near and far vision. For example, he will be unable to read and watch television at the same time. The use of two spectacles in ametropic patients and the lack of clear vision for intermediate distances in many presbyopes over the age of 50, are the two main disadvantages of reading glasses.

1.3.2 Multifocal lenses: bifocals and trifocals

The solution to the problem of two glasses for ametropic presbyopes was invented by Benjamin Franklin [Tunnacliffe 1993] around 1785. It consisted of two separate lenses which were cut in half and placed together in a frame, the upper one for distance vision and the other for near vision. Since then many types of bifocal lenses have been developed to combine the distance portion, also called main lens, and the reading zone that is also called segment [Jalie 1994, Tunnacliffe 1995]. The fused bifocal appeared in 1904, and nowadays it is still one of the most popular designs. The reading addition is produced by fusing a segment lens of higher refractive index glass into a depression worked on the main lens. Before 1910, bifocals lenses were manufactured in a single piece of glass with different curvature for distance and near portions. At present, these lenses, called solid bifocals, are mainly fabricated in plastic materials, with the change of curvature in the first surface of the lens. Figure 9 shows a bifocal lens with a near portion with a curved top. Nowadays, this bifocal is very common and it can be found in fused glass or in plastic material from a single lens (solid). In general, bifocal lenses are fitted with segment top at the level of the lowest point of the corneal-scleral limbus in primary position of gaze [Tunnacliffe 1993], as is shown in figure 9. The horizontal position of the top must coincide with near pupil centre. So, patients have a wide visual field in far vision, and when the eyes rotate downwards and converge for near vision they look, more or less, through the centre of the segment. Presbyopes using bifocal lenses have a good visual quality for both distance and near tasks.

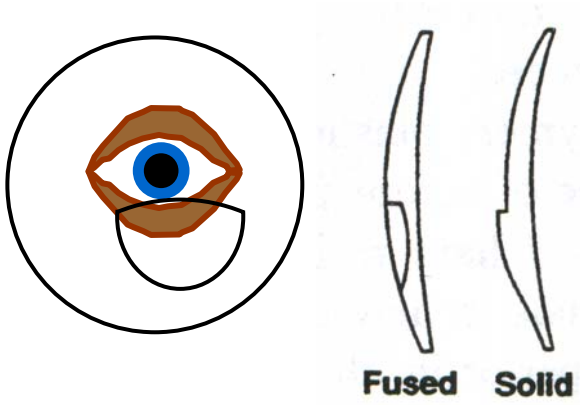

Figure 9. Example of bifocal lens for glasses with curved near portion fabricated with fused segment or in a single lens with different curvatures (solid)
[Tunnacliffe 1995]

The optical centre of the segment is localized in the centre of the circle that circumscribes its actual shape. Due to the different prismatic effects between far and near points closer to segment top, patients perceive an image jump when they change from far to near vision. So, this effect is null in flat tops. For 2 D of addition power in the segment, the image jump is around one prismatic dioptre in curved tops and more than two prismatic dioptres in round segments. After 50 years of age, the ability to accommodation is reduced to such an extent that bifocal wearers cannot focus objects at intermediate distances properly neither through the distance portion nor through the segment [Tunnacliffe 1995]. A possible solution is trifocal lenses which include an intermediate portion between the upper distance and lower reading portions. Nevertheless, this type of lenses has a reduced vertical field of view through the three zones and two image jumps. Indeed, in Spain, most practitioners barely dispense one pair of trifocal lenses per year. Other important drawback of bifocal and trifocal lenses is the cosmetic appeal, because the segment is seen on the face and, besides many presbyopes do not want to reveal their age.

1.4 PROGRESSIVE-POWER LENSES (PPLs)

Progressive addition lenses (PALs) or, as we will refer within this thesis, progressive power lenses (PPLs) is an alternative to bifocal and trifocal lenses. These are designed to provide continuous vision at all distances by means a progressive change in spherical power from upper to lower zones. PPLs are being increasingly used today to correct presbyopia. Around a third of presbyopic population living in Europe and in USA uses progressive lenses. The rest of the Europeans use mainly single lenses (60%), while bifocals are more used in the USA (40%) [Meslin 2007].

The first progressive lens was successfully commercialized by Essel (now called Essilor) in France in 1959. The front surface had a spherical upper portion and a continuous shortening of the radius of curvature from intermediate to lower portions allowing a progressive increase of positive power (figure 10). The main problem of progressive lenses is the presence of peripheral astigmatism induced by the continuous change in power through the lens. This inherent defect in design was well recognized from the early days: Minkwitz [Minkwitz 1963] stated that it was not possible to produce a progressive spherical power surface without astigmatism and distortion being present at some point. Residual astigmatism degrades vision through some parts of the lens and may play a role in reducing the success of the adaptation process.

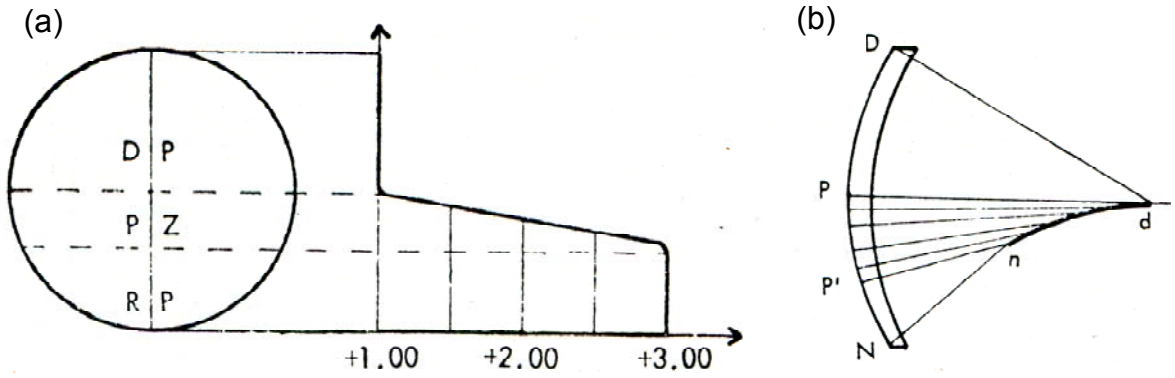

Figure 10. First commercialized PPL by Essel in 1959. (a) Different zones : distance portion ,DP; progression zone, PZ; and reading portion, RP. (b) Evolution of centres of curvature in the progression zone , PP', from distance to near portions.
[Jalie 1994]

To verify and to mount the PPLs in frames, two different types of makings are found: visible and invisible markings (see figure 11). The first ones are removed after mounting. In the upper area of the lens, the cross fitting and horizontal lines are the reference points for mounting, while the upper and dower circles are for checking the powers of the distance and near prescriptions respectively [Jalie 1994, Brooks 1983]. Because the front progressive surface has gradually reducing radii of curvature towards the bottom of the lens, the lower edge thickness is noticeably less than the thickness of the upper edge. Nowadays, the second surface of PPLs is tilted with respect to the first one in order to remove this excess thickness. So, a prismatic power of 0.6Δ base down per dioptre of addition is induced [Jalie 2000]. The prismatic power is measured in a painted point just under the fitting cross.

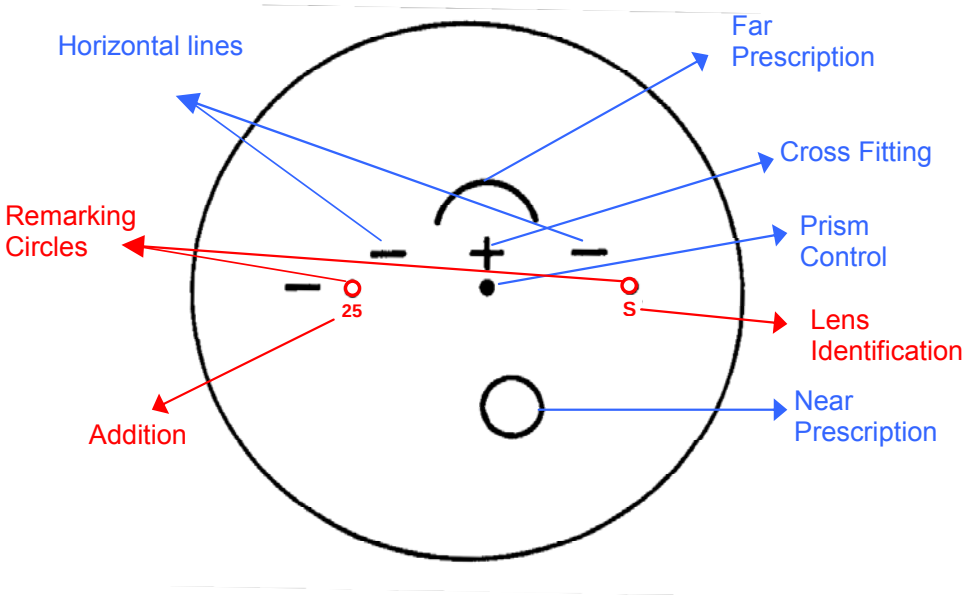

Figure 11. Marks in progressive lenses. After mounting, all marks are removed. To reconstruct the spotting, the hidden etch marks (in red) should be located by holding the lens under a bulb and placed on a verification card provided by the manufacturer.

1.4.1 Isocylinder and isopower lines. Power profile

To study the optical properties of PPLs and to compare different designs, three conventional diagrams are normally used [Tunnacliffe 1995]: isocylinder lines, isopower lines and power profile (figure 12). Isocylinder graphs show lines joining those points where astigmatism is the same (normally in steps of 0.5 D). The different zones of a PPL are delimited by the first 0.5 D isocylinder lines. We can estimate the widths of the distance, near and progression zones depending on the height on the lens, and we also can locate the zones with unwanted astigmatism. On the other hand, isopower lines show how the addition power (spherical power difference from far prescription) is distributed over the lens, normally in steps of 0.5 D. Evidently, the width of reading zone can be also delimited by the isopower line corresponding to addition power needed for reading. The power profiles show how the addition increases along the progression corridor (also called umbilical line).

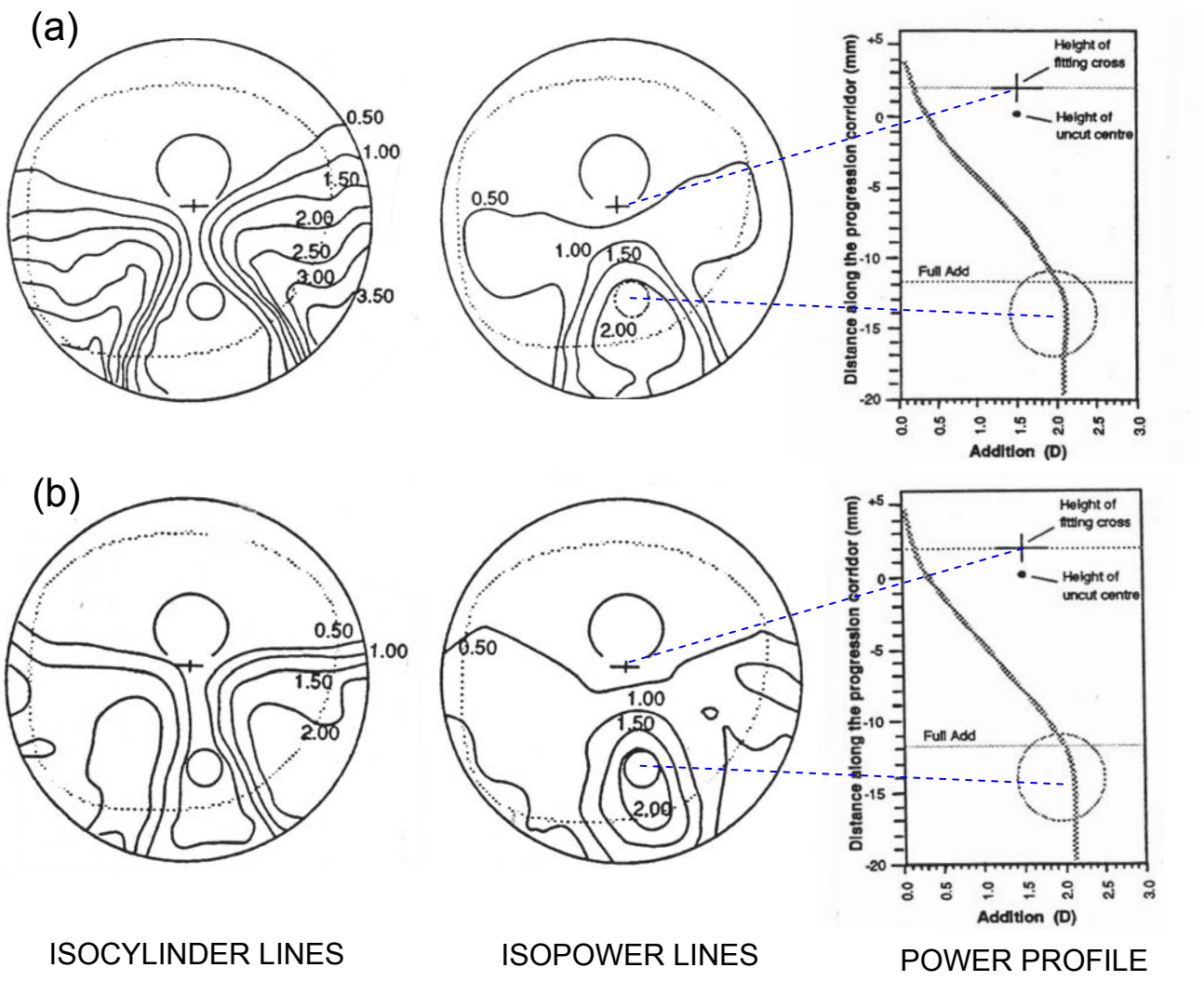

Figure 12. Typical graphs to evaluate the optical characteristics of progressive lenses. Lens (a) is a hard design and lens (b) is a soft design. *[Tunnacliffe 1995]*

1.4.2 Reading addition

In PPLs prescription, it is important to remind the importance in the selection of the addition power.

In clinical optometry, there is an old rule of that a person will find close work to be comfortable if no more than one-half of the accommodative amplitude must be used [Grosvernor 2002]. These estimations are useful for corrections with single or bifocal spectacle lenses. Nevertheless, in the case of PPLs the near-addition power must be the minimum necessary to see clearly at near distances. If the near prescription addition is higher than the exact value, patients will have adaptation problems because of two reasons.

Firstly, the peripheral astigmatism increases with the addition values. Moreover, to minimize the ocular effort in the rotation, the eyes will look through the first zone of the progression corridor with the exact addition. In this area the visual field is more restricted due to the fast increase of peripheral astigmatism from the centre of the corridor. Figure 13 shows the isocylinder plots of two PPLs with a near addition of 2.00 and 2.75 D. For people between the ages 50 and 55, the accommodative amplitude is around 1.5 D. If they need a total positive power of 3.5 D, the prescription of reading addition for single or bifocal spectacle could be 2.75 D. If this same prescription is dispensed in PPLs, the subject will look through the red circle of figure 13b which is very limited by the peripheral astigmatism. However, if we prescribe the exact addition power of 2.00 D, the subject will use the wider area designed for near vision, figure 13a.

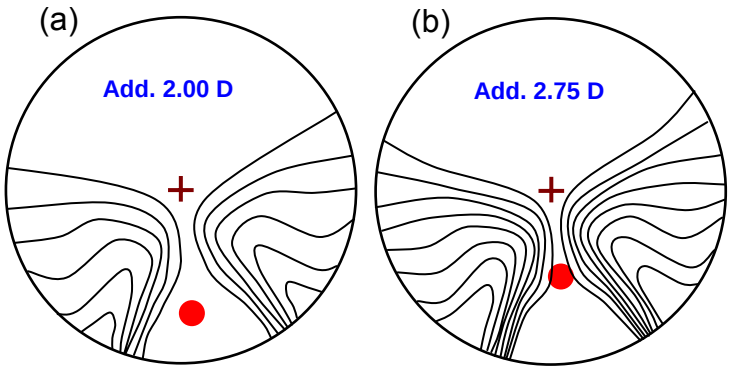

Figure 13. Graphs of 0.5 D-isocylinder lines of PPLs with reading additions of 2.00 and 2.75 D. The red circle indicates the zone used by a subject with a accommodative amplitude of 1.5 D to see clearly objects at a distance of 28.5 cm (vergence of 3.5 D)

1.4.3 Designs of PPLs

– Early designs

From the beginning of twentieth century, multitude of designs has been proposed to improve optical and visual performance of progressive lenses mainly limited by peripheral astigmatism. In this point, we revised the designs of the first part of the 20th century [Sullivan and Fowler 1988].

In 1907, Aves patented the first design of PPL. It consisted of a biconvex lens with two conical surfaces. One was the lower half of an ellipse with vertical axis, resembled a cylinder with horizontal axis in which the power increases downwards. The other one consisted of a

convex conical section with a horizontal increment of curvature downwards. But this lens corrected only hyperopia and could not incorporate astigmatic corrections.

In 1920, Poullain and Cornet produced a progressive single surface, known as “elephant trunk”. This type of surface, shown in figure 14, is not a surface of revolution what supposed important limitations of manufacturing at early part of the twentieth century. A combination of progressive cylindrical surfaces employed by Aves produce the same effect as the “elephant trunk” surface [Volk and Weinberg 1962]. An example of this is shown in figure 14. In the central part of the power progression, there is only a spherical power change, but in peripheral zones the unwanted astigmatism increases quickly.

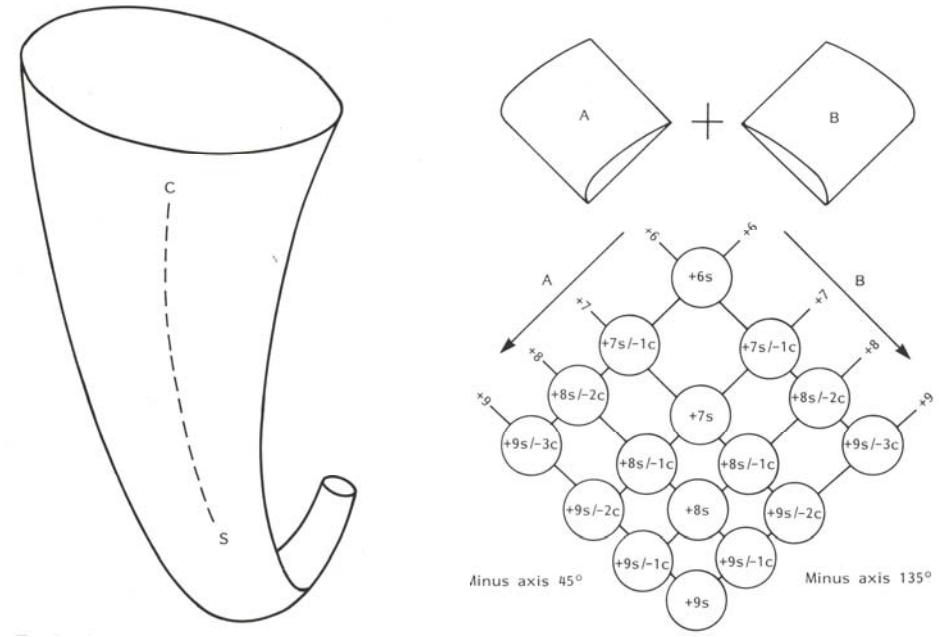

Figure 14. Example of “elephant trunk” surface and, its power and astigmatism distribution expressed by the combinations of progressive cylinders employed by Aves. *[Sullivan and Fowler 1988]*

In 1914, Gowlland produced a progressive lens with an anterior toroidal surface and a posterior paraboloidal surface. This lens was the first to be produced commercially. Bach, in 1958, proposed a new design with a better control of astigmatism. In this lens, a section of an ellipse with horizontal axis was tilted to equalize the astigmatism at all points, and this astigmatism was neutralized by a cylinder with opposite sign in the concave surface.

A concentric design, resembled a blended bifocal, were suggested by Paige (1918) and patented by Beach (1946). It supposed an annular zone of progression with a poor optical quality in the area between distance and near portions.

– Current designs

Many different types of PPLs have been commercialized since Maitenaz designed the first commercially successful PPL in the 1950s. As mentioned above, this lens was commercialized by Essel under the name of Varilux. It consisted of a spherical far area joined inferiorly to an “elephant trunk” construction which merged into a spherical near area. This lens had high values of aberrations (astigmatism, distortion and field of curvature) in peripheral zones. In 1970s, Maitenaz modified this design to reduce aberrations in the lateral areas of the near portion, although to do this, he had to increase the aberrations in the progression corridor [Sullivan and Fowler 1988].

PPLs designs are commonly described according to the astigmatism distribution over the progressive surface. PPLs use to be grouped in either *hard* or *soft* progressive designs (see figure 12) [Jalie 2000]. The lenses with *hard* design have wide astigmatism-free far and near vision areas, but astigmatism rapidly increases away from the corridor at intermediate zones. In the *soft* design, the astigmatism-free far and near areas are narrower but introduced at a more gradual pace, producing a slower increase of astigmatism in the lateral zones. First generation PPLs had a symmetrical distribution of astigmatism around the corridor (*symmetric* design). However, since in normal binocular vision the eyes move a slightly larger distance on the temporal side of a lens than on the nasal side, an *asymmetric* design (see lens b in figure 12) was proposed in which astigmatism changed more gradually towards the temporal area of the lenses [Tunnacliffe 1995]. Nowadays, moreover, for most PPL designs, the distribution of unwanted astigmatism varies with the addition power taking into account the differing needs of patients in different stages of presbyopia (also called *multi-designs*). For instance, under the age of 50, the amplitude of accommodation is sufficient to focus at all distances using only far and near zones, and the intermediate portion of the PPL is not so important.

In relation to Minkwitz statement [Minkwitz 1963], a slower rate of the power change provides a reduction in the astigmatism. So, sometimes, as shown in figure 12, the power progression starts about 2 to 3 mm above fitting cross which should be placed at the pupil centre with the eyes in the primary position. It supposes an additional correction of around +0.2 D, which appears acceptable in practice.

Despite numerical control lathe machines being able to generate aspheric surface sections, current designs of PPLs still present significant amounts of astigmatism. Beyond astigmatism, the other higher order aberrations in PPLs have been much less studied.

All designs noted above produce a power progression by a change in the shape of the surface. From 1950, when Spiegel patented a method of producing optical glass with variation of the refractive index [Sullivan and Fowler 1988], to nowadays, many designers have studied the use of gradient-index materials to manufacture progressive lenses. However, until now, any company commercializes this type of lenses.

1.5 OPTICAL QUALITY PARAMETERS

In this thesis, different optical parameters are used to describe the optical quality of the PPLs and the eyes. These metrics are based on the wavefront aberration.

When a free-aberration system forms the image of a point object, a spherical wave emerges from the exit pupil converging to the Gaussian image point. This surface passing through the center of the exit pupil is the reference wavefront $W_{ref}(\rho,\theta)$. If the system is aberrated, the **wavefront aberration** $WA(\rho,\theta)$ is expressed as the difference between the optical path of its wavefront $W(\rho,\theta)$ and that of the reference wave, on the exit pupil plane (figure 15).

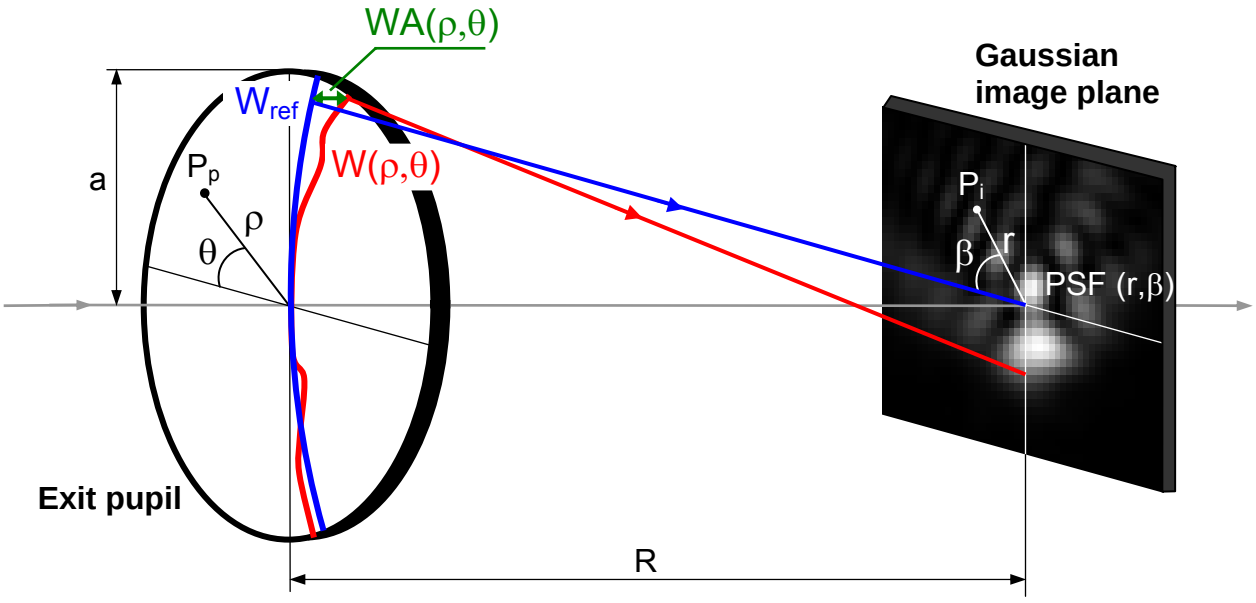

Figure 15. The function of wavefront aberration $WA(\rho,\theta)$ is expressed as the difference on the exit pupil plane between the optical path of the actual wavefront $W(\rho,\theta)$ and that of the reference wavefront $W_{ref}(\rho,\theta)$. P_p and P_i are the corresponding points of $WA(\rho,\theta)$ and PSF (r,β) respectively. R is the radius of the reference wavefront, and "a" is the pupil radius.

The point spread function (PSF) is defined as the irradiance distribution of the image of a point object. Assuming a uniformly illuminated aperture, the function $\exp[i\phi(\rho,\theta)]$ is the pupil function of the system. The PSF is proportional to the modulus square of the Fourier transform (FT) of the pupil function. The phase aberration in the exit pupil plane, $\phi(\rho,\theta)$, is related to the wavefront aberration in the same plane according to $\phi(\rho,\theta)=(2\pi/\lambda)WA(\rho,\theta)$. In our experiments, we can consider that the exit and entrance pupil coincide with the aperture of the system. Thus, the PSF in the Gaussian image plane is given by this formula:

$$PSF(r,\beta) = \left| FT\left\{ \exp\left(i\frac{2\pi}{\lambda} WA(\rho,\theta) \right) \right\} \right|^2 \qquad (1)$$

where (r,β) and (ρ,θ) are the polar coordinates in the image and pupil planes respectively, and λ is the wavelength. The Fourier transform integral for circular aperture gives the PSF normalized to the aberration-free central irradiance [Mahajan 2001]:

$$PSF(r,\beta) = \pi^{-2} \left| \int_0^1 \int_0^{2\pi} \exp\left[i\frac{2\pi}{\lambda} WA(\rho,\theta) \right] \exp\left[-i\frac{2\pi}{\lambda R} a\ r\rho\cos(\theta-\beta) \right] \rho d\rho d\theta \right|^2 \qquad (2)$$

The elements, points and coordinates of Eq. (2) are shown in figure 15.

The **Strehl ratio** characterizes the overall system performance, it relates the axial irradiance of the aberrated system and the system limited by diffraction. In this work, we calculated the Strehl ratio as the quotient between the intensity peak in the system's PSF and the diffraction-limited PSF.

Zernike polynomials are widely used to describe the wavefront aberration. These polynomials are orthogonal over the unit circle. In polar coordinates (ρ,θ), Zernike polynomials can be expressed as the product of angular functions and radial polynomials. In [Born and Wolf 1999, Malacara 1992] the angular coordinate (θ) is defined from the y (vertical) axis. In Ophthalmic Optics, the angular position is specified from x (horizontal) axis, commencing with 0 on the observer's right-hand [Thibos *et al*. 2000]. Each polynomial is composed of a radial-dependent polynomial and an angular-dependent sinusoidal component. Thus the Zernike polynomials are defined as:

$$Z_j(\rho,\theta) = Z_n^m(\rho,\theta) = \begin{cases} \sqrt{n+1}\ R_n^0(\rho) & \text{if } m = 0 \\ \sqrt{2(n+1)}\ R_n^{|m|}(\rho)\cos(m\theta) & \text{if } m > 0 \\ -\sqrt{2(n+1)}\ R_n^{|m|}(\rho)\sin(m\theta) & \text{if } m < 0 \end{cases} \tag{3}$$

where $R_n^{|m|}(\rho)$ is the radial polynomial expressed as:

$$R_n^{|m|}(\rho) = \sum_{s=0}^{(n-|m|)/2} \frac{(-1)^s (n-s)!}{s!\,[(n+|m|)/2-s]!\,[(n-|m|)/2-s]!}\rho^{n-2s} \tag{4}$$

The radial coordinate (ρ) is normalized to 1 and the angular coordinate (θ) ranges from 0 to 2π.

The Zernikes polynomials can be expressed with a single index (j), or with both the radial degree (n) and the angular frequency (m). For the *j*th polynomial, the radial order and the angular frequency are obtained as:

$$n = \text{roundup}\left[\frac{-3+\sqrt{9+8j}}{2}\right] \qquad m = 2j - n(n+2) \tag{5}$$

Figure 16 shows the 3D representations of the aberrated wavefront up to forth radial order.

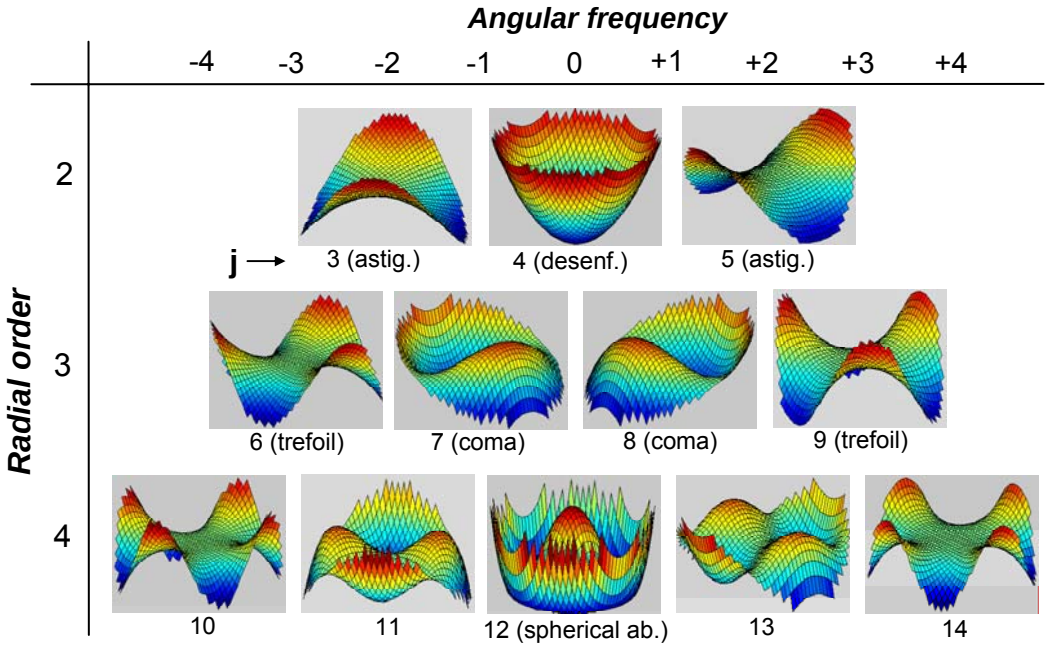

Figure 16. 3D representations of the aberrated wavefront for Zernike coefficients from second up to forth radial order. The Seidel aberrations corresponding to Zernike coefficients are also noted between brackets.

Table 1 shows the Zernike polynomials up to fifth order, that is the first 21st Zernike modes. The corresponding aberrations are also noted.

Index, j	Radial degree, n	Angular frequency, m	Zernike polynomial	Aberrations
0	0	0	1	Constant term (Piston)
1	1	-1	$2\rho\sin\theta$	Tilt in y direction
2	1	1	$2\rho\cos\theta$	Tilt in x direction
3	2	-2	$\sqrt{6}\,\rho^2\sin2\theta$	Astigmatism with axis at ±45º
4	2	0	$\sqrt{3}\,(2\rho^2-1)$	Defocus
5	2	2	$\sqrt{6}\,\rho^2\cos2\theta$	Astigmatism with axis at 0º or 90º
6	3	-3	$\sqrt{8}\,\rho^3\sin3\theta$	Vertical trefoil
7	3	-1	$\sqrt{8}\,(3\rho^3-2\rho)\sin\theta$	Coma along y axis
8	3	1	$\sqrt{8}\,(3\rho^3-2\rho)\cos\theta$	Coma along x axis
9	3	3	$\sqrt{8}\,\rho^3\cos3\theta$	Horizontal trefoil
10	4	-4	$\sqrt{10}\,\rho^4\sin4\theta$	
11	4	-2	$\sqrt{10}\,(4\rho^4-3\,\rho^2)\sin2\theta$	
12	4	0	$\sqrt{5}\,(6\rho^4-6\rho^2+1)$	Spherical aberration
13	4	2	$\sqrt{10}\,(4\rho^4-3\,\rho^2)\cos2\theta$	
14	4	4	$\sqrt{10}\,\rho^4\cos4\theta$	
15	5	-5	$\sqrt{12}\,\rho^5\sin5\theta$	
16	5	-3	$\sqrt{12}\,(5\rho^5-4\rho^3)\sin3\theta$	
17	5	-1	$\sqrt{12}\,(10\rho^5-12\rho^3+3\rho)\sin\theta$	
18	5	1	$\sqrt{12}\,(10\rho^5-12\rho^3+3\rho)\cos\theta$	
19	5	3	$\sqrt{12}\,(5\rho^5-4\rho^3)\cos3\theta$	
20	5	5	$\sqrt{12}\,\rho^5\cos5\theta$	

Table 1. Zernike polynomials up to fifth order according to OSA standards [Thibos *et al.* 2000] and the corresponding aberrations.

To an easier interpretation and manipulation of the Zernike polynomials, some properties have to be taken into account [Malacara 1992]:

1. Each polynomial mode, except C_0, has a mean value of zero.
2. The wavefront variance is equal to the sum of the variances of the individual polynomial mode.

3. Zernike polynomials present balanced aberrations. Each polynomial contains the proper amount of each of the lower order terms needed to minimize the variance of that term. For example, the polynomial Z_4 describes only the defocus of the circle of least confusion, and the amount of defocus (represented by ρ^2) needed to balance high order terms, such as spherical aberration, is already included in the polynomial describing those aberrations.
4. Adding or subtracting Zernike polynomials does not affect the fit coefficients of other polynomials.

The wavefront aberrations can be also expressed by a power expansions in terms of square polar coordinate (ρ) up to 4th degree in this way [Meeteren 1974, Wyant and Creath 1992]:

$$WA(\rho,\theta) = A_t\,\rho\cos\theta + A_d\,\rho^2 + A_a\,\rho^2\cos^2\theta + A_c\,\rho^3\cos\theta + A_s\,\rho^4 \qquad (6)$$

where aberrations are limited to tilt (A_t), defocus (A_d), astigmatism (A_a), coma (A_c) and spherical aberration (A_s). The primary or Seidel aberrations are also called third-order aberrations, because the ray aberrations associated with wave aberrations of this order are of the third degree in the coordinates [Born and Wolf 1999].

The Seidel coefficients (A_t, A_d, A_a…) can be expressed as functions of Zernike coefficients (C_1, C_2, C_3, C_4…). This is done by grouping the Zernike terms with the same degree and equaling them with the corresponding Seidel coefficient [Wyant and Creath 1992]. The magnitude and angle for each primary aberration are shown in table 2.

Defocus, astigmatism and spherical aberrations can be expressed in diopters from the Seidel aberrations [Meeteren 1974] (a is the pupil radius):

$$E = \frac{2A_d}{a^2} \qquad I = \frac{-2A_a}{a^2} \qquad S = \frac{-4A_s}{a^2} \qquad (7)$$

where E, taking into account the positive sign of coefficient A_d in table 2, is the sphere of the sphero-cylindrical form with negative cylinder. The value of this cylinder is I, that is the Sturm's interval. The negative cylinder axis is that shown in table 2. According to OSA standards [Thibos *et al.* 2000], the wavefront aberration function must be positive (W>0) for a myopic eye. In this case, the Zernike coefficient C_4 is positive and therefore our value of E

is also positive. Thus, the **sphero-cylindrical form** obtained from E and I values corresponds to the powers of the tested system. In the case of the eye, both isolated and in combination with a ophthalmic lens, the sphero-cylindrical form express the powers with opposite signs to the prescription. In the case of the isolated lens testing, the sphero-cylindrical form directly gives the power signs of the lens. In Eq.(7) it is also shown the longitudinal spherical aberration in diopters, S.

Coefficient	Aberration	Magnitude	Angle
A_t	Tilt	$\sqrt{(2C_2-2\sqrt{8}C_8)^2+(2C_1-2\sqrt{8}C_7)^2}$	$\tan^{-1}\left(\frac{2C_1+2\sqrt{8}C_7}{2C_2-2\sqrt{8}C_8}\right)$
A_d	Defocus	$2\sqrt{3}C_4-6\sqrt{5}C_{12}\pm\sqrt{6C_5^2+6C_3^2}$ positive sign to obtain the sphere of the sphero-cylindrical form with negative cylinder	
A_a	Astigmatism	$\pm 2\sqrt{6C_5^2+6C_3^2}$ sign opposite that chosen in defocus term	$\frac{1}{2}\tan^{-1}\left(\frac{-C_3}{C_5}\right)$ Angle of the negative cylinder axis (if Z_5<0, then angle=angle+90º)
A_c	Coma	$3\sqrt{8C_8^2+8C_7^2}$	$\tan^{-1}\left(\frac{-C_7}{C_8}\right)$
A_s	Spherical aberration	$6\sqrt{5}C_{12}$	

Table 2. Magnitude and orientation of Seidel aberrations as function of Zernike coefficients.

On the other hand, the **RMS** is a parameter of the wavefront error that characterizes the overall system performance. It is defined as the square root of the wavefront variance. If the mean value of the wavefront surface is zero, such as a flat reference wavefront without piston (C_0=0), the wavefront variance (σ_W^2) is just the mean squared value of the wavefront over the pupil [Malacara 1992]:

$$\sigma_W^2=\frac{1}{\pi}\int_0^1\int_0^{2\pi}W^2\rho d\rho d\theta \qquad (8)$$

From the orthogonal properties of the Zernike polynomials, the wavefront variance is equal to the sum of the variances of each polynomial mode that corresponds to the summing

of the squares of the Zernike coefficients. Thus, we calculated the RMS as the root square of the sum of the squares of the Zernike coefficients:

$$RMS = \sqrt{\sigma_W^2} = \sqrt{\sum_{3}^{j_{max}} C_j^2} \qquad (9)$$

In this thesis, for all optical measurements, we calculate Zernike coefficients up to fifth order, the RMS of the WA, the PSF from the WA and the Strehl ratio.

1.6 OPTICAL TECHNIQUES FOR TESTING OPHTHALMIC LENSES

There are different methods for measuring and evaluating the performance of optical elements. In the area of Visual Optics, several techniques are routinely applied for testing contact lenses, intraocular lenses or ophthalmic lenses.

1.6.1 Lensmeters

These instruments are normally used to measure spherical, cylindrical and prismatic powers in ophthalmic lenses. Several studies [Sheedy *et al.* 1987, Diepes and Tameling 1988] has been undertaken to evaluate PPLs using this kind of apparatus.

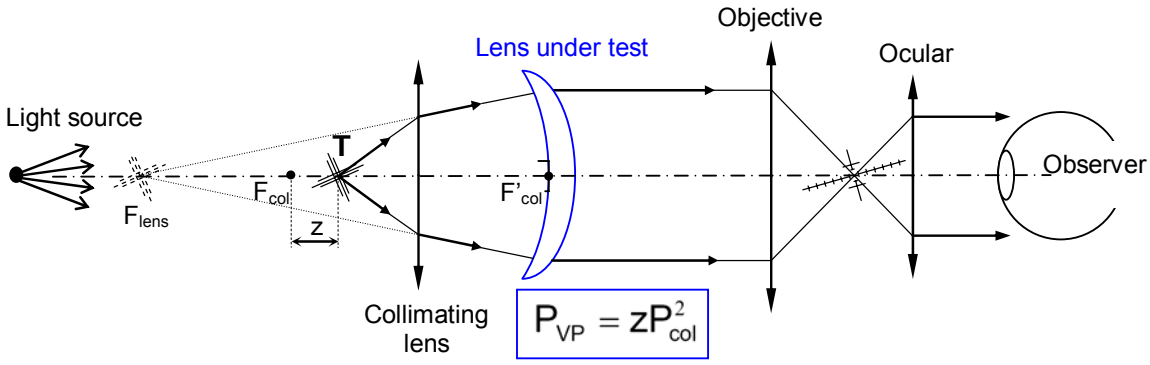

Figure 17. A schematic diagram of a lensmeter measring a positive ophthalmic lens. F_{lens} is the object focal point of lens under test, F_{col} amd F'_{col} are the object and image focal points of the collimating lens respectively, T is the target, z is the displacement of the target, P_{col} is the power of the collimating lens and P_{vp} is the posterior vertex power of the lens under test.

Figure 17 shows a schematic diagram of a manual lensmeter. The posterior surface of ophthalmic lens under test is placed at the image focal point of the collimating lens (CL). The

target (typically a crossed sets of lines) is moved from the object focal point of the CL up to get its image through the CL at the object focal point of the tested lens. So, a collimated beam arrives to the objective lens, and the observer sees sharply the target. Ocular lens allows to correct the spherical refractive error of the observer. The power, measured from the posterior vertex, of the lens under test is calculated as the product between displacement (z) of the target and the square power of the CL. Conventional lensmeters has a typical accuracy of 0.125 D.

1.6.2 Interferometers

There are many types of interferometers which could be used to test optical elements. In particular, shearing interferometers are widely used for many applications [Leibbrandt *et al.* 1996, Harbers *et al.* 1996] such as the testing of ophthalmic lenses [Wyant and Smith 1975]. In this method, the initial wavefront is duplicated and displaced laterally by a small amount (figure 18). The interference between the original and the displaced wavefronts gives the interferogram. The shape of the wavefront aberration can be determined from the lateral shearing interferogram [Malacara 1992]. The precision of this instrument can be controlled by varying the amount of shear. Figure 18 shows a lateral shearing interferometer used to measure monofocal ophthalmic lenses [Wyant and Smith 1975] and examples of interference patterns for different pure wavefront aberrations [Malacara 1992]. In the interferometer shown in figure 18, the collimated beam is duplicated using a plane parallel glass plate where part of the beam is reflected from the front surface and part of it is reflected from the back surface. In the interferograms, we can see the both beams for circular aperture and the fringes appear only in the area of overlap of the two wavefronts.

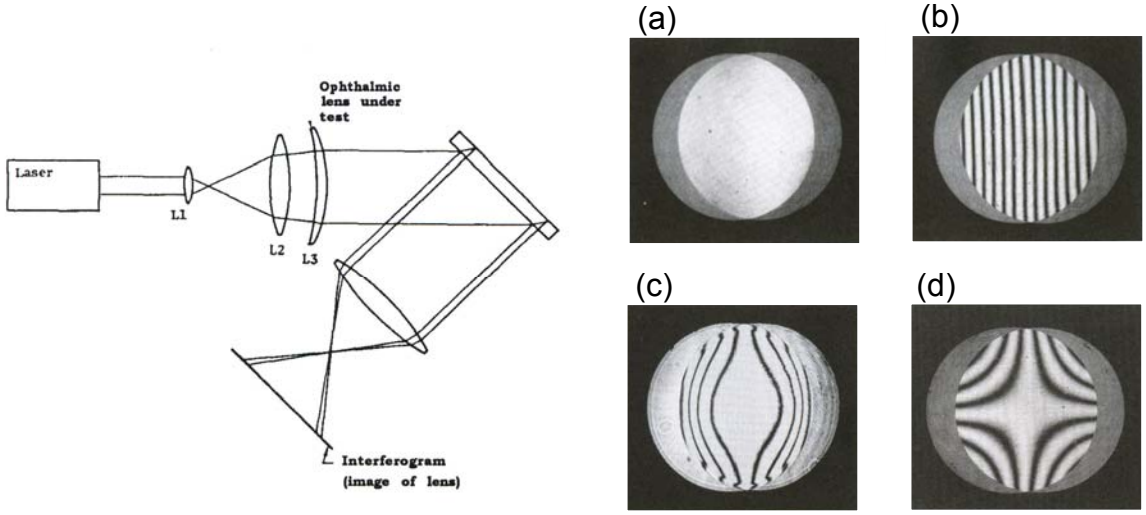

Figure 18. Lateral shearing interferometer for measuring ophthalmic lenses *[Wyant and Smith 1975]*, and interferograms for: (a) flat wavefront, (b) defocus, (c) spherical aberration and (d) coma with shear direction in horizontal axis *[Malacara 1992]*.

[Acosta *et al.* 2006] built a modified point diffraction interferometer (PDI) to test ophthalmic lenses which allows to obtain interferograms of large areas of progressive lenses (see figure 19). The PDI is a two-beam interferometer in which a spherical reference beam is generated by a small pinhole that is located in a semitransparent coating. As shown in figure 19, the wavefront coming from the lens under test passes through the semitransparent coating and interferes with the reference wavefront.

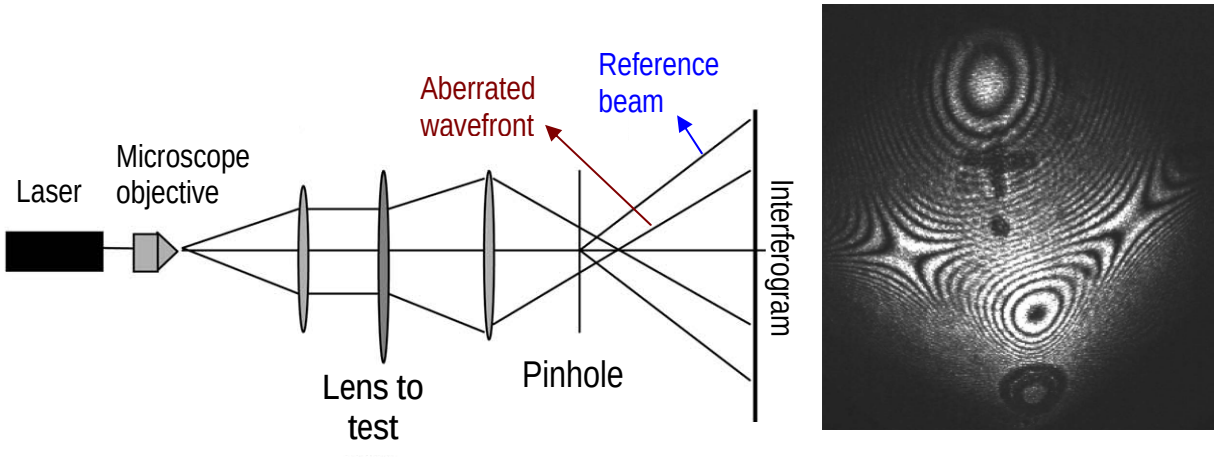

Figure 19. Experimental setup of a PDI used to measure ophthalmic lenses. In the interferogram of a PPL, we can see the change of sign in defocus from the upper part (far zone) to lower part (near zone) and the changes due to astigmatism near the progressive corridor *[Acosta et al. 2006]*

1.6.3 Ronchi tests

In 1923, the Italian physicist Ronchi describes at the first time this type of test to evaluate the aberrations of mirrors. It consisted of a ruling placed near to the center of curvature of the mirror and the image of the grating was superimposed on the grating itself. It produced fringes patterns which depended on aberrations of the mirror [Malacara 1992].

A variation of this technique allows to measure other optical systems, such as intraocular lenses. A diffraction grating is placed near to the image focal point of the lens under test producing interferograms fringes on a screen. This method permits to measure the power of the monofocal and bifocal intraocular lenses with high precision, less than 0.1 D [González *et al.* 1997], and also high order aberrations. To measure the spherical aberration [Carretero *et al.* 1992], the most predominant in intraocular lenses, the diffraction grating is moved slowly up to get a “fusiform” pattern with a very broad central fringe, as is presented in figure 20. In this position, the paraxial defocus is zero and the spherical

aberration is calculated from the direct relation between wavefront aberration and the interferogram.

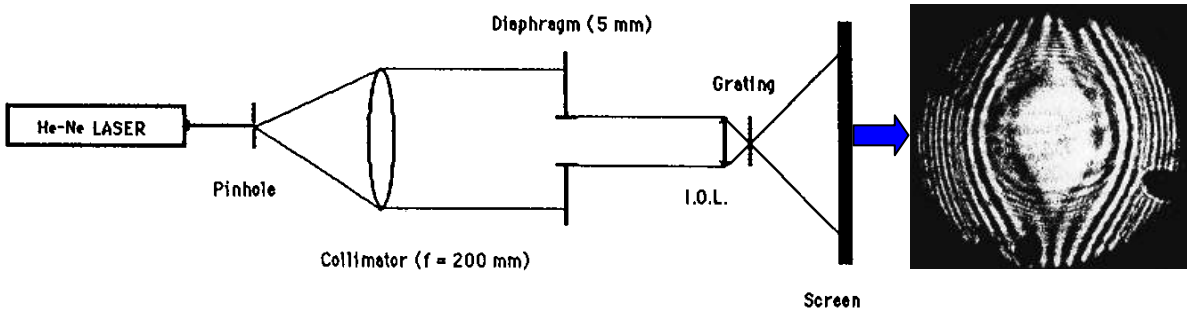

Figure 20. An experimental setup of the Ronchi test using a diffraction grating to measure the spherical aberration of intraocular lenses (IOL), and Ronchi interferogram with spherical aberration in absence of defocusing *[Carretero et al. 1992]*

1.6.4 Moiré deflectometry

In this kind of systems, the wavefront coming from the element under test passes through two gratings forming a moiré pattern. This technique can be used to measure both optical elements in transmission and ophthalmic surfaces in reflection [Rottenkolber and Podbielska 1996]. Figure 21 shows a setup of a moiré deflectometer which is prepared to measure the corneal topography [Mejía-Barbosa and Malacara-Hernández 2001]. In this case, the lens L_1 focuses the collimated beam nearly on the centre of the corneal surface. If the wavefront coming from cornea is not flat, after passing through the first grating (G1), a distorted image of the grating is superimposed on the second grating (G2), producing a moiré pattern that is projected on the CCD camera with the lens L_2. The pattern gives information about ray deflections that is used to calculate the slopes of the tested surface in the direction perpendicular to the grating lines. But these calculations only allow to obtain the wavefront aberrations in one direction. To obtain the complete wavefront aberration, it is necessary to measure the ray deflections in two orthogonal directions. The accuracy of the measurements depends on the distance between the gratings (d) and on the spatial frequency (1/p) of the gratings.

To measure ophthalmic lenses, the initial collimated beam is replaced by a laser point source. This is placed perpendicular to the lens surfaces and the axial position varies depending on the power of the lens. The wavefront coming from the lens pass through the two gratings and form a moiré pattern on a diffusive screen. A commercial instrument (Rotlex Class Plus lens analyzer) based in this technique measures local spherical and

cylindrical powers with high accuracy [Sheedy *et al.* 2005]. In figure 22, we show an example of the isopower and isocylinder maps of a progressive lens given by this instrument.

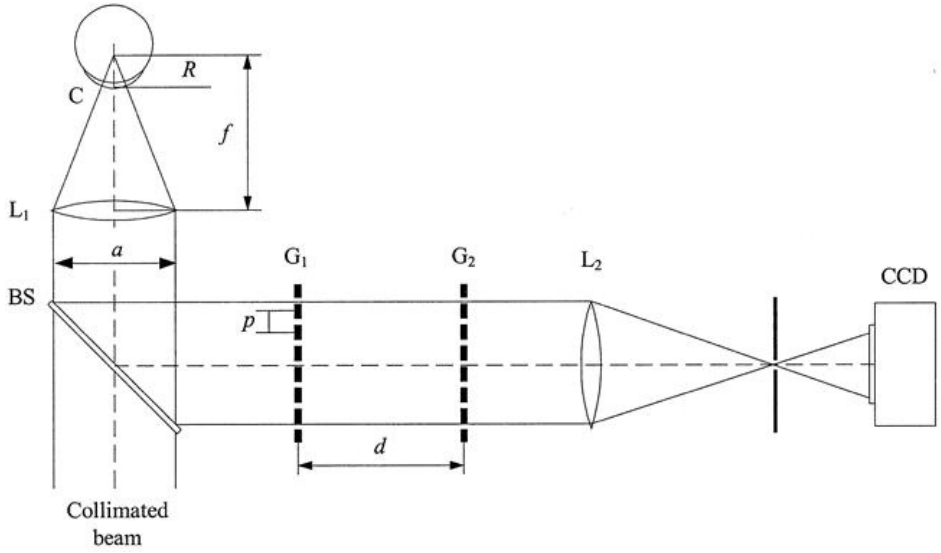

Figure 21. Basic morié deflectometer setup for measuring ophthalmic surfaces. BS is a beam splitter, C is the surface under test (in this case the cornea), R is the curvature radius, G_1 and G_2 are the gratings, p is the grating pitch, d is the distance between gratings, L_1 and L_2 are lenses to focus the beams *[Mejía-Barbosa and Malacara-Hernández 2001]*

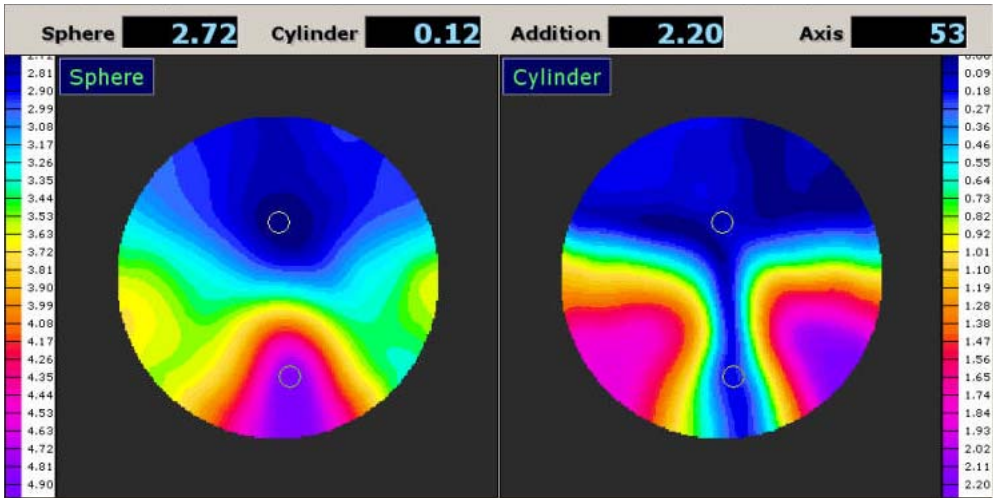

Figure 22. Examples of isopower and isocylinder maps of a PPL given by the Rotlex Class Plus lens analyzer. This instrument is based in moiré deflectometry. Note the high precision in contours maps of 0.09 D (*Image published in the web site: www.rotlex.com/class.asp)*

The experimental ray tracing is other method to measure the ray deflections. It consists of obtaining the deflection of a narrow laser beam refracted by a lens, measuring

the positions of the incident and refracted beam. The accuracy of this technique is better when the ray positions are measured at two planes behind the lens [Canabal *et al.* 2001].

1.7 HARTMANN-SHACK (HS) WAVEFRONT SENSOR

Over the last few decades, researchers have measured the ocular optical quality using several methods. In 1619, C. Scheiner devised the first optometer for measuring refractive errors of the eye [Thibos 2000]. The Scheiner Disk was an opaque disk with two pinholes. If an optically imperfect eye views through it, two images of a single point are formed on the retina. When defocus is the only optical imperfection, a simple lens will be able to bring the two retinal images into coincidence. [Smirnov 1961] was the first to measure the wave aberration of the human eye. He measured the ocular wave aberration from subjective measurement of the lateral aberration over the entire area of the entry pupil. [Howland and Howland 1977] designed a subjective method consisting of relating the ocular image of a grid through a crossed cylinder lens to the wave aberration of the eye. [Walsh *et al.* 1984] modified this method by the addition of a beam splitter and a camera to permit objective recording of the distorted retinal image of the grid. The retinal image quality has been also measured using double-pass systems [Santamaría *et al.* 1987, Artal *et al.* 1995(a), Guirao *et al.* 1999, Villegas *et al.* 2002]. [Iglesias *et al.* 1998] estimated the ocular aberrations using double-pass retinal images recorded at different pupil diameters. Some works [Porter *et al.* 2001, Castejón-Monchón *et al.* 2002] have reported on the wavefront aberrations (WAs) in a large population using a HS sensor. [Moreno-Barriuso *et al*. 2001] compared three different techniques to measure the ocular WAs: laser ray tracing, the spatially resolved refractometer and the HS sensor. In the other hand, the majority of current adaptive optics systems for the human eye use a HS sensor to measure the WAs [Liang *et al.* 1997, Fernández *et al.* 2001]. In some of these prototypes, the ocular aberrations are compensated by use of deformable mirrors [Liang *et al.* 1997, Fernández *et al.* 2001], technique also used in the telescopes to compensate the optical turbulence of the earth´s atmosphere.

In addition to testing the ophthalmic elements in optical bench, some studies have estimated the optical performance of contact lenses and IOLs with the eye (*in situ).* Eyes implanted with both monofocal and bifocal IOLs were measured with a double-pass system [Navarro *et al.* 1993, Artal *et al.* 1995(b)]. The image quality in eyes with contact lenses was also estimated by using a double pass apparatus [Artal *et al.* 1999] and a HS wavefront sensor [Hong *et al.* 2001].

In this thesis, the wavefront aberrations of progressive lenses, both isolated or in combination with eyes, will be measured using a home built system with a Hartmann-Shack sensor. So, in the following, we undertake an exhaustive revision of this technique.

1.7.1 Revision and description of HS sensor

In 1900s, an astrophysicist named J. Hartmann [Hartmann 1900, Hartmann 1904] used for the first time a metal disk perforated with regularly spaced holes [Malacara 1992] (figure 23) for measuring the rays aberrations of mirrors and lenses. This disk was placed over the optical element that was to be tested and the distribution of spots was analysed at the focus plane using a photographic plate. The aberrations could be determined by estimating the displacements of spots from their regularly spaced positions.

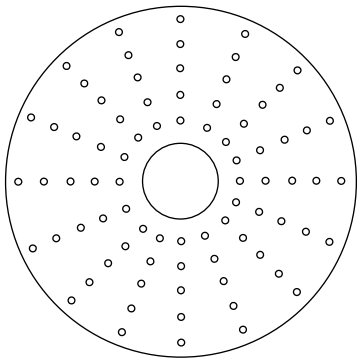

Figure 23. Classical Hartmann radial disk. *[Malacara 1992]*

In the late 1960s, US Air Force proposed to the Optical Sciences Center (OSC), at the University of Arizona, to improve the images of satellites taken from earth. Mienel, astronomer and director of the OSC, used the standard Hartmann test to calculate figures of merit for large telescopes. In order to measure the wavefront error, at the same time an image of the satellite was taken, Mienel collimated the beam and placed a plate with holes in the image of the pupil. However, this configuration produced a weak intensity of the spots and a lack of accuracy for placing the centroids of these blurry spots. These problems were involved by R. Shack [Shack and Platt 1971], who proposed to replace the holes of the plate by tiny lenses. So, it was the first configuration of a HS sensor [Platt and Shack 2001] (figure 24). However, in those years no one was able to fabricate the lenses required with a diameter of 1 mm and focal length of 100 to 150 mm. Platt decided that the only way to make the long focal lengths with 1 mm center-to-center distances was to use crossed cylindrical lenses. After many attempts, Platt got to fabricate good quality lens arrays of thermal plastic (Plexiglass). A complete system with a Hartmann-Shack sensor was delivered to the Air Forced to be used in satellite-tracking telescopes, but this system was never installed. In the early 1980s, all the large telescopes at the European Sothern Observatories (ESO) were tested and aligned by R. Wilson using a wavefront sensor with lens arrays sent by Shack. During the late 1970s, Adaptive Optics Associates (AOA) developed techniques to compensate the optical turbulence of earth´s atmosphere, using

the HS wavefront sensor to measure the atmosphere aberrations. Nowadays, many researchers use Hartmann-Shack sensors in their experiments.

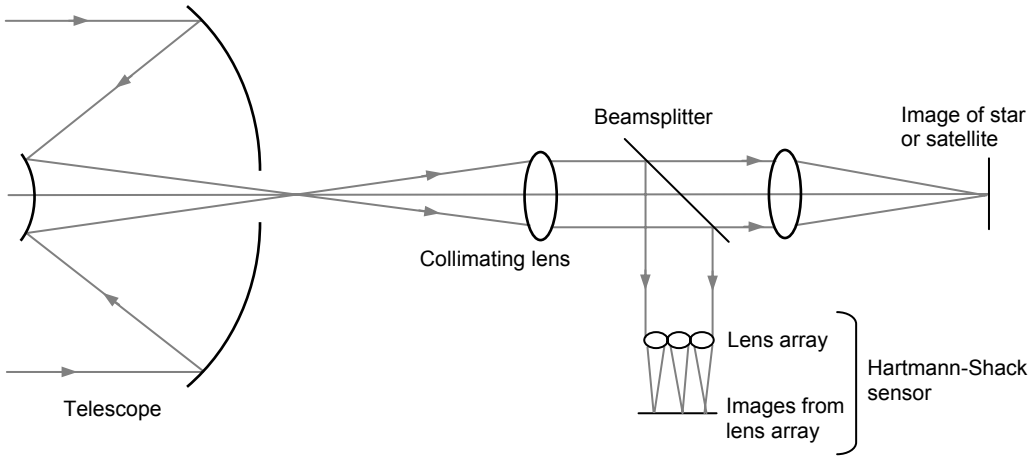

Figure 24. Schematic diagram of the first Hartmann-Shack sensor *[Platt and Shack 2001]*

Liang and collaborators [Liang *et al.* 1994] used for the first time a Hartmann-Shack sensor for measuring the wave aberrations of the eye. In this study they generated a point source on the retina and measured the aberrations of the wavefront emerging of the eye by using a HS sensor. Thus, the wave aberrations of the eye are expressed as the difference of the deformed wavefront and a plane wave in front of the eye at the same plane (figure 25a). These wave aberrations are equivalent to those in the image space of the eye defined as the differences between the real wavefront at the exit pupil of the eye and the spherical wavefront converging to a reference point on the retina (figure 25b). Liang´s aberrometer is shown in figure 26. This system is divided in two parts: illuminator arm and detector arm. The illuminator arm brings a focus point on the retina. Defocus errors of the tested eye is corrected by movement of the lens L1 with respect to lens L2. The subject has to view a fixation target T to stabilize the accommodation. The light coming from the retina passes through the ocular media in direction to Hartmann-Shack detector. In this configuration the WAs are measured at the pupil plane of the eye, since this plane and the lens array are conjugate. The wavefront was reconstructed by using Zernike polynomials. Nowadays, many researchers use this process to obtain the WAs of the eye, even several companies are selling Hartmann-Shack sensors commercially.

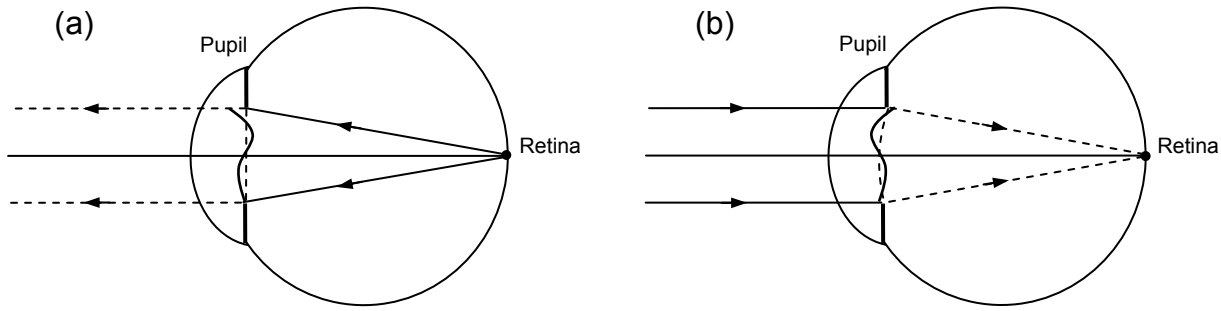

Figure 25. Definitions of the wavefront aberrations of the eye.
(a) In the object space. The solid curve is the real wavefront and the dashed lines represent the reference plane wave. (b) In the image space. The dashed lines are the reference sphere.

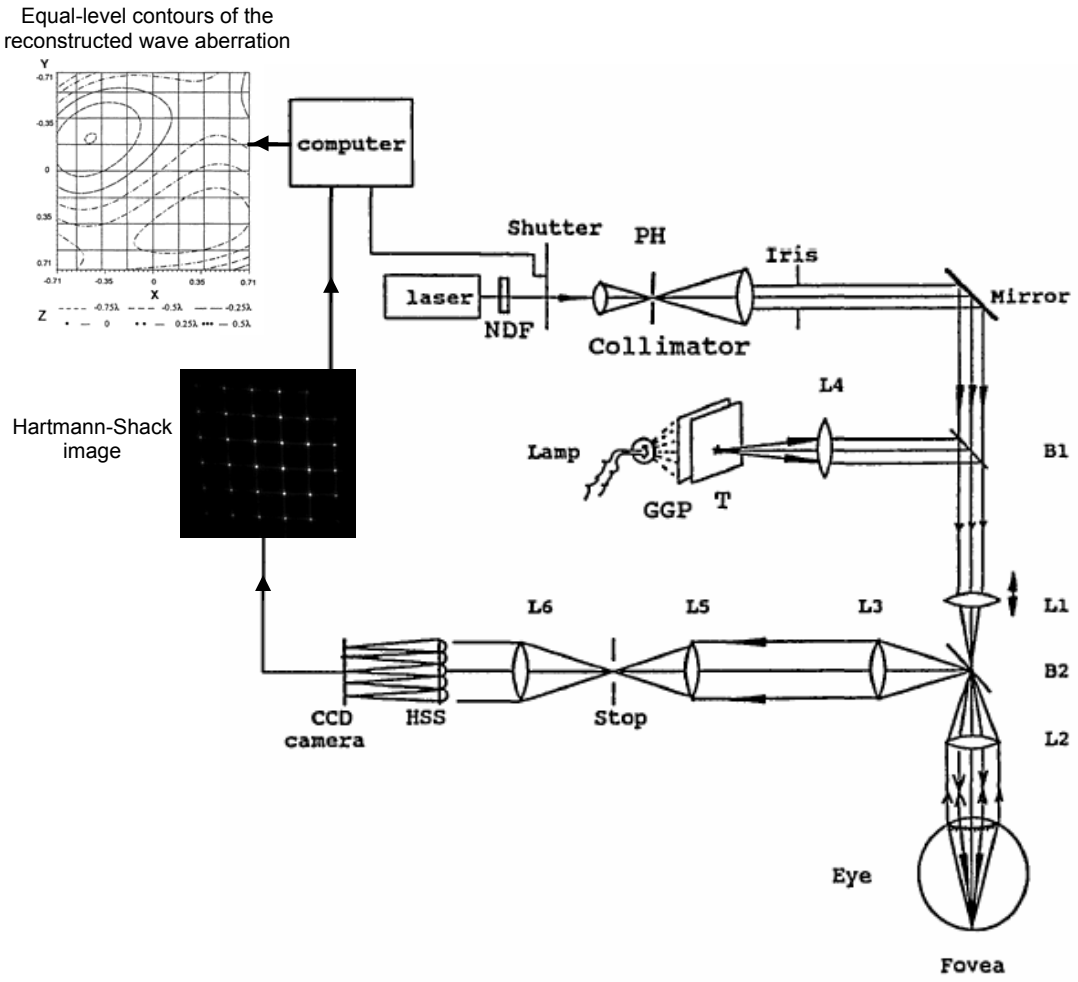

Figure 26. The first experimental system with a Hartmann-Shack sensor for measuring the wave aberrations of the eye. NDF, neutral density filter; B1 and B2, beam splitters; L1-L6, lenses; T, target; GGP, ground-glass plate; HSS, Hartmann-Shack sensor. *[Liang et al. 1994]*

The Hartmann test is also used to test lenses [Morales and Malacara 1983, Malacara and Malacara 1992]. In particular, [Castellini *et al.* 1994] proposed a modified version of the

Hartmann test to measure the spherical power, astigmatism and prismatic deviation of progressive power lenses. Castellini´s system is shown in figure 27. The lens was tested with a 2-mm laser beam diameter, in 280 points over nine concentric circles. Two angular movements of the lens, ϑ and α, permit to reproduce the real behavior of the eye.

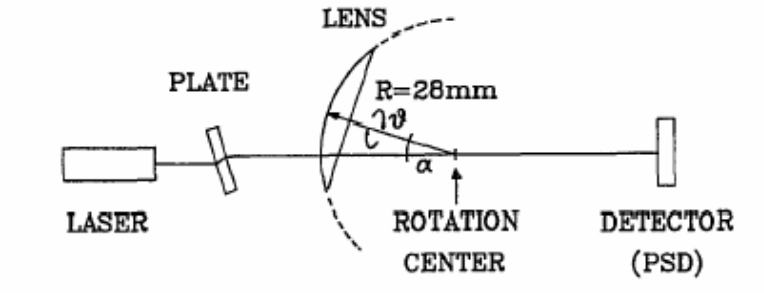

Figure 27. A modified version of the Hartmann test to measure the spherical power, astigmatism and prismatic deviation of progressive power lenses. *[Castellini et al. 1994]*

Nowadays, the company Nidek commercializes an instrument based in a Hartmann sensor that is used as a lensmeter of high accuracy and reliability [*http://www.nidek-intl.com/lensmetr.html*].

1.7.2 Processing of HS images

The principle of the Hartmann-Shack wavefront sensor is shown in figure 28. Each microlens produces an extended spot corresponding to the wavefront section it covers. For a flat wavefront, the HS image is a regular matrix of spots. When the wavefront is aberrated, the spot matrix is distorted. The displacement of each spot provides the local slope of the wavefront over the corresponding microlens.

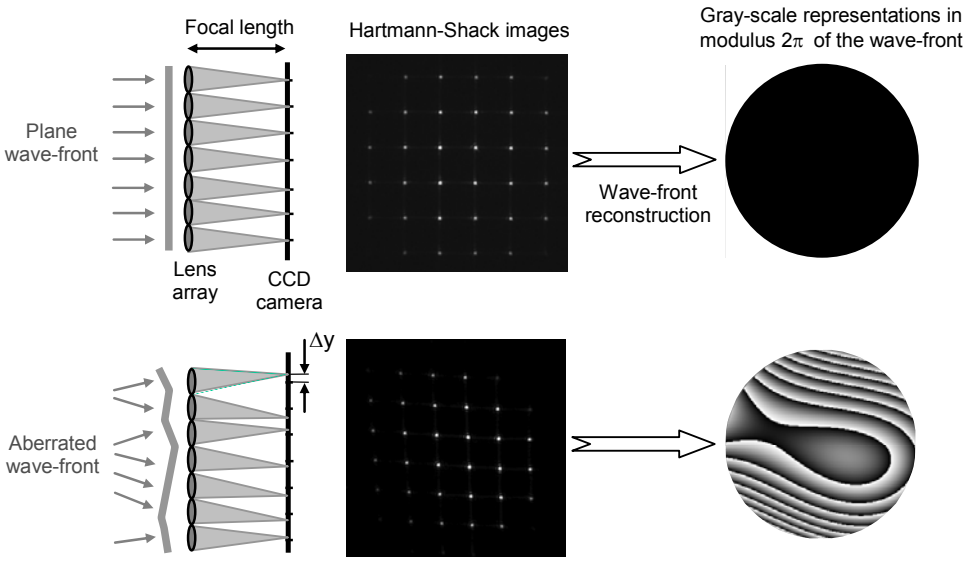

Figure 28. Wavefront aberration estimation from a Hartmann-Shack sensor.

In this thesis, the wavefront aberrations will be fitted to Zernike polynomials using the method described by [Prieto *et al.* 2000]. This process is implemented in a computer program. The strategy of the centre of gravity, or centroid, is used to position the extended spots. The centroid (X_i, Y_i) of the *i*th spot (or microlens) is defined as:

$$X_i = \frac{\int_{A_i} xI(x,y)dxdy}{\int_{A_i} I(x,y)dxdy} \qquad Y_i = \frac{\int_{A_i} yI(x,y)dxdy}{\int_{A_i} I(x,y)dxdy} \tag{10}$$

where A_i is the area associated with the *i*th microlens and I(x,y) is the image intensity. The displacement of the centroid (Δx_i, Δy_i) is proportional to the average of the wavefront derivative across the microlens:

$$\Delta x_i = \frac{f}{A}\int_{A_i} \frac{\partial WA(x,y)}{\partial x}dxdy \qquad \Delta y_i = \frac{f}{A}\int_{A_i} \frac{\partial WA(x,y)}{\partial y}dxdy \tag{11}$$

where f and A are the focal length and the area of the microlens respectively. The relations $\Delta x_i/f$ and $\Delta y_i/f$ are the wavefront slopes of the centroid in the x and y directions. The displacements (x_i, y_i) represent the spots shifts between the tested image and the reference image for the isolated system. Therefore, WA(x,y) is the wavefront aberration of the optical element (for example eye, ophthalmic lens...) measured in radians.

To reconstruct the WA from the averaged derivatives, the lineal combination of elements of a functional basis or modes is widely used. In particular, for circular pupils, the Zernike circle polynomials [Noll 1976] are commonly used. So, the WA can be expressed as:

$$WA(x,y) = \sum_{j}^{j_{max}} C_j Z_j(x,y) \tag{12}$$

with $Z_j(x,y)$ being the *j*th mode (i.e. Zernike polynomial), C_j is its coefficient and j_{max} is the expansion truncation mode. If partial derivatives of Eq. (12) are integrated across each microlens area, substituting in Eq. (11), we obtain the relationship between centroids displacements and Zernike polynomials:

$$\Delta x_i = \frac{f}{A}\sum_{j}^{j_{max}} C_j \int_{A_i} \frac{\partial Z_j(x,y)}{\partial x}dxdy \qquad \Delta y_i = \frac{f}{A}\sum_{j}^{j_{max}} C_j \int_{A_i} \frac{\partial Z_j(x,y)}{\partial y}dxdy \tag{13}$$

We have two systems of N equations, being N the number of spots. These two systems can be mixed and expressed in matrix notation as:

$$\Delta = M \cdot C \tag{14}$$

where Δ and c are 2N column vectors. Δ includes the spot displacements in the x and y direction, and c represents the unknown coefficients. M is the $j_{max} \times 2N$ matrix of partial derivatives of the polynomials averaged across each microlens.

$$\Delta = \begin{vmatrix} \Delta x_1 \\ \vdots \\ \Delta x_{i_{max}} \\ \Delta y_1 \\ \vdots \\ \Delta y_{i_{max}} \end{vmatrix} \qquad C = \begin{vmatrix} C_1 \\ \vdots \\ C_{j_{max}} \end{vmatrix} \qquad M = \frac{f}{A} \begin{vmatrix} \int_{A_1} \frac{\partial Z_1(x,y)}{\partial x} dxdy & \cdots & \int_{A_1} \frac{\partial Z_{j_{max}}(x,y)}{\partial x} dxdy \\ \vdots & \ddots & \\ \int_{A_{i_{max}}} \frac{\partial Z_1(x,y)}{\partial x} dxdy & & \int_{A_{i_{max}}} \frac{\partial Z_{j_{max}}(x,y)}{\partial x} dxdy \\ \int_{A_1} \frac{\partial Z_1(x,y)}{\partial y} dxdy & \cdots & \int_{A_1} \frac{\partial Z_{j_{max}}(x,y)}{\partial y} dxdy \\ \vdots & \ddots & \\ \int_{A_{i_{max}}} \frac{\partial Z_1(x,y)}{\partial y} dxdy & \cdots & \int_{A_{i_{max}}} \frac{\partial Z_{j_{max}}(x,y)}{\partial y} dxdy \end{vmatrix} \tag{15}$$

Since the number of microlenses is usually higher than the Zernike modes, the system is redundant. The system is solved by estimating the inverse matrix M^{-1}, and the Zernike coefficients are obtained as least-squares values.

1.8 PSYCHOPHYSICAL ASSESSMENT

Although there are different ways for measuring the visual performance of the human eye, testings of contrast sensitivity and visual acuity (VA) are widely used. VA is defined as the smallest spatial detail that the subject can resolve [Elliot *et al.* 1995]. Different tests [Grosvernor 2002, Keeney *et al.* 1995] have been proposed for measuring the minimum detail that the eye can discriminate. The most commonly used optotypes are Landolt C (broken ring) and the letters charts. The Landolt C, introduced in 1888 by Parisian opthalmologist Edmond Landolt, is a ring with a gap which is presented in different directions. In 1862, the Utrecht ophthalmologist Herman Snellen designed the universal letters chart for measuring VA. Figure 29 shows an example of this type of visual acuity test. In 1976, the Australian optometrists I.L. Bailey and J.E. Lovie introduced a letters chart

based on the Snellen test, but with equal numbers of letters on each line and the letters size varies in a regular progression of 0.1 log MAR (logarithm of minimum angle of resolution) from line to line. The “tumbling E” is also widely used to measure the MAR. It consists in presenting a capital “E” in different directions and the person being tested should determine which direction the “E” was pointing. The width of the strokes and the gaps are one fifth of the height of the optotype character.

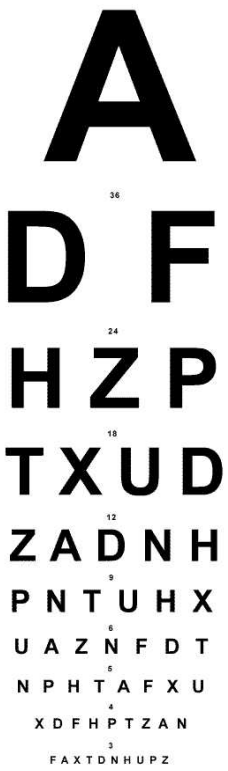

Figure 29. Snellen letters chart. Although this figure is reduced respect to the original size, the numbers between lines correspond to the viewing distances for which the letters subtend 5-min. angle (i.e. the minimum detail subtends 1-min. angle).

In the last decades, psychophysical assessments of the performance of progressive-power lenses have been undertaken in different ways. Grating VA is not significantly deteriorated when looking through low eccentricities [Sullivan and Fowler 1989(b)]. For typical intermediate office tasks, this kind of lenses provides marginally diminished performance compared with single-vision lenses [Selenow *et al.* 2002]. Clinical surveys of patient acceptance [Kris 1999, Boroyan *et al.* 1995, Sullivan and Fowler 1989(a)] show a small percentage of progressive-lenses wearers (around 10-15%) with adaptation problems, that could be produced by different factors: distortion, the need of head movements, defocus errors, astigmatism or perhaps high order aberrations. Some researchers [Fauquier *et al.* 1995, Sullivan and Fowler 1988] have evaluated the amount of astigmatism that is tolerated by patients wearing PPL´s. In relation to defocus tolerance, visual performance for different values of defocus [Legge *et al.* 1987, Campbell and Green 1965, Woods *et al.* 1996, Charman and Jennings 1976, Miller *et al.* 1997, Sullivan and Fowler 1988, Villegas *et al.* 2002] and depth of focus [Campbell 1957, Tucker and Charman 1975, Atchison *et al.* 1997, Marcos *et al.* 1999] in the eye have been widely studied.

In order to predict visual performance, some optical parameters (for example the radius of 84% encircled energy of the point-spread function or the integral of the modulation transfer function across the frequency range of interest) have been proposed for assessing the image quality of visual instruments, such as telescopes, but only for small sizes of pupil [Mouroulis and Zhang 1992]. Other metrics calculated from double-pass retinal images have been relatively well correlated with VA and CSF measurements for different amounts of defocus [Villegas *et al.* 2002]. Recently, the VA using computationally-aberrated letters have

been correlated with a great number of optical metrics derived from wavefront aberration assigned to the letters [Marsack 2004].

Chapter 2

JUSTIFICATION AND OBJECTIVES

2.1 JUSTIFICATION

Although, both theoretical [Minkwitz 1963, Bourdoncle et al. 1992] and empirical results [Fowler and Sullivan 1989, Spiers and Hull 2000, Castellini *et al.* 1994] have well documented the presence of astigmatism in PPLs, little is known about the high order aberrations of these lenses. Some previous studies [Jalie 1994, Burns 1995, Maitenaz 1967, Bourdoncle *et al.* 1992] concentrated in the theoretical shape and size of the image of a point through a progressive spherical power surface, but as far as we known there are no experimental results on the aberrations at different locations of PPLs.

The retinal image quality of an eye wearing an ophthalmic lens depends on both the ocular quality and the lens quality. However, the above-described techniques used to evaluate ophthalmic lenses (lensmeters, interferometry, Ronchi test and deflectometry) usually estimate the optical quality of the isolated lenses without taking into account the optical performance of the human eye or the combination of the lenses with the eye.

In the process of designing a PPL, it is very advantageous to be able to predict the visual performance from the optical parameters. Thus, the designers can a priori know what will be the level of acceptance and satisfaction of the future users of the PPL. The reduction of visual performance due to astigmatism and defocus errors in PPLs has been widely studied in different studies. But, the visual impact of high order aberrations of this kind of lenses and the effect of the combination with the ocular aberrations is not still well known.

Just after dispensing PPLs, the optometrist informs patients on the adaptation process to his new lenses. But, what does adaptation period consist of? It has been demonstrated the adaptation to the distortion aberration [O'Leary and McMahon 1991, Wendy *et al.* 2001], however there is not documented information on the possible adaptation of the visual system to the deterioration of the foveal vision due to the aberrations of PPLs. In relation to this topic, previous works have reported the adaptation of the eye to its particular aberrations [Artal *et al.* 2004].

There are many PPLs available in the market, but little information on their optical characteristics. Although, as mentioned above, different optical methods have been proposed for designing and evaluating PPLs, there is a significant lack of studies presenting objective measurements on different designs of PPLs.

2.2 OBJECTIVES

- In this context, the first objective of this thesis is to measure the spatially resolved aberrations in PPLs. In order to do it, we will design and build a system with a HS wavefront sensor, where the lenses will be measured in different zones simulating real directions of sight.

- The nature of the aberration coupling between the PPL and the eye will be also studied. The ocular aberrations should be measured with the same system used to evaluate PPLs.

- In order to evaluate the retinal image quality of older eyes with progressive lenses, we will compare PPLs aberrations with those of presbyopic eyes.

- Another important point in this thesis is to know the impact of aberrations of PPLs on VA for different viewing conditions. To control the positions of the eye respect the different zones of the PPL, the VA measurements should be taken with the same system used to measure the wavefront aberrations.

- In this study, we will try to find the optical parameter that better predicts the visual quality. These results could be useful in the process of design of PPLs in which a previous knowledge of the relation between optical parameters and final visual performance is fundamental to get a successful prototype.

- In order to study the possible adaptation of the foveal vision to the optical aberrations of the PPLs, we will measure VA through relevant controlled zones of PPLs during the first week wearing this type of lenses.

- Another goal of the present thesis is to evaluate the optical quality of different PPL designs currently commercialized. So, we could evaluate the differences between the lenses offered by the companies.

Chapter 3

METHODS

3.1 EXPERIMENTAL SYSTEM

In this thesis, an experimental system with a Hartmann-Shack wavefront sensor has been designed and built to perform spatially resolved aberration measurements in ophthalmic lenses, in particular in PPLs, either isolated or in combination with the eye.

This apparatus has several advantages over previous existing techniques. For instance, the conventional lensmeters only allow measuring spherical power and astigmatism, while our system also measures high order aberrations, and resembling real viewing conditions. In contrast to lensometers and other typical methods of optical bench such as interferometry, Ronchi test or Moiré deflectometry, our technique allows to measure the lens and eye aberrations under the same optical conditions, and to predict easily the final optical quality of the entire system eye with lens for any viewing position.

3.1.1 Description of the system

A schematic view of the apparatus used is shown in the figure 30, and a picture of the system measuring a subject in the figure 31.

Illumination arm

The measurements are obtained using monochromatic green light (543 nm) from a He-Ne laser. This enable comparison with later psychophysical measurements performed also in visible (green) light.

The beam first passes through a linear polarizer (pol) and a neutral density filter (NDF) to control the intensity of light. A spatial filter (M&PH), consisting of a 20x microscope objective and a 10-μm pinhole, creates a point source. The emerging beam is collimated by lens C. A revolver of circular apertures (P1) controls the beam size. Using a removable mirror (m3) the system can measure either only the ophthalmic lens (OL) or the eye, with or without the OL. To measure only OLs, one more removable mirror (m4) directs the beam to the posterior surface of the lens. The size of aperture P1 limits the maximum size of the OL on which the wave aberration can be measured.

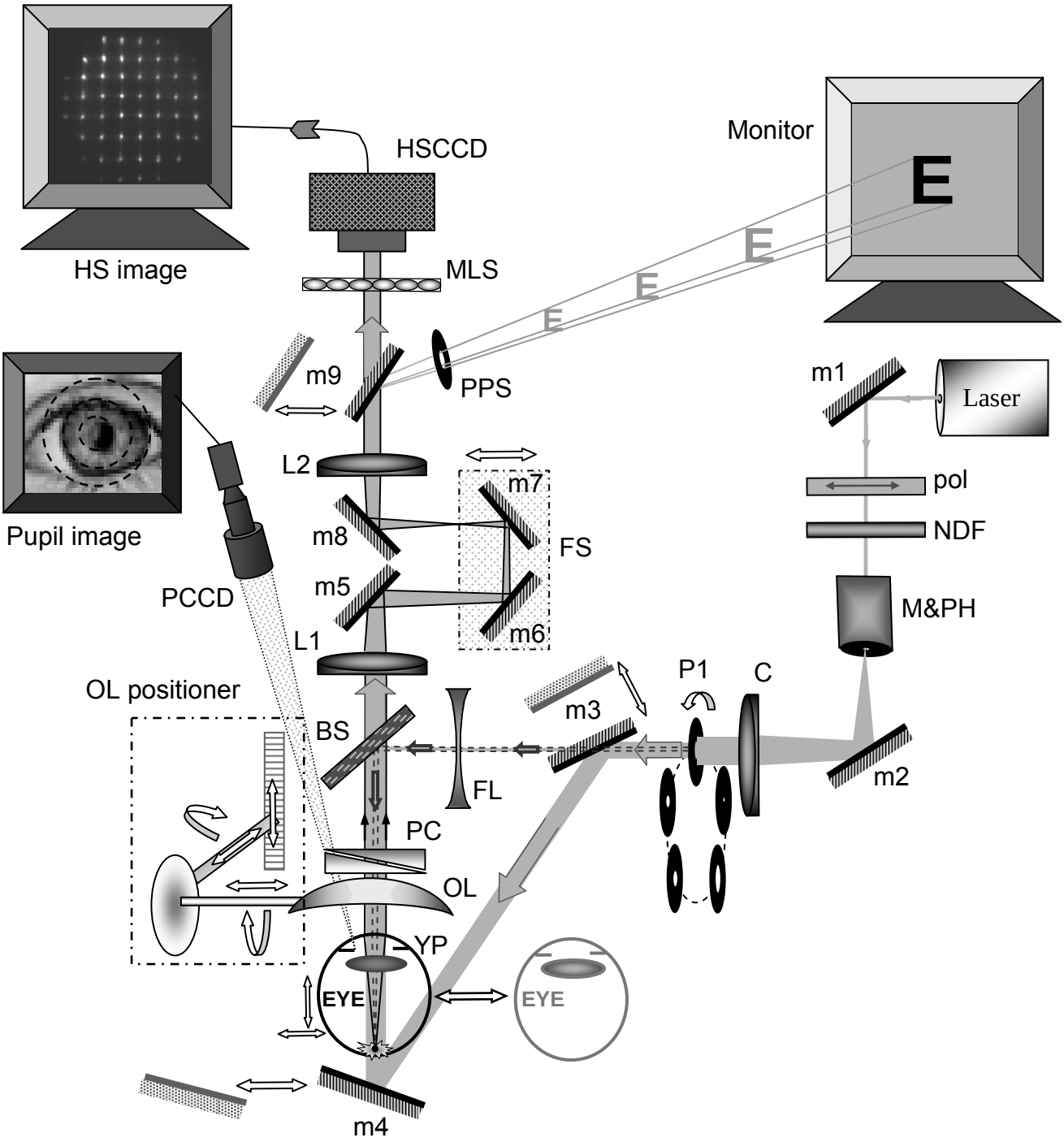

Figure 30. Experimental setup. Pol, lineal polarizer; NDF, variable neutral density filters; M&PH, microscope objective and pinhole; C, collimator achromatic lens; P1, aperture; OL, ophthalmic lens (in our particular experiment, this is a PPL); YP, eye pupil; PC, prism compensator; FL, focus lens; BS, beam splitter; FS, focus corrector system; L1, L2, achromatic lenses; m1-m9, mirrors; MLS, microlenses; PCCD, CCD for pupil centering; HSCCD, CCD to capture HS images; PPS, pupil for psychophysical measurements.

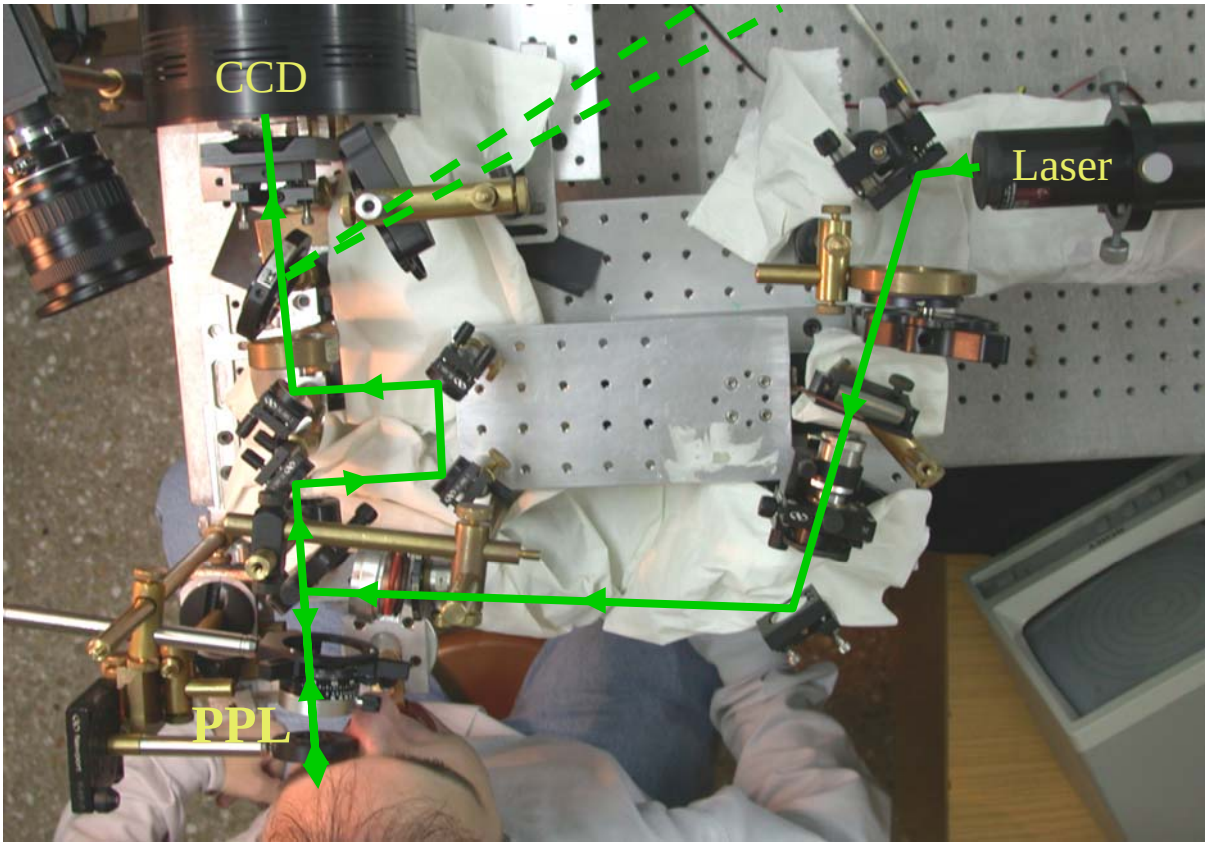

Figure 31. Picture of the experimental set-up.

In order to measure the ocular WA, a point-like source is formed on the retina. A narrow beam is produced by a 1.5-mm aperture (P1). Lens FL corrects the focus errors of the eye (with or without OL). A pellicle beam splitter (BS) reflects the light toward the eye. The exposure level at the cornea was always lower than 50 nW for a 3-s exposure. This corresponds to approximately 3 nW/cm^2 for a 1.5-mm diameter incoming beam, more than one order of magnitude below the limit set by safety standards [ANSI 1993]. Using a bite-bar attached to a three-axis micropositioner minimizes head movements. A CCD video camera (PCCD) monitors the axial position and the centration of the natural pupil with respect to the measuring beam. The light coming from the retina passes through the ocular media and OL in direction to lens L1.

Detection arm

A removable prism compensator (PC) is placed as near the lens as possible, if a large prismatic power is induced by the tested zone of the OL. This allows the beam to stay aligned through our system avoiding extra aberrations by oblique incidence on the lenses.

A focus corrector system is used to remove, or to change, the defocus of the OL, the eye or both combined. This allows measurement even in cases of large amounts of defocus.

The arrangement consists of two achromatic doublets, L1 (148-mm focal length) and L2 (100-mm focal length), and two mirrors mounted on a moving stage (FS) that increase or decrease the optical path between L1 and L2. As is shown in figure 32a, the refraction change (Rx) is the quotient between the displacement of the FS (distance d) and the square of the focal of the lens L1. The FS is moving towards and away from the mirrors m5 and m8 to compensate myopic and hypermetropic errors respectively.

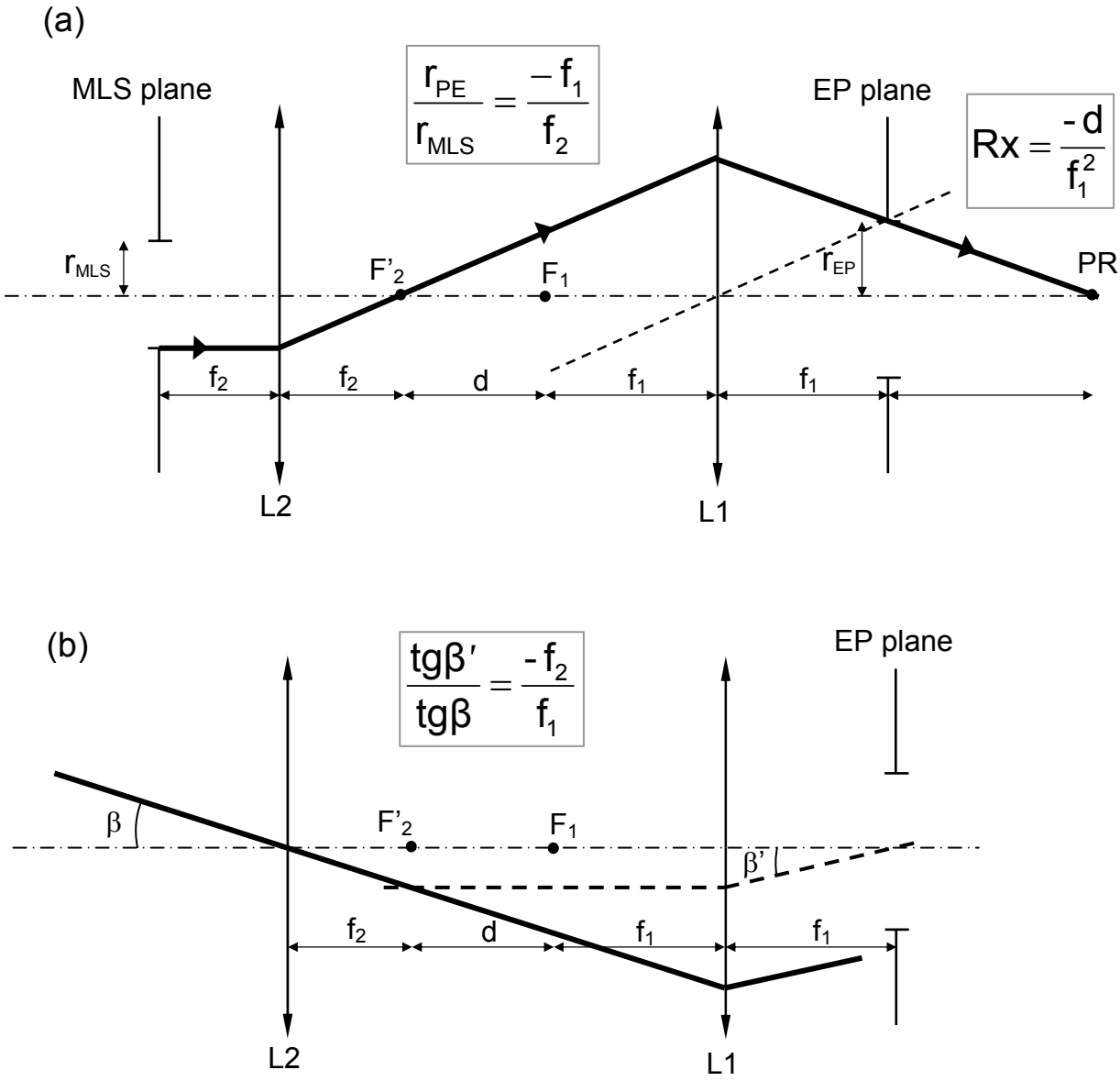

Figure 32. Variations of (a) defocus and pupil size, and (b) field of view, through the focus corrector system. f_1 and f_2

Finally, the beam coming from L2 is sampled by the microlens array (MLS). These microlenses have a square geometry, a 40-mm focal length, and a single microlens aperture

of 0.6 mm. The camera used was a cooled CCD camera (HSCCD) placed at the focus location of the MLS records the HS images. The camera is connected to the PC's parallel port with a parallel interface port (DB25). It is a CompuScope CCD800 Integrating Camera with a CCD size of 768x512 pixels, square pixels of 9x9μm and a quantum efficiency of 40% at 543 nm.

The MLS are placed at one focal distance of lens L2. The entrance pupil (EP) of the tested system must be placed at the focus of the lens L1 to be conjugated with the MLS plane. Thus, the wavefront aberration estimated in the MLS plane corresponds to that in the pupil plane. In this way, the OL is placed at this point to be measured it isolated. In the case of the direct measurements of the eye plus the OL, the entrance pupil of the entire system in real conditions is placed at the focus of L1.

Psychophysical channel

By means of a removable mirror (m9), the monitor used to perform psychophysical measurements is seen through the same optical path as that used for HS measurements. An artificial aperture (PPS) is used to choice the pupil diameter size in the eye pupil plane.

The focus corrector acts as a telescopic system, which in the variations in the sizes of the pupil (figure 32a) and the field of view (figure 32b) depend on quotient between focal lengths of the lenses. In our configuration, the diameter of entrance pupil (EP) of the tested system is magnified a factor of 1.48 with respect to the MLS plane. The smaller lateral dimension of the CCD camera (512 pixels) limits the maximum diameter of the pupil to 4.6 mm at the MLS plane, that corresponds to 6.8 mm of the EP. In the same way, in the psychophysical measurements, the system reduces the field of view in a factor of 0.68, which is taken into account in the size of the letters used to measure the VA.

3.1.2 Simulation of normal viewing conditions

To design any ophthalmic lens, it is essential to know the position of the lens in relation to the human eye. In our experiments, the values of the distances and the tilts of the lens with respect the eye are those that are considered commonly in designing of progressive lenses. The distance between the back vertex of the PPL and the centre of rotation of the eye is considered to be 27 mm. The vertex distance between the back vertex of the progressive lens and the cornea is 13 mm in primary position. In other sight directions, this distance changes and it is considered in the displacements of the lens.

When the isolated lens is measured, the tested zone size (TZ, figure 33) is selected with the revolver of apertures (P1, figure 30). However, in natural viewing conditions, the aperture is the natural pupil of the eye (NP), which coincides approximately with the entrance pupil of the naked eye. It is placed around 3 mm back the anterior vertex of cornea. For the entire system eye with lens, the entrance pupil (EP) is approximately the object of the natural pupil through the progressive lens. Figure 33 shows the position and size of the entrance pupil of the entire system, and its relation with the tested zone of the lens. In our experiments, we use progressive lenses with plano distance power and 2 D power addition. Thus, the maximum power of the lens (P_{OL}) will be 2 D. For this value the entrance pupil of the system is placed only 0.53 mm (s=16.53 mm) from the natural pupil, and its diameter (ϕ_{EP}) is a factor of 1.033 (3.3%) larger. Furthermore, for the nearest object distance in normal viewing conditions (a=250 mm), the entrance pupil is only a factor of 1.064 (6.4 %) larger than the tested zone of the lens. For these reasons, we consider the EP of the entire system at the same place that the natural pupil, and its size equals to the tested zone size (TZ) of the lens.

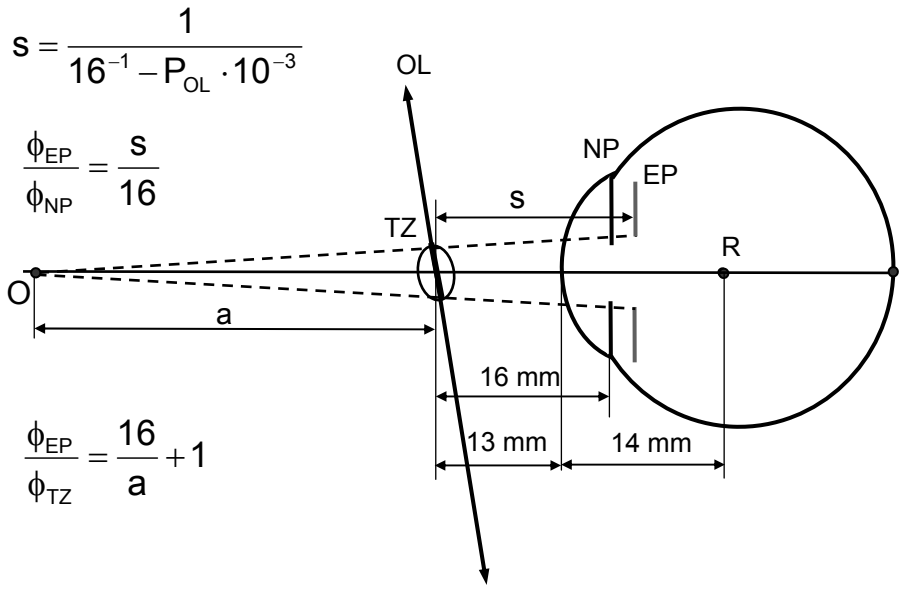

Figure 33. Position of entrance pupil, EP, of the entire system eye plus lens; and its diameter, ϕ_{EP}, in relation to that of the natural pupil of the eye, ϕ_{NP}. The ratio of EP diameter to tested zone size, ϕ_{TZ}, of the ophthalmic lens as function of object distance "a" is also shown. R, centre of rotation of the eye; s, distance between OL and EP; P_{OL}, power of the ophthalmic lens in diopters. All distances in mm.

The visual axis of the eye is the line from the point of fixation to the fovea, passing through the nodal points of the eye. Supposing this axis passes through the rotation centre of the eye is a good approach, and it makes easy to study the ophthalmic lenses in front of the eye. The visual axis pass through the different zones of the progressive lens depending

on the viewing distances and the lateral eccentricity of the fixation point. As it is logical, in the experimental setup, the optical bench can not be tilted to follow the eye rotations. To reproduce the actual behavior of the eye, the ophthalmic lens is displaced in the three directions and tilted around horizontal and vertical axes by means of a positioner system (shown in figure 30). The combination of these movements and rotations permits us to explore different zones of the lens.

In practice, spectacle lenses are tilted with respect to the vertical plane. This ensures that the eye sees through the lens when looking downwards. This tilt is called pantoscopic tilt [Tunnacliffe 1995]. To estimate the displacements and the tilts, the pantoscopic tilt (τ) is assumed as 12º. Figure 34 shows an example on how the eye looks through a zone of the lens to a near object in real conditions, and how this is simulated in our measuring system.

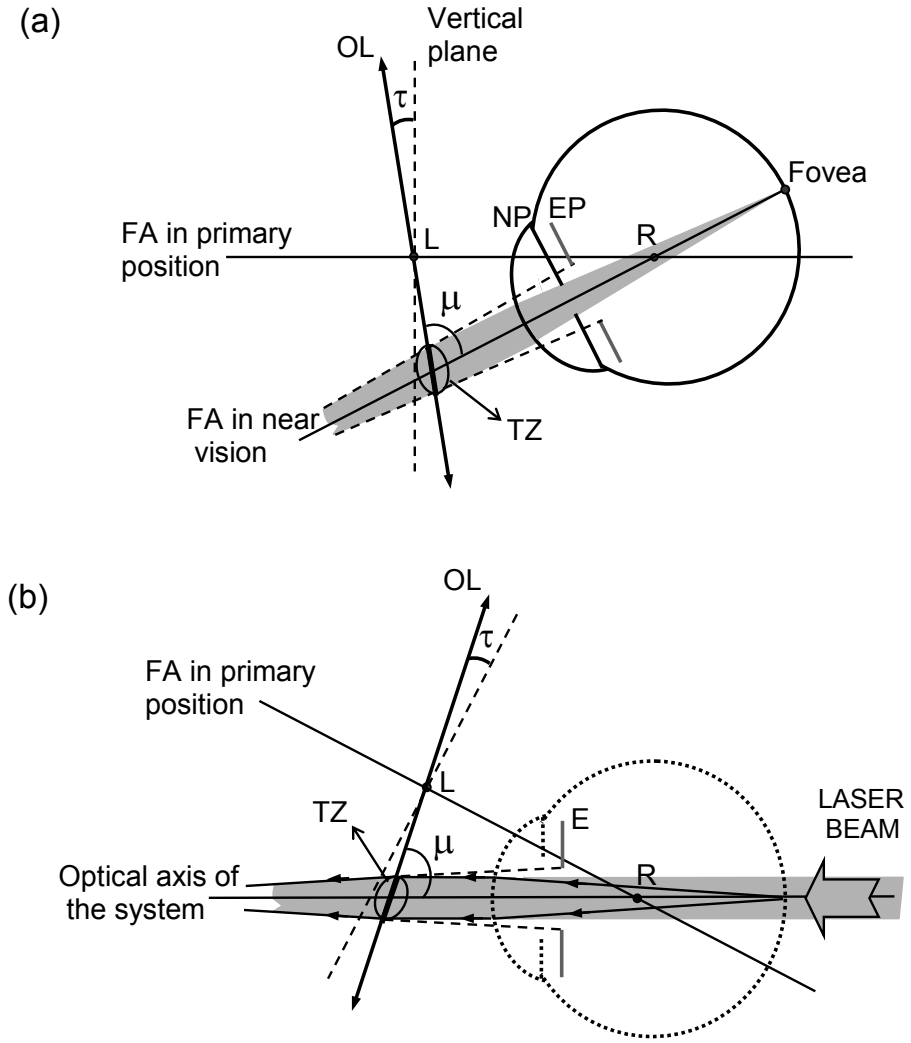

Figure 34. (a) Schematic behavior of the eye when looking to a near object. (b) Simulation of the same situation in our system. Shaded area represents the laser beam to measure the OL alone. Dotted contour represents the position of the eye. Ray tracing shows the direction of the laser beam when entire system eye and OL is measured. FA, fixation axis (visual axis); L, distant intersection point; R, rotation center of the eye; τ, pantoscopic tilt; μ, angle between lens and FA; NP, eye pupil; EP, entrance pupil of the system eye and OL; TZ, tested zone.

The tilts and displacements of the lens, with the corresponding equations, are shown in figures 35 and 36, in the horizontal and vertical planes respectively. The equations show the tilts and displacements as function of following fixed parameters: distance from the fitting cross (L) of the lens to the rotation center of the eye (LR=27 mm), distance from the anterior apex of the cornea to the rotation center of the eye (AR=14 mm), pantoscopic tilt (τ=12º), horizontal and vertical coordinates (LP_H, LP_V) of the selected point of the lens from the fitting cross, distances of the rotations centers in the horizontal (LG_H) and in the vertical (LG_V) planes from the fitting cross. In order to make easier the process, at the beginning the laser beam is normal to the lens and it passes through the fitting cross. In this position, the fitting cross is the reference point (O) for the movements. In both the horizontal and vertical planes, the movements were carried out following these steps:

1. Tilting the lens.

2. Moving the lens to place the selected point (P) of the lens on the measuring beam.

3. Placing the lens at the correct axial position. For measurements in the isolated PPLs, the selected point is placed at the focus of the lens L1 which coincides with the reference point (O). The final axial movement is the addition of the axial displacements in both the horizontal (P_HO) and vertical (P_VO) planes. For the entire system, eye plus lens, the eye pupil is place at the focus of the lens L1, and the selected point of the lens is placed to the vertex distance in front of the anterior apex of the cornea. Figure 37 shows how the vertex distance is calculated for any sight direction. This distance is the hypotenuse of the triangle formed by the tested point of the lens (P), its projection on the vertical axis of the lens (P_V) and the rotation center of the eye (R). The distance between P_V and R has been calculated in figure 36.

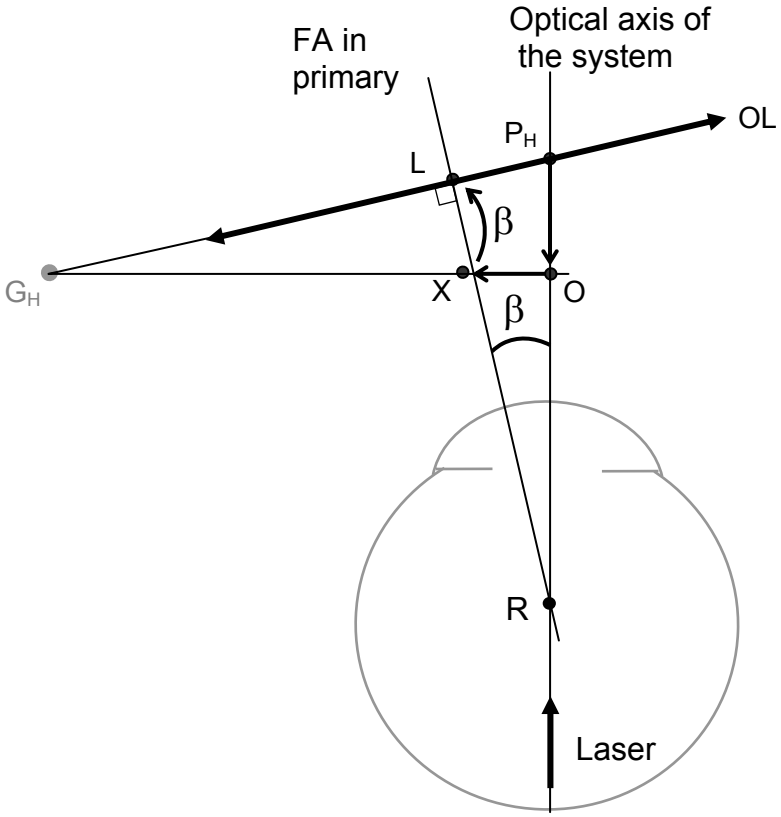

Horizontal tilt	$\mathrm{tg}\beta = \frac{LP_H}{LR}$
Horizontal displacement	$OX = (LG_H - LP_H)\cdot\cos\beta - LG_H$
Axial displacement for measurements in isolated lenses	$P_HO = -(LG_H - LP_H)\cdot\sin\beta$

Figure 35. Tilts and displacements in the horizontal plane. β, tilt angle; OX, horizontal displacement; P_HO, axial displacement for measurements in isolated lenses; O, reference point (for measurements in isolated lenses this point coincides with focus of lens L1); L, distant intersection point (fitting cross of the lens); X, point L before tilting ; P_H, projection of the tested point of the lens on the horizontal axis of the lens; R, rotation center of the eye; G_H, horizontal rotation center of the lens in our system; FA, fixation axis. Sign convention for the lens tilts: *clockwise* angles are negative, *anticlockwise* angles are positive (example of the figure). Distances from the lens to the rotation center of the eye (LR) are positive. Horizontal distances towards the right are positive and towards the left are negative. The axial displacement (P_HO) toward lens L1 is negative. Fixed values in our experiments: LR=27mm, LG_H=90mm.

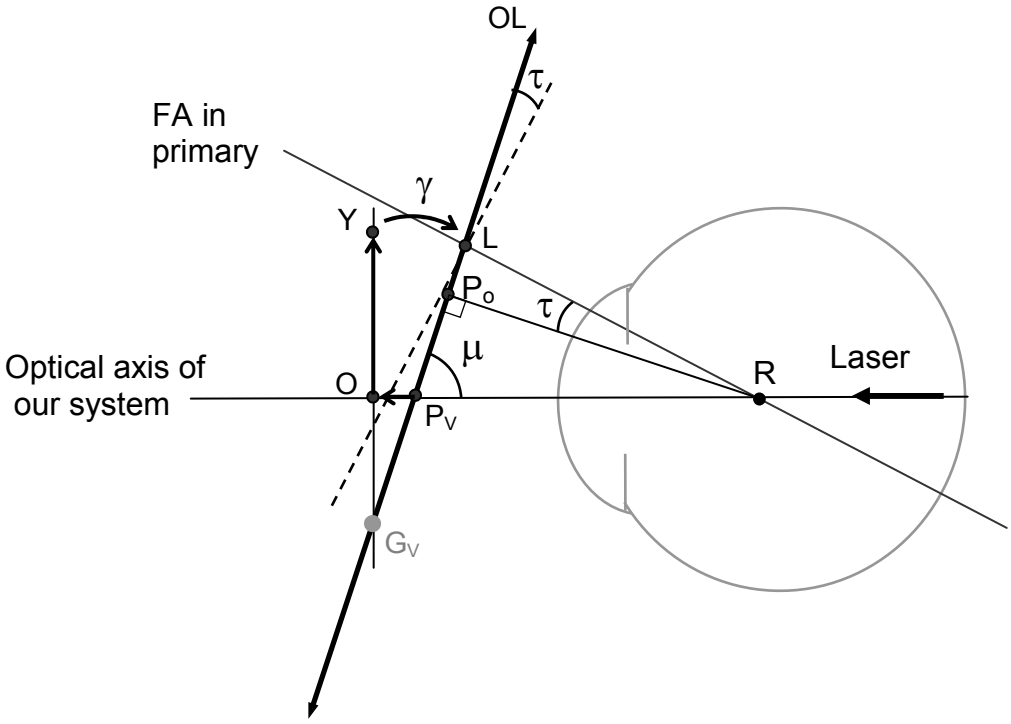

Vertical tilt	γ=-90-μ for $\mu<0$ γ=90-μ for $\mu>0$	$\mathrm{tg}\,\mu = \frac{P_0R}{P_0P_V} = \frac{LR\cdot\cos\tau}{LP_V + LR\cdot\sin\tau}$
Vertical displacement		$OY = (LG_V - LP_V)\cdot\cos\gamma - LG_V$
Axial displacement for measurements in isolated lenses		$P_VO = -(LG_V - LP_V)\cdot\sin\gamma$
Distance from tested point to rotation center of the eye		$P_VR = \frac{LR\cdot\cos\tau}{\sin\mu}$

Figure 36. Tilts and displacements in the vertical plane. γ, tilt angle; OY, vertical displacement; P_VO, axial displacement for measurements in isolated lenses; P_VR, distance from tested point of the lens to rotation center of the eye for measurements in entire system eye plus lens; O, reference point (for measurements in isolated lenses, this point coincides with focus of lens L1); L, distant intersection point (fitting cross of the lens); Y, point L before tilting; P_V, projection of the tested point of the lens on the vertical axis of the lens; P_o, intersection point of the lens with the perpendicular visual axis; R, rotation center of the eye; G_V, vertical rotation center of the lens in our system; FA, fixation axis; μ, angle between lens and FA; τ, pantoscopic angle. Sign convention for the lens tilts: *clockwise* angles are negative (example of the figure), *anticlockwise* angles are positive. Pantoscopic angle and distances from the lens to the rotation center of the eye (P_oR, LR) are positive. Vertical distances and displacements taken upwards are positive and downwards are negative. The axial displacement (P_VO) toward lens L1 is negative. Fixed values in our experiments: τ=12º, LR=27mm, LG_V=9mm.

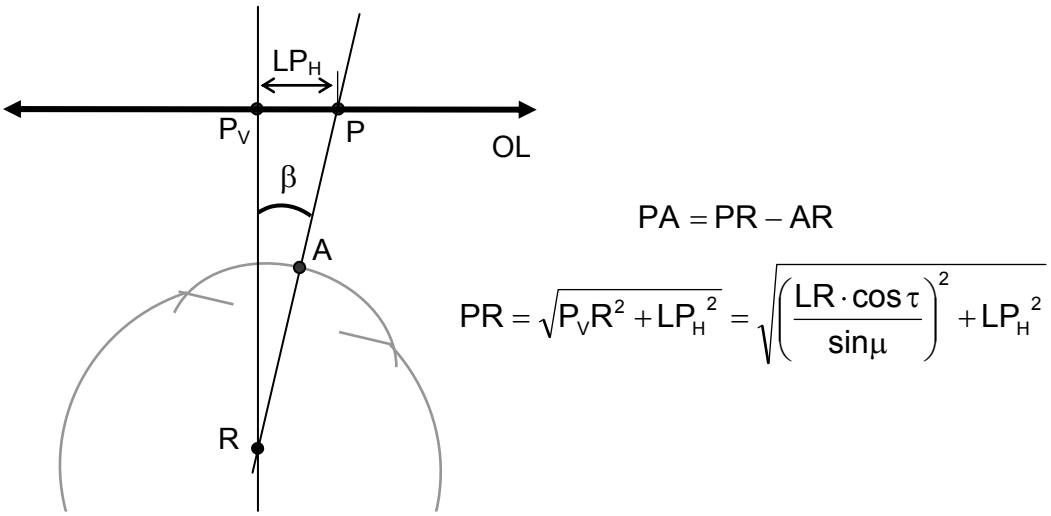

Figure 37. Vertex distance (PA) from the selected point of the lens to the cornea. This figure corresponds to the plane that contains the selected point of the lens (P), its projection on the vertical axis of the lens (P_V) and the rotation center of the eye (R). The expression of the distance P_V R has been obtained in figure 35.

3.2 OPTICAL MEASUREMENTS

In this section, the general aspects of the optical measurements will be described.

3.2.1 Calibration of the system

The calibration is done with the system mounted for measuring isolated lenses but without any lens for testing. Firstly, we place the CCD camera (HSCCD) of the HS sensor at the exact position of the MLS focus. Taking into account the focal lengths of the lenses L1 and L2, the moving stage (FS) of the focus corrector sub-system is moved to obtain an approximately collimated beam entering the MLS. The exact axial location of the CCD camera is found by moving it with a positioner up to find the highest peak intensity of the spots. In order to obtain the exact position of the FS that produces a perfectly collimated beam, HS images are registered, and defocus is processed for small displacements of the FS.

To test the defocus calibration, the focus corrector also moved in steps of 5 mm, which supposes changes of 10 mm in the optical path (d). Figure 38 shows a very good linear correlation between the values of theoretical defocus and the values obtained from the HS images.

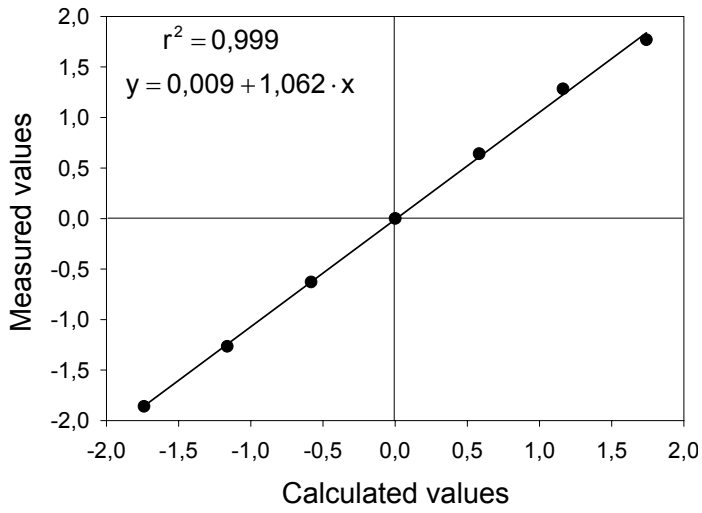

Figure 38. Calibration of defocus, moving the focus corrector (FS) in steps of 5 mm (d=10mm). Defocus is expressed as Zernike coefficient 4, in microns. 5.9-mm pupil diameter.

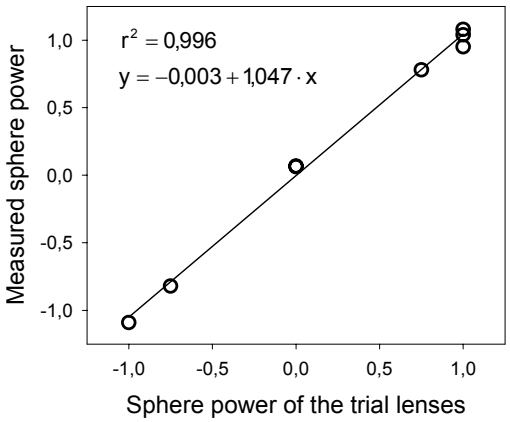

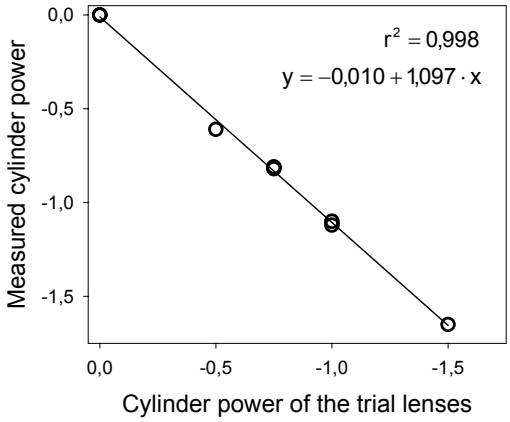

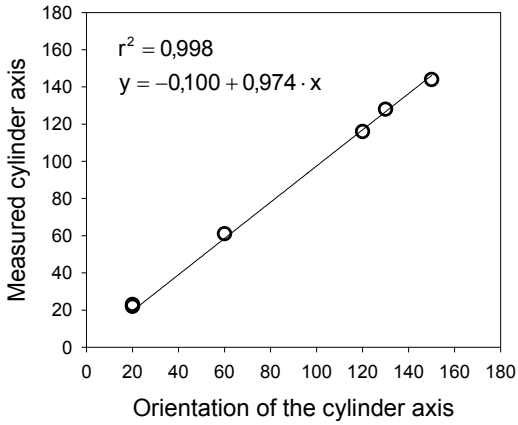

Figure 39. Calibration of defocus and astigmatism (power and orientation), expressed as sphero-cylindrical form, using trial lenses. Values for negative cylinder. Powers in diopters and orientation of the axis in degrees.

Astigmatism, both isolated cylinder powers and in combination with defocus, was tested using trial lenses. Figure 39 shows a very good linear correlation between the values of the trial lenses and the measured values. The data are shown in sphero-cylindrical form, that is, sphere power, negative cylinder power and orientation of the cylinder axis.

The wave aberrations of the system were also measured, obtaining values of Zernike coefficients below 0.01μm for both 4 and 6-mm pupil diameters (figure 40). Thus, the contribution of the system to the final wavefront aberration can be considered negligible.

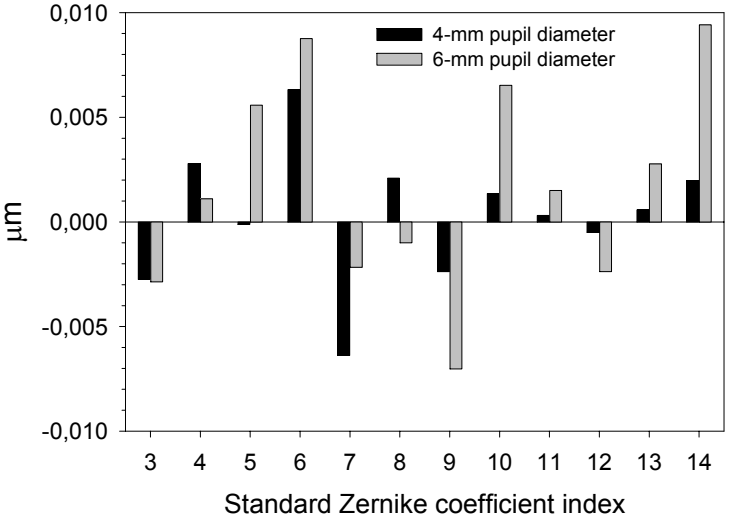

Figure 40. Aberrations values given only by the experimental system.

3.2.2 Progressive power lenses (PPLS)

All lenses used in the experiments, except those in the neural adaptation experiment (chapter 7), have in common the following characteristics: the progressive surface is on the front of the lens, plano distance power, 2D power addition, 18-mm corridor length (vertical measurement from the fitting cross to the centre of the near verification circle) and 2.5-mm inset of the near vision. In the chapter 7, the power in the far zone and the addition depend on the refraction of the subjects.

A Varilux Comfort progressive lens (Essilor International, France), is used to study the wavefront aberrations (chapter 4), the influence of the lens aberrations in visual quality (chapter 5) and the relation with optical metrics (chapter 6).

In the section of optical comparison of different PPLs (chapter 8), the lenses are simply called A, B and C, because we do not have any commercial interest in any product

and the main goal of this study is to evaluate the optical quality of the current PPL designs and to show the differences between them.

The HS systems measure the ocular aberrations in the object space that is in front of the eye. For this reason, when measuring isolated PPLs, the in-coming beam is directed on the posterior surface of the lenses. For all measurements, the lenses were placed and tilted accordingly to simulate natural viewing conditions.

3.2.3 Combining eyes with PPLs

The final image quality in retina is given by the complete system: eye plus the progressive lens. Testing directly a large number of zones in the lenses *in situ* is time consuming and requires the collaboration of the subject. An alternative method is to estimate wavefront aberration (WA) of the whole system by adding those of the two elements. For six zones of the Varilux Comfort lens and two subjects, the WAs of the whole system are obtained in two ways: (1) by direct measurement of the system and (2) by adding the individual WAs of the eye and the lens for selected zone. The aberration coupling between the lens and the eye is explored by comparing the two methods. The possible differences between both methods will be due to the propagation distance of the wavefront between eye and lens (that we consider 14 mm), in addition to the experimental errors.

3.3 MEASUREMENTS OF VISUAL ACUITY

Visual acuity was measured using the “tumbling E” (figure 30). Capital letter "E" was presented in four possible orientations (right, left, up and down). A computer program developed from the VSG2/5 (Visual Stimulus Generator from Cambridge Research System, UK) produced the video signal input to a Sony GDM-F520 monitor. In a first adjustment, the letter size was reduced by steps of 0.2 arc-min up to the smallest letter that the subject saw in the best focus. From this reference size, four sizes more (two-up and two-down) were randomly presented for 1 second up to 80 times (20 times for each size).

In order to compare optical and psychophysical parameters in visible green light, the green gun of the monitor was used. The luminance of the screen was 80 cd/m^2 with the visual field subtending 7.5º.

Visual acuity measurements were taken with two different artificial pupil diameters (figure 30, PPS): 4.5 and 3 mm, and for two different contrast values, 100% and 15%.

By counting the number of letters orientations correctly identified by the subject for each size, a four-parameter sigmoidal fit (constraining correct responses to 25% and 100% when MAR is zero and infinity respectively) was used to obtain the value of visual acuity. We chose the value of MAR for the 75% of correct responses. Figure 41 shows the sigmoidal fits of MAR for subject when is looking through an intermediate location of the PPL for high and low contrast letters. Finally, the VA is expressed in decimal units (1/MAR).

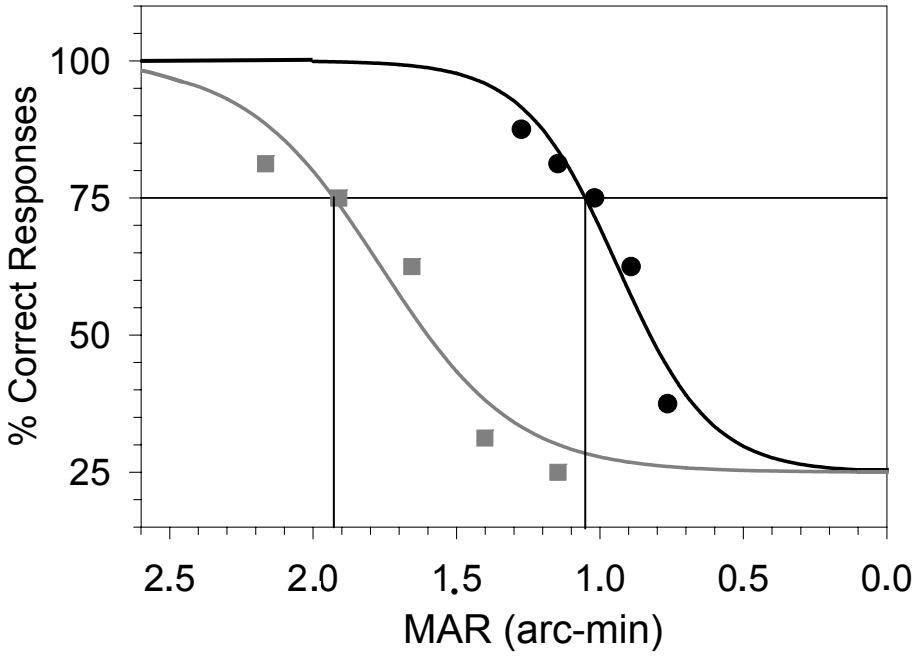

Figure 41. Examples of sigmoidal fits of MAR. Contrast 100% (circles) and contrast 15% (squares). 4.5-mm pupil diameter.

.

3.4 SELECTION OF TESTING AREA AND PUPIL DIAMETER

In this section, we analyse what is the convenient area of the progressive lenses for testing and what is the adequate pupil diameter. The concrete conditions of each experiment will be described in the results chapters.

In order to select the locations for testing the lenses, we consider locations along the corridor and nearby peripheral zones, because these are very frequently used by subjects and have no negligible values of aberrations. The horizontal width of the tested area is selected taking into account the amplitude of horizontal eye movements. The field of foveal gaze is determined by the coordination of horizontal eye and head movements. The complete amplitude of the horizontal eye movement is described as the movement between the extreme positions (nasal-to-temporal). Usually, this horizontal amplitude is less than 30º

[*Progressive addition lenses. Ophthalmic optics files. Essilor International 2007, Paris*], and the rest of the movement necessary to keep the gaze in a peripheral object is given by the head or even by the body. In a recent work [Han *et al.* 2003(b)] the amplitude of horizontal eye movement was less than 25º for an object with an amplitude of 37º placed at a intermediate distance of 60 cm. As an example, figure 42 shows the eye movements of 15º and the head movement of 10º for an object with an eccentricity of 25º in far vision. For these reasons, we tested mainly zones located to less than 13º from the corridor (complete amplitude of 26º), although we wide this area to 20º when comparing different designs of PPLs. In any way, in each section of results, we specify the measured zones.

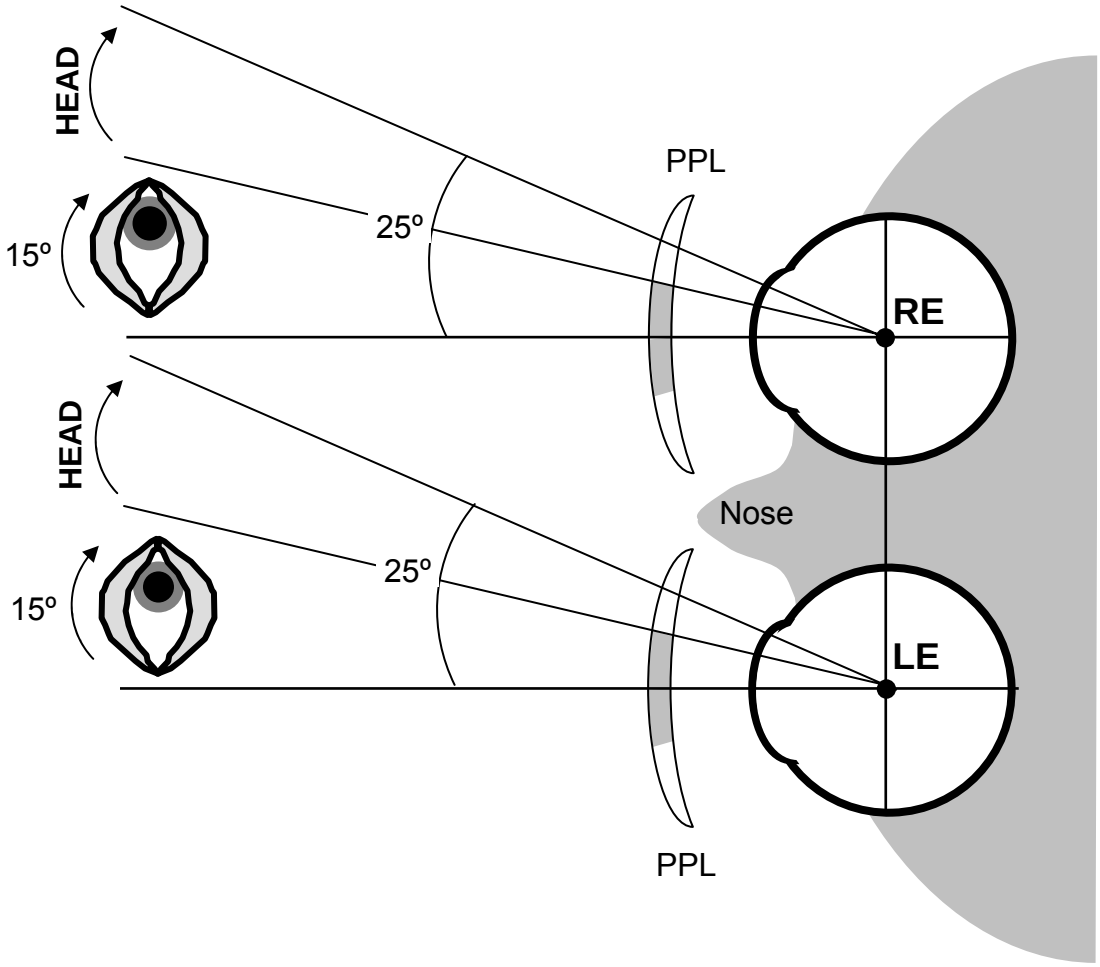

Figure 42. Horizontal movements of the eye and head for gazing a peripheral object with a eccentricity of 25º in far vision, taking into account the maximum normal movement of the eyes (around 15º, that corresponds with a complete amplitude of 30º). The subject uses the shadowed zones of the progressive lenses for foveal vision.

The optical and visual results are obtained for a pupil diameter equal or lower than 4.5 mm, since larger pupils are uncommon in presbyopic eyes [Chateau *et al.* 1996]. However,

WA and PSF maps presented in some of the figures corresponds to a larger pupil diameter (6-mm) to better show the effect of aberrations in each lens zone.

Chapter 4

RESULTS (I):

WAVEFRONT ABERRATIONS IN PPLS: ISOLATED AND IN SITU

In this chapter, we present the spatially resolved aberrations measured in a PPL. We also compare the high order aberrations for all zones of the PPL with three normal older eyes. Finally, we explore the nature of the aberration coupling between the lens and the eye, by comparing the aberrations of the lens plus eye system with those in the lens and the eye measured separately.

4.1 TESTED ZONES

We measure the WA at 21 relevant locations across a PPL (Varilux Comfort; Essilor International, France), with plano distance power, 2 D power addition. Figure 43 shows the specific area of interest on the lens (the dashed contour line) covered by the 21 zones where the aberrations were measured.

In six representative locations (from the 21), we measure the WA of the eyes plus the PPL. The selected zones are (shadowed zones in figure 43): within the corridor, 1 and 8; nearby to the corridor in intermediate vision, 7 and 9; near vision, 18; and a peripheral location, 14.

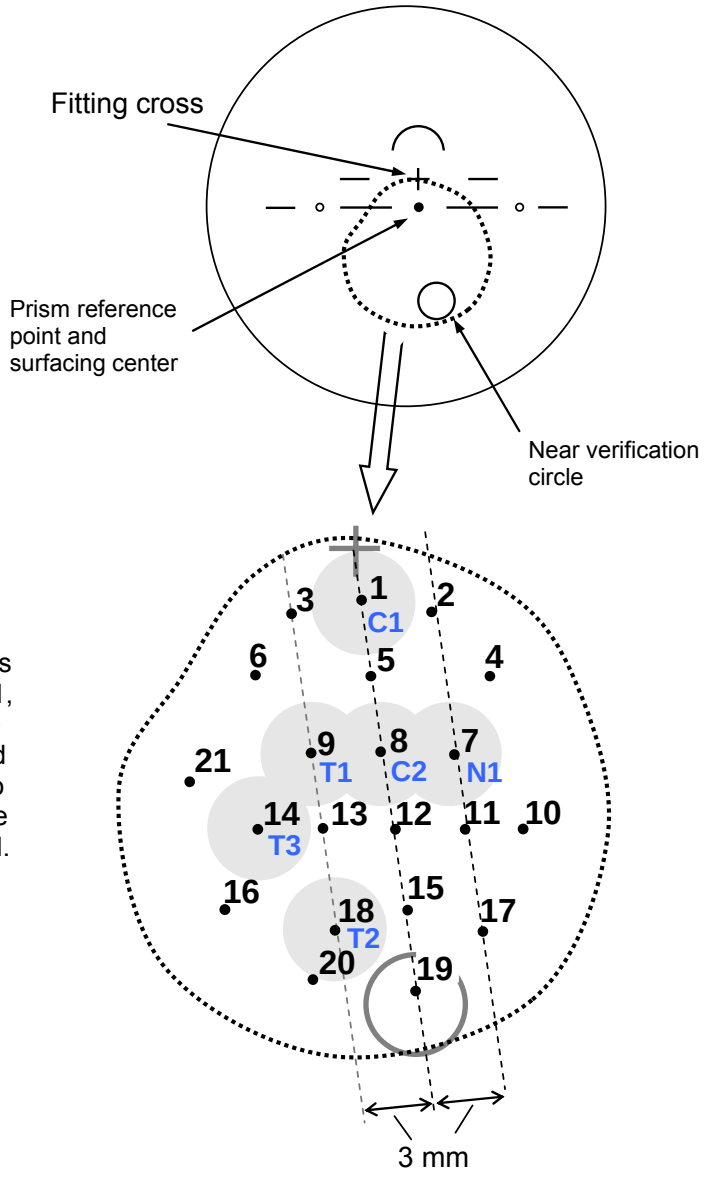

Figure 43. Locations of the measured zones in the isolated PPL. The shadowed zones (1, 7, 8, 9, 14 and 18), 4.5-mm diameter, were also selected to study the coupling lens and eye aberrations. In these locations, we also test the visual acuity in the chapter 5, where blue notation with letters C, N and T is used.

4.2 SPATIALLY RESOLVED WA IN THE CORRIDOR AND NEARBY ZONES OF A PPL

The estimated WA can be divided in two parts, the second order and the high order aberrations. The second order includes defocus (Zernike coefficient 4) and astigmatism (Zernike coefficients 3 and 5), and the high order the remaining aberrations. We show the defocus distribution in the PPL, the WA and PSF maps for all zones, the spatially resolved RMS and Strehl ratio, and finally, the Zernike coefficients.

4.2.1 Defocus

In PPLs, the defocus is distributed around the lens increasing from far to near areas for allowing to keep focus for different viewing distances. In the near circle, the defocus must be the addition power which subject needs for seeing clearly in near tasks.

The global performance of PPLs depends on the power distribution. From the point of view of ergonomics, the power profile along the corridor and the lateral inset of the near circle are two important parameters taken into account when designing PPLs. On the other hand, the values and the distribution of the residual optical aberrations (astigmatism and others which we will show later) depend directly on the power progression on the lens. Figure 44 shows the power distribution in the tested lens. A 3D representation of the defocus Zernike coefficient can be seen in figure 44a and the iso-power lines plot is shown in figure 44b. In these graphs, we can see that the power of 2 D is reached to 17 mm below the fitting cross and around 2.5 mm at the nasal side. It agrees with the data of the lens given by Essilor: plano distance power, 2D power addition, 18-mm corridor length and 2.5-mm inset. In the tested lens, the power progression is faster in the middle of the corridor, between 4 and 12.5 mm below fitting cross, where the power increases from 0.4 to 1.6 D. In peripheral areas the progression is slower, and the total addition is not got. Along the corridor, the 80% of the total addition is reached around 12.5 mm below fitting cross. It supposes an ergonomic benefit, because the subject has not to turn downwards the eyes too much to see objects at a relatively nearby distance.

In this work, we assume that in normal viewing conditions the remaining accommodation of the subjects compensate the small amounts of defocus induced by the difference between the power of the zone of the lens and the object distance. For this reason, in the following chapters, the value of Zernike coefficient for defocus is set to zero for estimating the optical quality (i.e. WA, PSF, RMS, Strehl ratio…) of the lens.

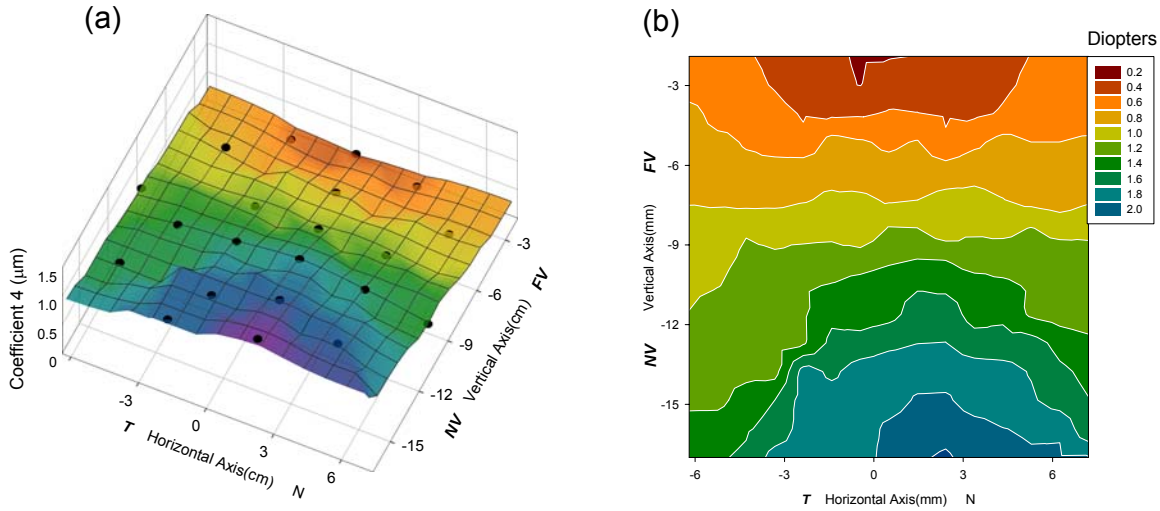

Figure 44. (a) Spatially resolved defocus (power), expressed by Zernike coefficient 4, for 4.5-mm zones diameter. (b) contour plots of power in diopters,.

4.2.2 WA and PSF maps

Figures 45a and 46a show the WA and PSF maps with defocus Zernike coefficient set to zero for 20 relevant zones of the PPL for 6-mm pupil diameter. Zone number 20 (not shown for clarity) is very similar to 18. The PSF maps were calculated at the circle of least confusion. The plots for zones of the corridor show typical shapes of coma with a small amount of astigmatism. However, in locations of the PPL outside the corridor, astigmatism increases and becomes the dominant aberration, while coma remains fairly similar to the center. Figures 45b and 46b show the WA and PSF maps of zone number 9 with defocus and astigmatism set to zero (the other zones present similar aberration maps for this condition). As shown in figure 45b, in addition to coma, there is also some trefoil. Figure 46b corresponds to a typical coma-shape PSF.

There are many previous theoretical works [Piers *et al.* 2000, Jalie 1994, Fowler and Sullivan 1989, Bourdoncle *et al.* 1991] about the shape and size of the image of a point through a progressive spherical power surface. Maitenaz claimed a V-shaped unevenly illuminated. Jalie considered a blur image composed of two superimposed ellipses. Bourdoncle and collaborators found that coma affected the nature of the image when pupil size changed. Burns proposed a retinal blur as a circle increasing the light going down the image. Our results of PSFs in the corridor show typical shapes of coma modified by astigmatism and trefoil. Actually, as we can see in these plots, the intensity is higher at the bottom of the images, due to the orientation of the coma. However, in areas of the PPL outside the corridor, the images are dominated by the astigmatic shape.

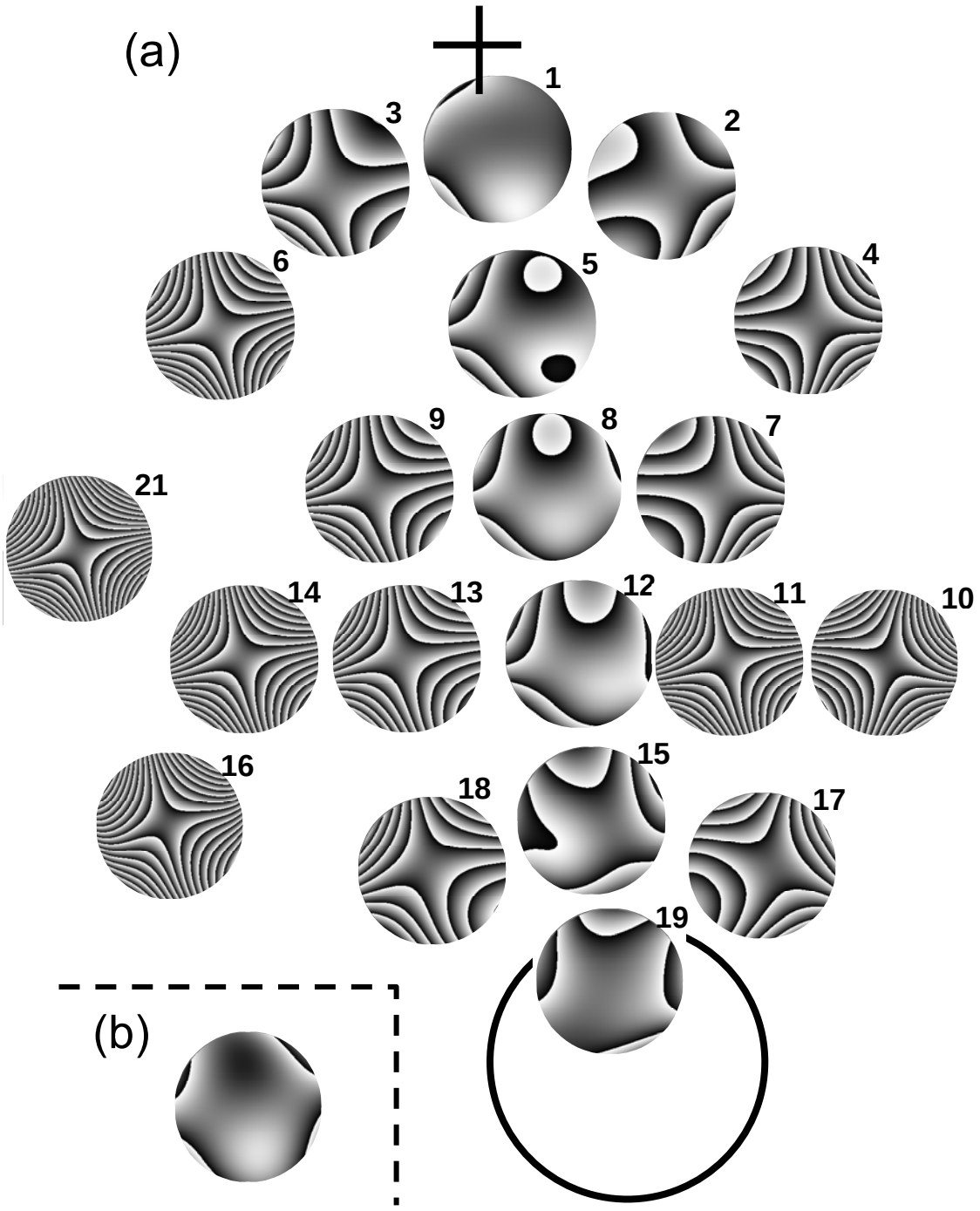

Figure 45. (a) A modulus 2π representation of the WA maps at 20 locations across the PPL, with the defocus Zernike coefficient 4 set to zero. Zone number 20 (not shown for clarity) equals zone 18. WAs maps are calculated for 6-mm zones diameter, but in order to place the maps on the lens without crossing themselves like is shown in figure 43, the maps are presented with a minor relative size. (b) WA map for zone 9 considering defocus (Zernike coefficient 4) and astigmatism (Zernike coefficients 5 and 6) zero. The maps of the rest of the zones equal this.

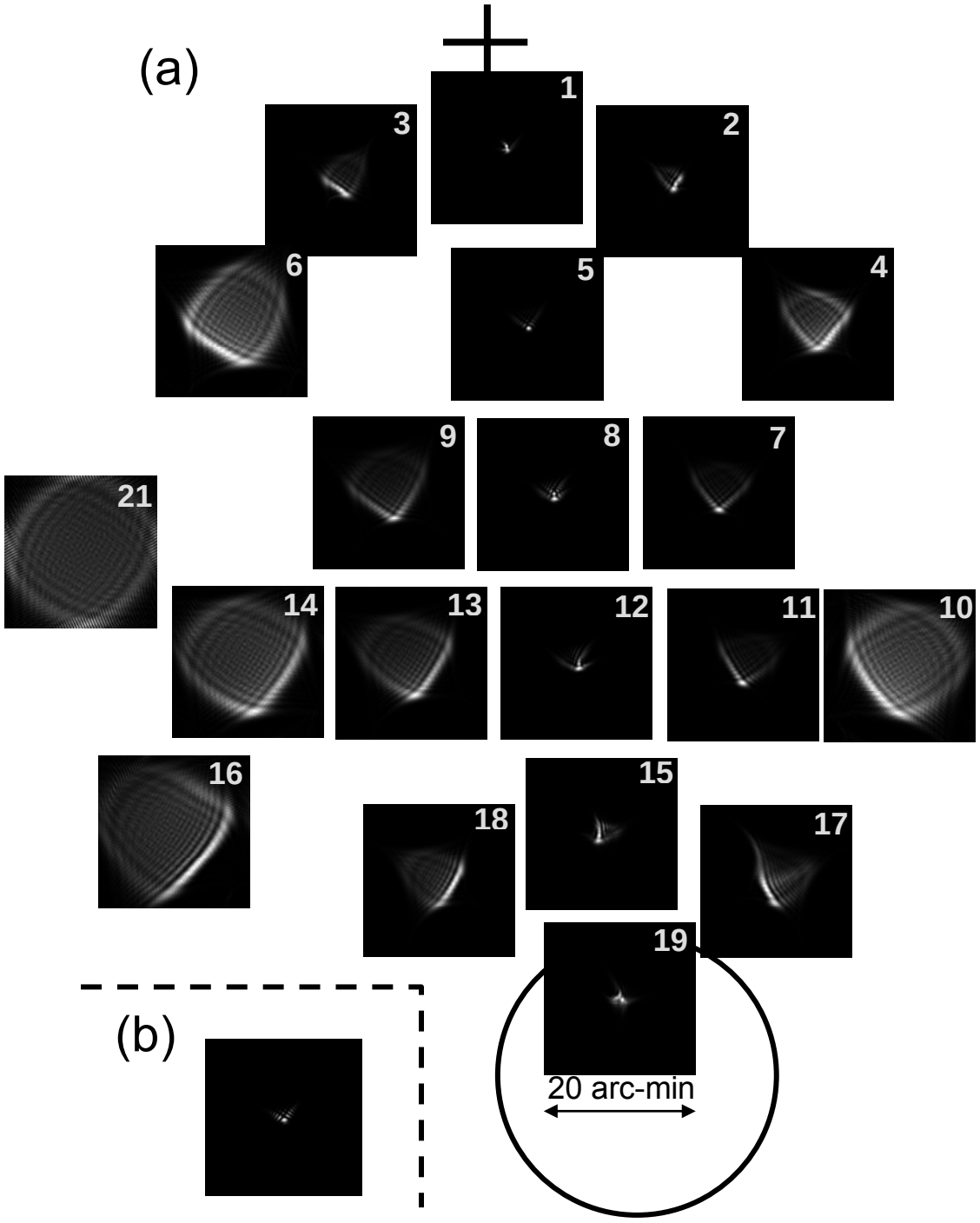

Figure 46. (a) PSFs maps at 20 locations across the PPL for 6-mm zones diameter, considering defocus (Zernike coefficient 4) zero. Zone number 20 (not shown for clarity) equals zone 18, and it isn't shown to do clearer the representation. (b) PSF map for zone 9 considering defocus (Zernike coefficient 4) and astigmatism (Zernike coefficients 5 and 6) zero. The maps of the rest of the zones equal this.

4.2.3 RMS and Strehl ratio

Figures 47 and 48 present the spatially resolved values of the RMS and the Strehl Ratio respectively, for the PPL, considering defocus zero (a) and both astigmatism and defocus zero (b), for 4.5-mm zones diameter.

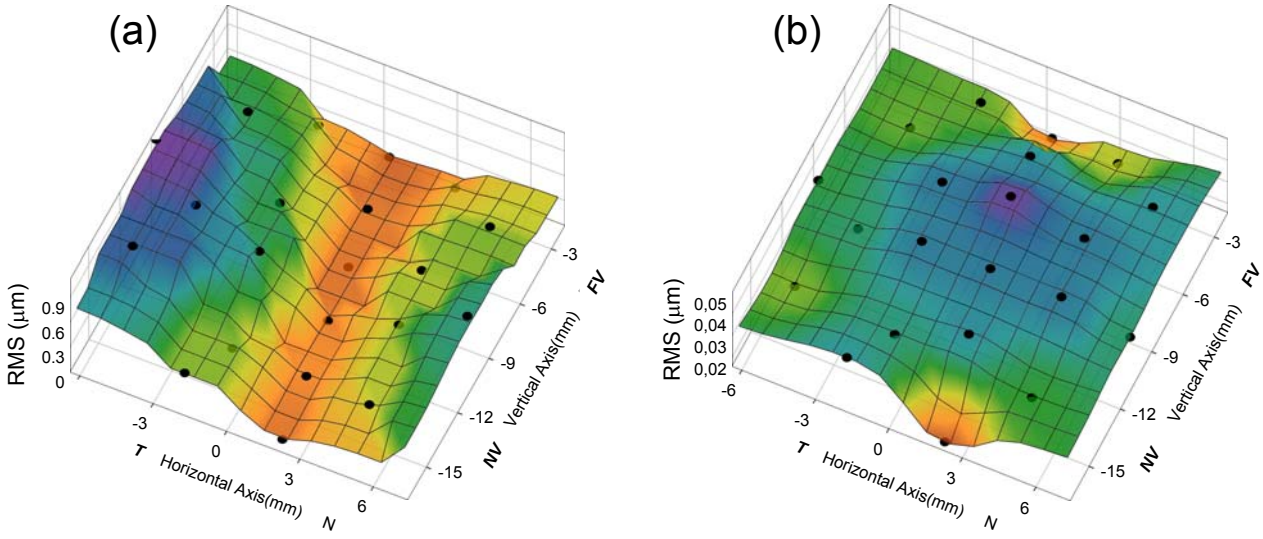

Figure 47. Spatially resolved RMS of the isolated PPL for 4.5-mm zones diameter, considering (a) defocus (Zernike coefficient 4) zero and (b) astigmatism (Zernike coefficients 5 and 6) and defocus (Zernike coefficient 4) set to zero. Circles show the results for each zone. FV and NV indicate the area of far and near vision respectively. N and T indicate the nasal and temporal areas respectively. The distances on the horizontal and vertical axe are taken from the fitting cross. Note the different values of the scale for the RMS in the two figures.

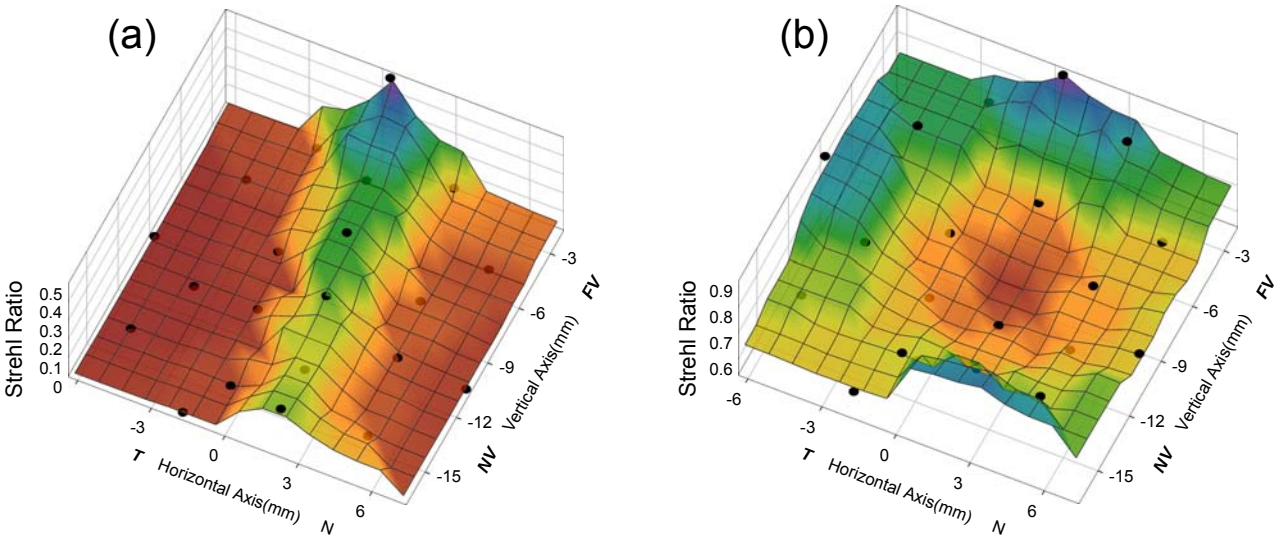

Figure 48. Spatially resolved Strehl Ratio of the isolated PPL for 4.5-mm zones diameter, considering (a) defocus (Zernike coefficient 4) zero and (b) astigmatism (Zernike coefficients 5 and 6) and defocus (Zernike coefficient 4) set to zero.

If astigmatism is included, the RMS values are around 0.10 μm for the distance and near reference centers. In the corridor, the total RMS values are between 0.10 and 0.20 μm depending on the zone. These values are similar to those of the measured naked eyes, 0.19 μm for eye SI and 0.23 μm for eye RU. The RMS of the lens at locations 3 and 6 mm from the corridor central line is around 0.60 and 0.90 μm respectively. However, if astigmatism is removed, the RMS is between 0.03 and 0.06 μm for all tested zones, finding the highest values in the middle of the corridor. These high order aberrations are mainly coma and trefoil.

The Strehl Ratio from all aberrations except defocus is high in the far zone 1, around 0.5. In the corridor, this parameter is lower, around 0.20, due to the increase of coma and trefoil. This effect can be seen very clear in the graph without astigmatism, where the Strehl Ratio decreases mainly in the middle of the corridor.

In both graphs without astigmatism, figures 47b and 48b, the optical quality is lower in the center of the corridor. In this area, the power progression is higher, providing an increment of coma and trefoil. In any way, without astigmatism the optical quality of the PPL is very good, since the Strehl Ratio is higher than 0.5 and the RMS is lower than 0.06 μm for all tested zones.

4.2.4 Wavefront aberrations. Zernike coefficients

Figure 49 shows all the Zernike values for the central and peripheral, nasal and temporal, zones of the lens considering 4.5-mm pupil diameter. The defocus coefficient is also included to note the evolution of the power over the lens. In addition to astigmatism (coefficients 3 and 5), the most significant aberrations for peripheral zones are coma (coefficients 7 and 8) and trefoil (coefficients 6 and 9). Other higher order aberrations are nearly negligible for every zone in the lens (in figure 50 we can see the higher order coefficients for every locations in a larger scale for 4.0-mm pupil diameter). In the nasal and temporal locations, astigmatism coefficient 3 is opposite in sign, while the coefficients 5 have the same sign. In this way, the orientation of the astigmatism is nearly vertically symmetric, and for zones on the same side of the corridor the behavior is similar. The negative cylinder axis is around 55º for temporal zones and 125º for nasal zones. In relation to the orientation of coma and trefoil, in the corridor zones, the coefficients 6 and 7 are significantly higher than coefficients 8 and 9, that means that coma and trefoil along the corridor are vertically orientated. In the rest of the zones, the orientation of these aberrations depends on the direction of the power progression.

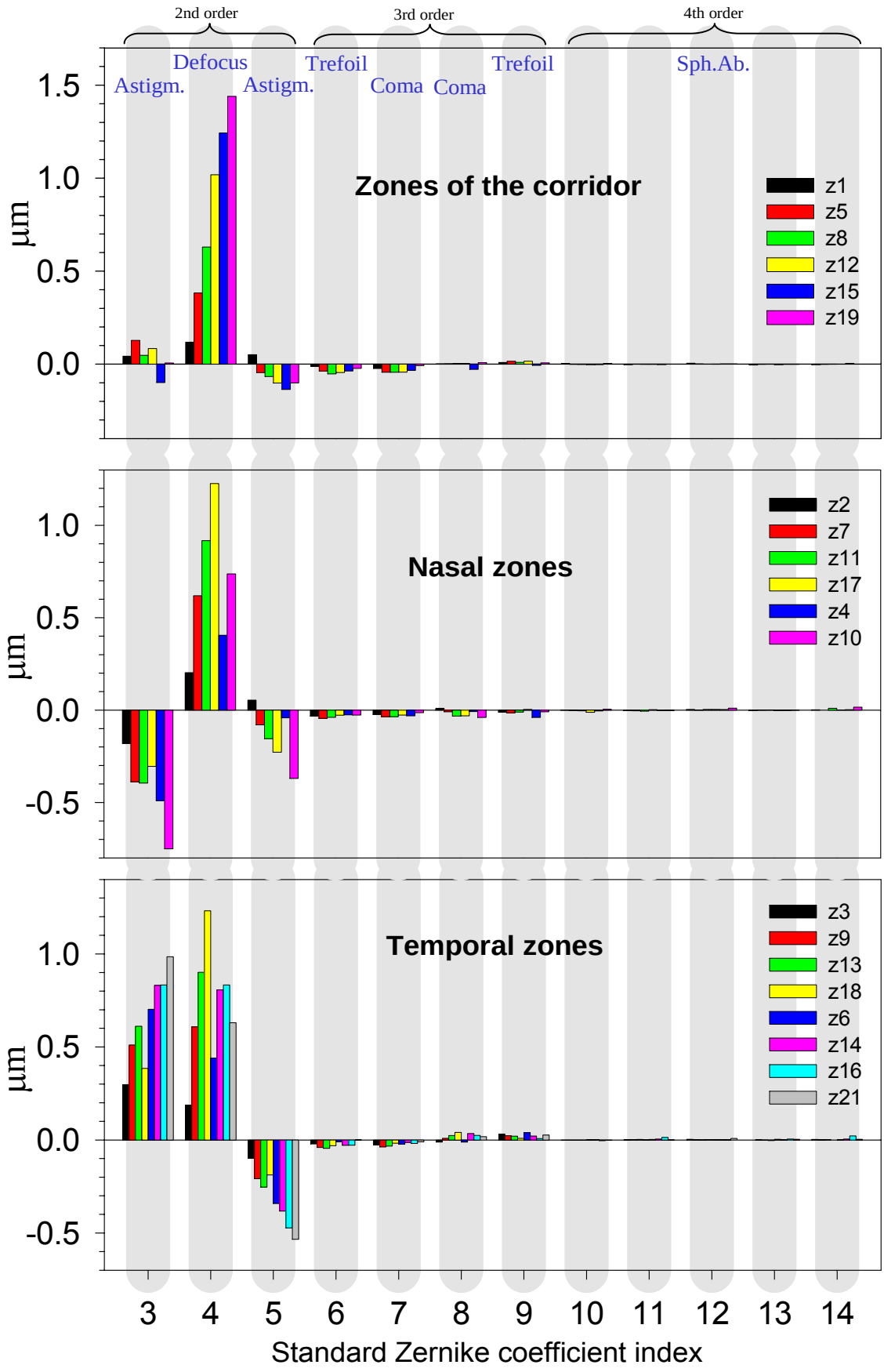

Figure 49. Zernike values for the central and peripheral (nasal and temporal) zones of the PPL for 4.5-mm pupil diameter. The Seidel aberrations corresponding to Zernike coefficients are shown on top of the graph.

Our results show, as it was well known, that astigmatism is the most important aberration found in progressive power lenses. In the last few years, computer numerical control lathes have been able to generate new complex aspheric surfaces. However, it will be difficult to completely eliminate astigmatism, as it is intrinsic to the design of progressive power surfaces. This is in accordance with Minkwitz [Minkwitz 1963] who stated that it was not possible to produce a progressive power lens without surface astigmatism and distortion being present at some point [Sullivan and Fowler 1988]. Coma and trefoil are the other dominant aberrations that appear in these lenses when defocus changes along the area of the tested zone. In the corridor and nearby locations of the lens, theses aberrations are slightly larger due to the faster rate of defocus change.

In the appendix of this work, we show an analytical model describing aberrations in PPLs.

4.2.5 Comparison with presbyopic eyes

It is interesting to compare the magnitude of the high order aberrations of the lens alone with the typical aberrations appearing in normal older eyes. This is shown in figure 50 for the 21 locations of the lens (green bars) and for three older eyes (P1, 2 and 3) from [Artal *et al.* 2002(a)]. In general, older eyes present larger aberrations than the PPL. In some cases, coma and trefoil coefficients have similar magnitude in the eye and in the lens. However, in every eye and location of the lens, spherical aberration is larger in the eye.

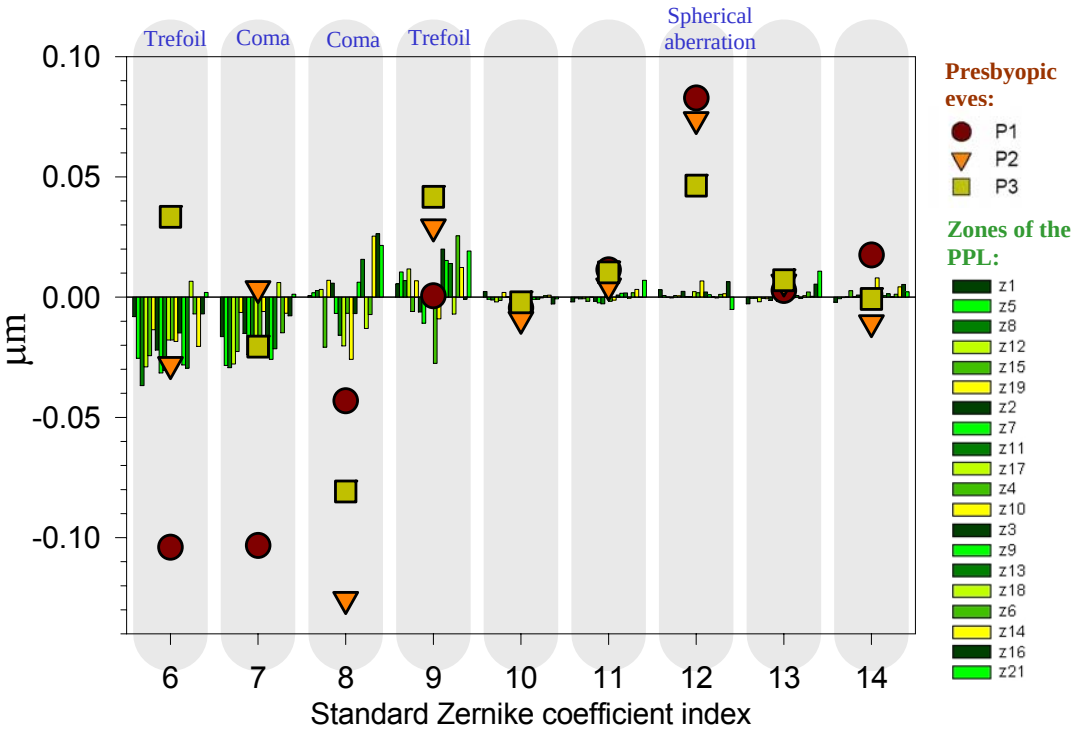

Figure 50. High order aberrations for all zones of the PPL compared with three normal older eyes obtained from *[Artal et al. 2002(a)]*. 4.0-mm pupil diameter.

4.3 WA MEASUREMENTS OF THE PPL IN COMBINATION WITH EYES

The optical tests are commonly made in isolated lenses, but the image quality on retina is due to the entire system eye with lens. In order to obtain the final optical quality of the entire system eye with PPLs, in this section, we study the aberration coupling between both for two eyes and six zones of the lens.

4.3.1 Measurements in the "naked" eyes

The left eyes of two 29-year-old normal males subjects (SI and RU) were measured. From the HS measurements, their refractions were estimated: subject SI -3.10-0.35 $\times$ 45 and subject RU –1.00-0.35 $\times$ 95. These low amounts of astigmatism were not compensated in order to study the coupling with the astigmatism of the PPL. They had a corrected decimal VA better than 1. Accommodation was paralyzed and the pupil was dilated with two drops of tropicamide (1%). Three HS measurements were obtained and the standard deviation calculated. The study followed the tenets of the Declaration of Helsinki, and signed informed consent was obtained from the subjects after the nature and all possible consequences of the study had been explained.

4.3.2 Direct measurements of the eyes with the lens

After measuring the isolated eyes, we measured the eyes wearing the PPL when they were looking through the six zones of the lens. The chosen zones are those shadowed in figure 43. Thus, we obtain the direct wavefront aberrations of the entire system eye plus lens. In the next section, we compare these aberrations measured directly with the sum of the eye plus lens aberrations measured separately.

4.3.3 Coupling of aberrations of the naked eyes and the PPL

In order to compare directly the optical quality of different zones of the PPL and the naked eyes, in figure 51, we can see the Zernike coefficients and the WA and PSF maps of the shadowed zones of figure 43 and the naked eyes (RU and SI). Figures 52 and 53, for the eye RU and eye SI respectively, show the comparison between direct measurements of eyes looking through the zones of the PPL and the results by adding the Zernike coefficients of the lens and the eye measured independently. Practically in all cases, the differences of Zernike coefficients estimated from both methods are smaller than the experimental errors. So, the WA and PSF maps are also very similar. Figure 54 shows the RMS of the system eye with lens both measured directly and adding aberrations. These results support the idea

that optical aberrations of the entire system eye with an ophthalmic lens can be predicted by adding the Zernike coefficients of both elements.

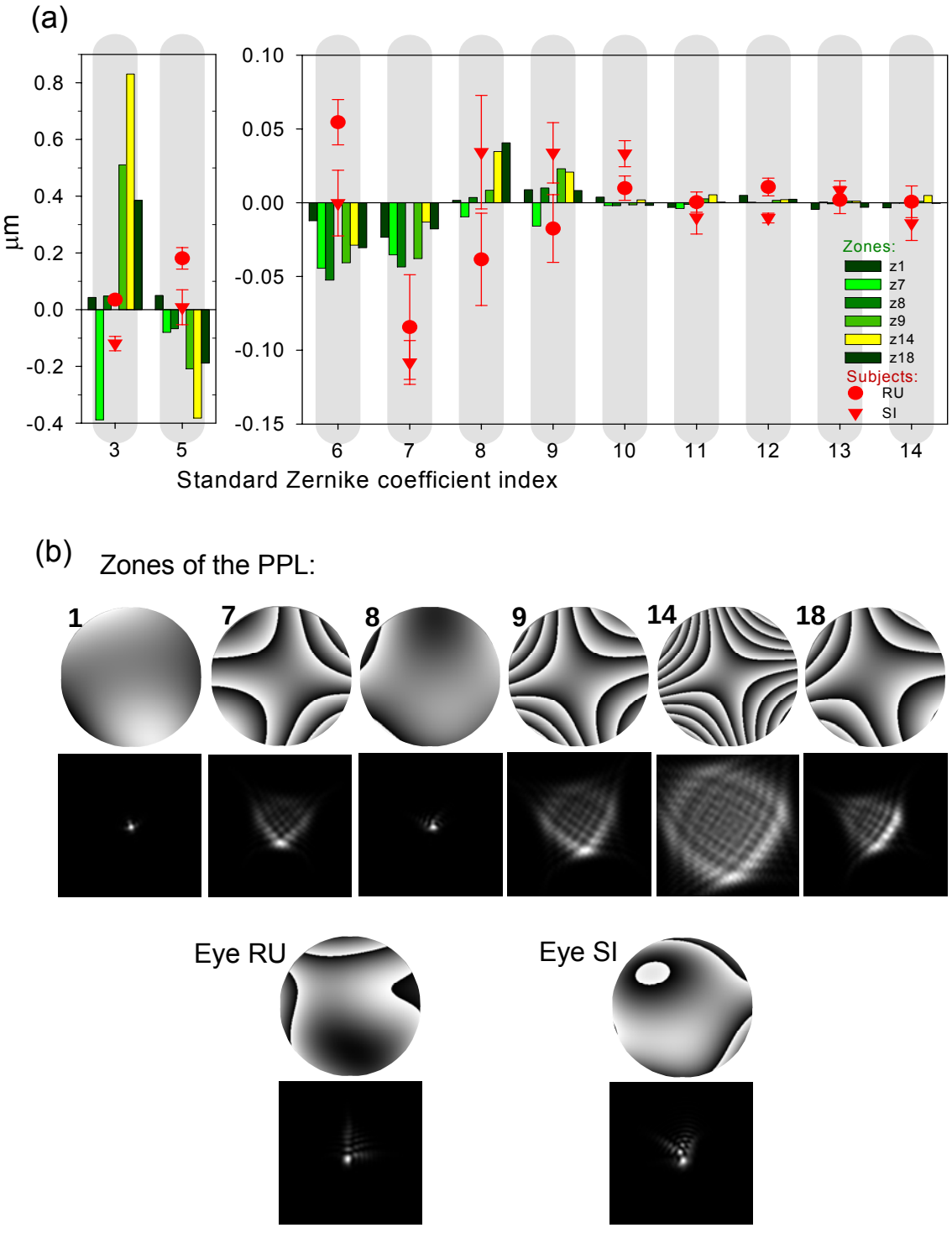

Figure 51. Comparison between the naked eyes and the zones of the PPL chosen to study the coupling of aberrations. (a) Zernike coefficients of the naked eyes (symbols) and tested zones 1, 7, 8, 9, 14 and 18 (bars) of the PPL. (b) A modulus 2π representation of the WAs and associated PSFs. 4.5-mm pupil diameter.

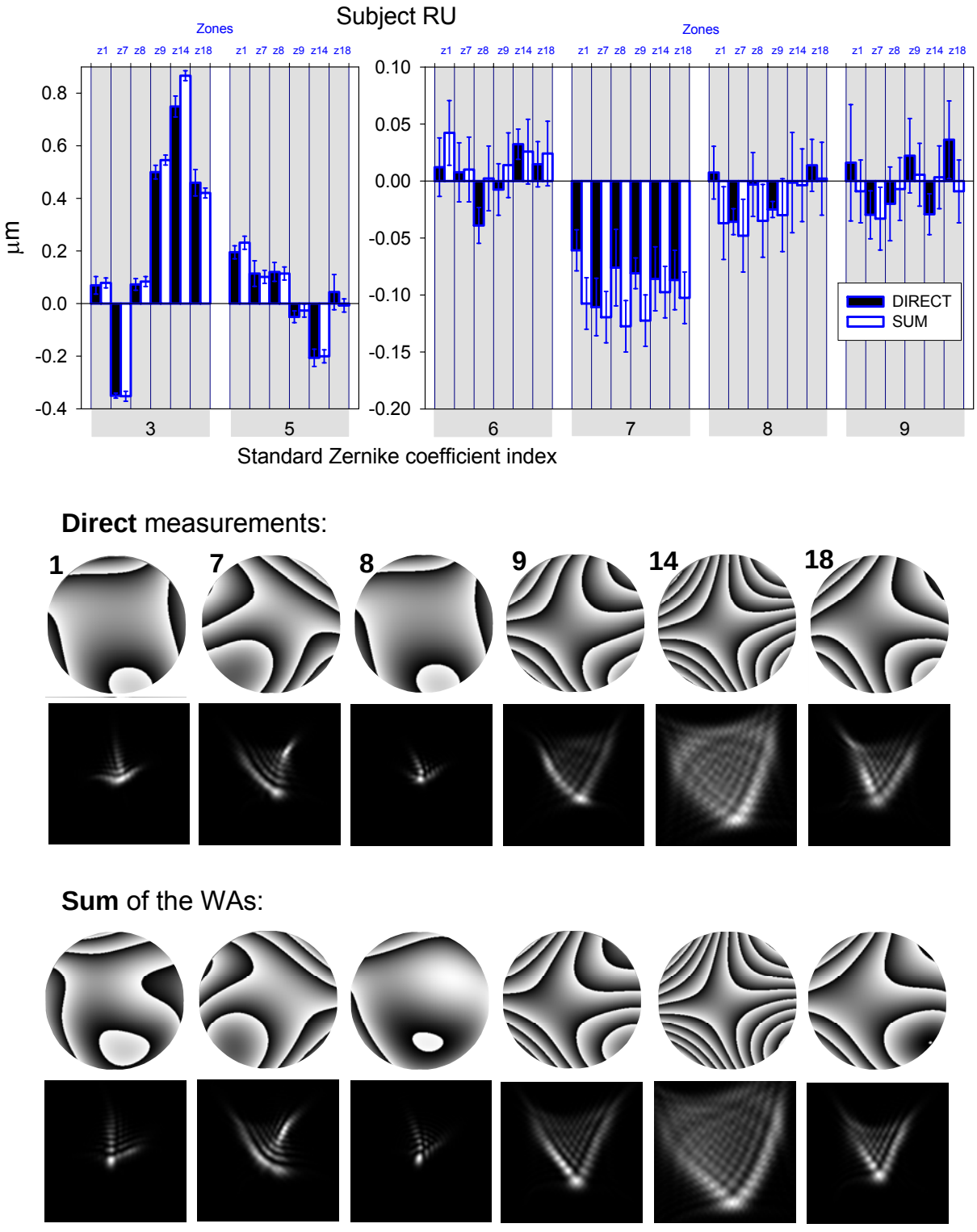

Figure 52. Comparison of optical quality (Zernike coefficients, and WA and PSF maps) of the eye of subject RU in combination with six zones of the PPL, obtained directly and by adding WAs. 4.5-mm pupil diameter.

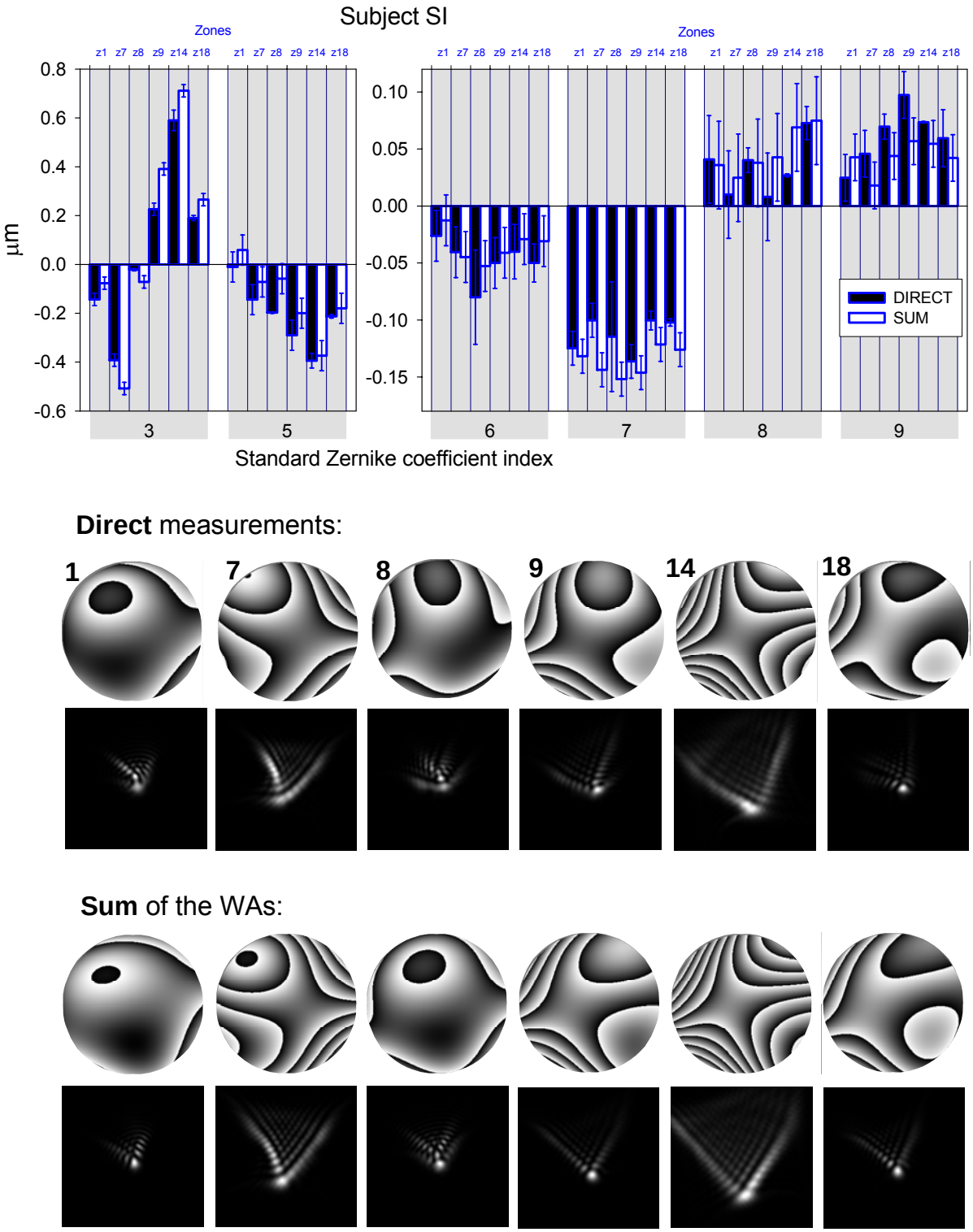

Figure 53. Comparison of optical quality (Zernike coefficients, and WA and PSF maps) of the eye of subject SI in combination with six zones of the PPL, obtained directly and by adding WAs. 4.5-mm pupil diameter.

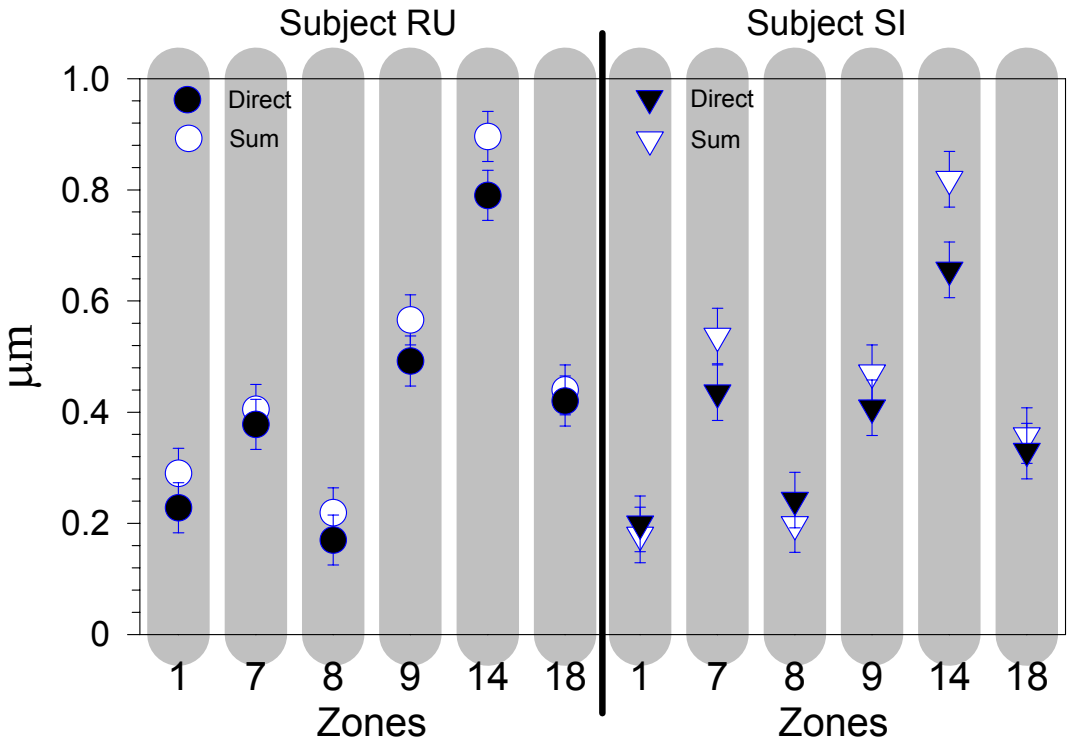

Figure 54. RMS of the eyes RU and SI looking through the six zones of the PPL, by measuring directly the WA (black symbols) and adding eye and zone of the lens WAs (white symbols). 4.5-mm pupil diameter.

In the following, to have a testing of lenses plus eye faster and more comfortable, we propose to obtain the WA of the entire system by adding WAs of the eye and those obtained for different zones of the lens. In this way, determining the aberration of the system only requires measurements of the eye and the zones of the lenses independently. We have compared this approach with results directly obtained from direct measurements on the eye plus the lens, for six relevant zones of a PPL. In general, as figures 52, 53 and 54 show, the difference between the measured and calculated methods is smaller than errors bars. However, some sources of error could affect this approach. Errors in lens alignment and/or lens tilt. Eye movements can produce small displacements in the location of the lens with respect the eye. In addition, for zones of the lens with high prismatic deviation that have to be tilted to replicate the normal viewing conditions, the prism compensator may be too separated from the selected zone, causing additional small aberrations because of a too oblique incident beam. When the vertex distance between the lens and eye is zero, the results from adding the WAs of both elements should equal the results from direct measurements. As the vertex distance increases, the predicted results by adding WAs will not be exact, due to the wavefront propagation along this distance. As expected, the

conventional vertex distance of 14-mm is small enough to produce substantial differences between the two approaches.

Since coma and trefoil are also common in the human eye, the aberration coupling between eye and lens may produce different values of these aberrations. It has been reported that aberration compensation is also present in normal young eyes, where corneal and crystalline lens aberrations tend to partially compensate [Artal *et al.* 2001]. A somehow similar situation may happen in some lens zones, the aberrations of the lens may be compensated by the particular aberrations of the eye yielding an improved optical performance than that present in the lens alone. For example, when subject SI looks through zone 18 of the PPL, the astigmatism of the lens is reduced by the small astigmatism of the eye due to the combination of Zernike coefficient 3 with opposite signs (see figure 51), which provides a lower RMS of the entire system (eye plus lens).

Chapter 5

RESULTS (II):

IMPACT OF ABERRATIONS OF PPLS ON VISUAL ACUITY

After the optical properties of PPLs have been measured, the relative impact of the aberrations present in this type of lenses on visual performance has been studied. In the following, we describe the procedure and results of measurements of VA in three eyes of different young subjects, when they are looking through the shadowed zones of figure 43 of the PPL (Varilux Comfort; Essilor International, with plano distance power, 2 D power addition). In this section we rename the selected zones of the lens with letters C, N and T to note the location (see blue notation in figure 43). So, zones in the corridor (1 and 8) are C1 and C2; nearby zones at 3-mm outside (7, 9 and 18) are N1 (in the nasal side), T1 and T2 (in the temporal side) respectively; and the other one 5.5 mm away from corridor in the temporal side (zone 14) is T3.

5.1 SUBJECTS AND EXPERIMENTAL CONDITIONS

VA was measured for the naked eyes and when looking through the different zones of the PPL. Accommodation was paralyzed and the pupil was dilated with two drops of tropicamide (1%) for each hour. The study followed the tenets of the Declaration of Helsinki, and signed informed consent was obtained from the subjects after the nature and all possible consequences of the study had been explained.

The VA measurements were taken with two different artificial pupil diameters: 4.5 and 3 mm. Two different contrast values, 100% and 15%, were measured.

The left eyes of three normal male subjects were measured. From HS measurements, their refractions were estimated:

MA (29 year old): -2.50 –0.25 × 50º

JO (26 year old): +0.60 –0.60 × 20º

EL (29 year old): -1.50 –0.20 × 100º

The low amounts of ocular astigmatism were not compensated to study the coupling with the astigmatism of the PPL and its influence on the visual performance. The largest value of astigmatism of our subjects (0.60 D) is inside the tolerable interval of astigmatism proposed in many previous studies. All subjects had a spherical corrected decimal VA better than 1.

During the procedure of VA measurements, the selected zone of the lens was carefully positioned using the laser beam. The axial position and the centration of the natural

pupil was controlled with the CCD video camera, and the subject had to see the laser beam on the center of the visual test.

5.2 VISUAL ACUITY THOUGH RELEVANT ZONES OF THE PPL

VA measured with naked eyes and looking through the selected zones of the PPL is presented in figure 55.

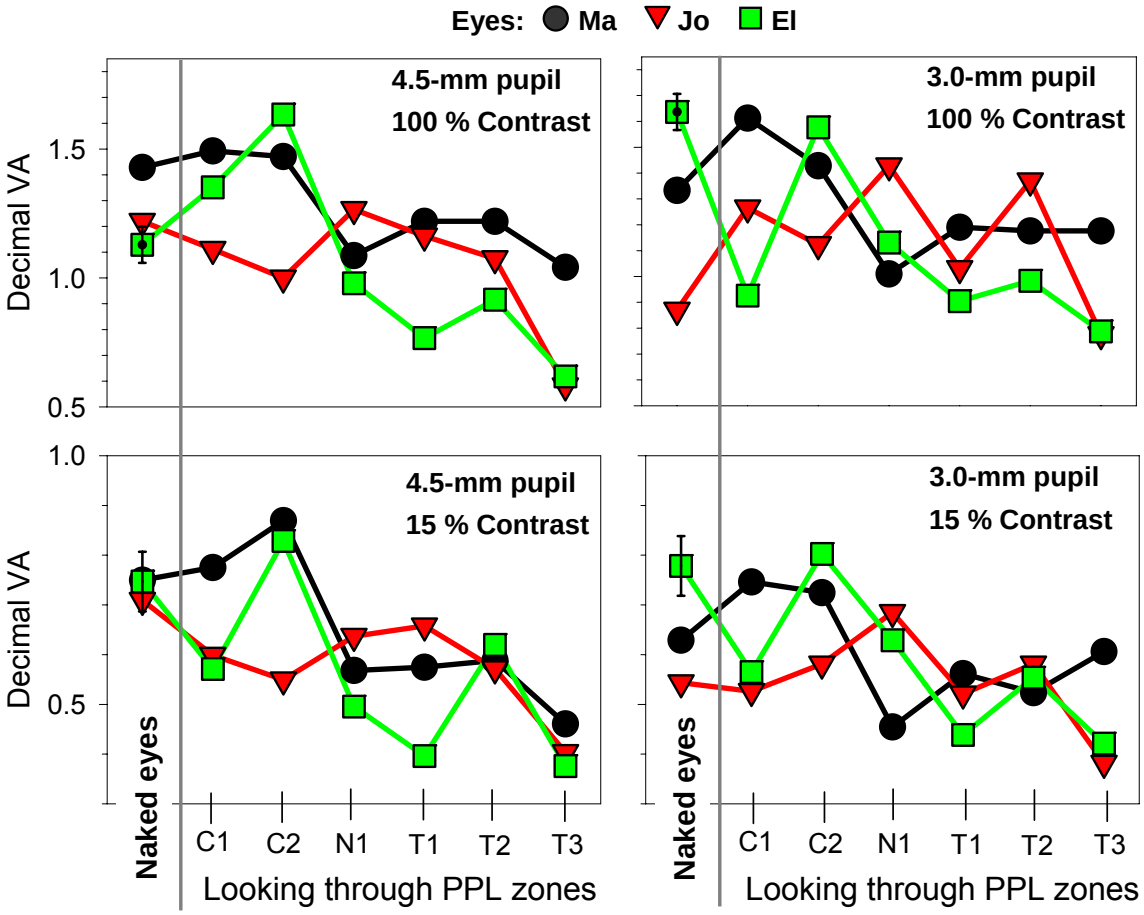

Figure 55. . Decimal VA of the eyes, both isolated and when looking across the six zones of the PPL. Experimental errors are equal or lower than the bars presented in the naked eye of the subject El.

As expected, VA for 100% contrast value is better than for 15%, but the behaviour in the different locations of the lens is similar for both contrast values. We have not found significant differences between the results of both pupil sizes. The visual quality when the eyes are looking through the corridor areas of the PPL is similar to those of the naked eye, even in some cases better. In these zones, high and low contrast VA ranges between 0.9-1.65 and 0.55-0.85 respectively. In general, the visual degradation is not so important in the

zones nearer to the corridor (locations N1, T1 and T2), although the behaviour depends on subject. For subject JO, VA is only decreased by the high astigmatism in zone T3. The high contrast VA of subject MA remains very stable in all zones. The larger changes from corridor to peripheral zones are present in the low contrast VA of subject MA and in both contrast values of subject EL. All results of high contrast VA at locations 3 mm (N1, T1 and T2) and 5.5 mm (T3) away from the corridor ranges between 0.75-1.4 and 0.55-1.20 respectively. The values for low contrast VA ranges between 0.40-0.65 and 0.35-0.60. In every case, the experimental error, expressed by standard deviation, is equal or lower than 0.07. In the figure 55, this maximum error bar is presented in the naked eye of the subject EL.

Figure 56 shows the average results of VA for every tested condition compared with the range of intersubject variability (standard deviation) of the eyes without lens. VA decreases moderately from the corridor to the peripheral zones. VA through the corridor and in nearby zones is similar or slightly lower than that found in eyes without lens. The abrupt change is observed from 3 to 5.5 mm outside locations. No important differences are found between high and low contrast VA. In the case of 3-mm pupil size, VA remains more stable for all zones.

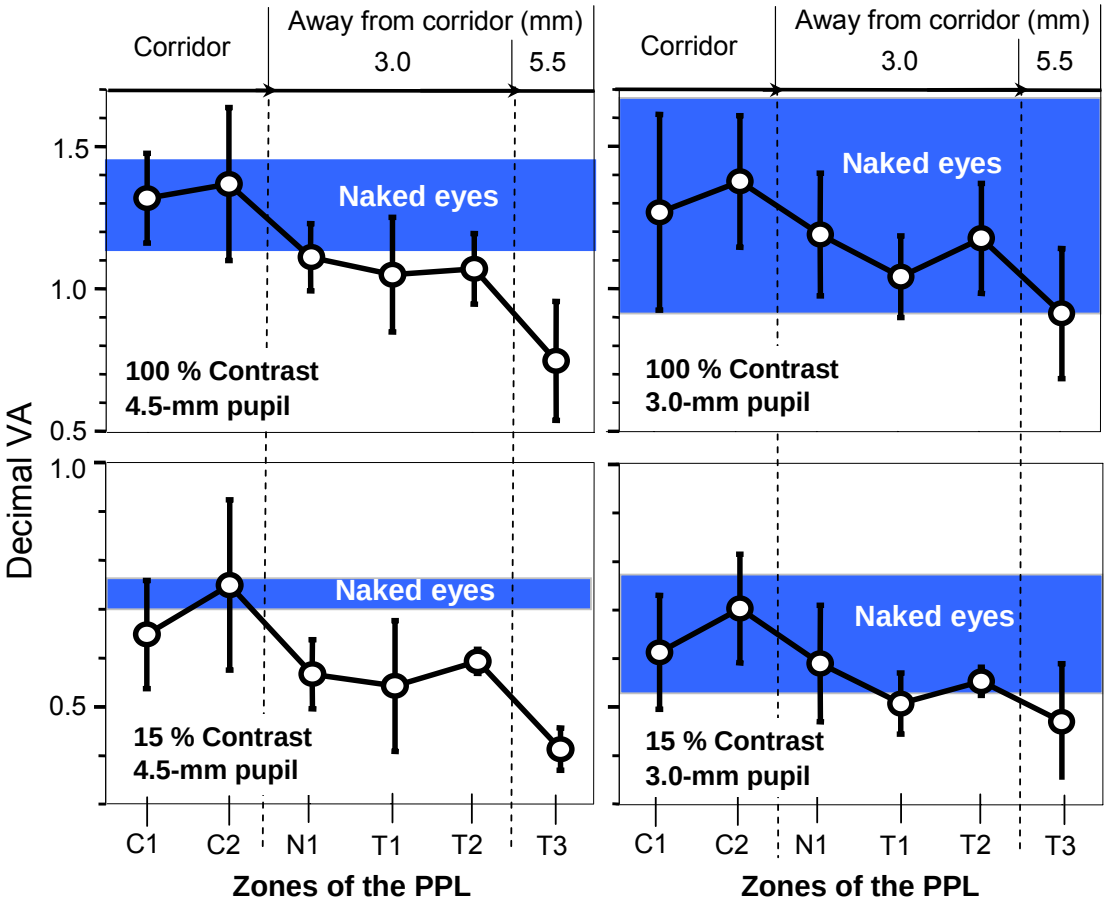

Figure 56. . Average VA of the eyes with the PPL in comparison with range of intersubject variability (standard deviation) of the eyes without lens for every pupil diameter (4.5- and 3-mm diameter) and contrast value (100% and 15%).

Chapter 6

RESULTS (III):

VISUAL ACUITY AND OPTICAL PARAMETERS

Psychophysical estimates, such as visual acuity (VA) and contrast sensitivity function (CSF), are quite useful for evaluating both visual performance and possible adaptation problems in PPLs. However, obtaining accurate visual measurements for different conditions is time-consuming and requires the collaboration of the subject. In order to predict visual performance, optical tests are commonly made in isolated lenses, but the image quality on the retina is due to the entire system eye with lens. In the current section, we study the correlations between different optical parameters and VA results, taking into account both the isolated lens and in combination with eyes. From these linear correlations, we obtain the optical parameter which better predicts visual performance in PPLs. Furthermore, the visual tolerance to optical aberrations in this kind of lenses is also studied.

The subjects and the experimental conditions have been described in chapter 5.

6.1 OPTICAL METRICS

In this section, firstly we described the parameters used to evaluate optical quality. The values of these parameters were estimated in the tested eyes and in the selected zones of the PPLs, both independently and in combination. The relation between the different optical parameters is discussed in other paragraph.

6.1.1 Description of optical metrics

In addition to the RMS, three other optical parameters were also computed from PSF´s: (1) the Strehl ratio, (2) the natural logarithm, or logarithm to the base e, of the Strehl ratio (Ln_Strehl_R.), and (3) the common, or base 10, logarithm of the volume under the PSF when the maximum was normalized to one (Log_Vol_PSF). The Strehl ratio was strictly computed as the quotient between the intensity peak in the system´s PSF and the diffraction-limited PSF. The volume of the PSF was calculated by adding the intensity of each pixel of the image when all intensity values were normalized between 0 and 1. This parameter is similar to that used with double-pass images [Villegas *et al.* 2002]. In figure 57, we can see a schematic representation on the parameters used to evaluate the optical quality of PPLs.

Although all metrics were obtained from WA, the RMS was calculated from coefficients of the wave aberration on pupil plane while the parameters from PSF (Strehl ratio and Log_Vol_PSF) give direct information on retinal image quality.

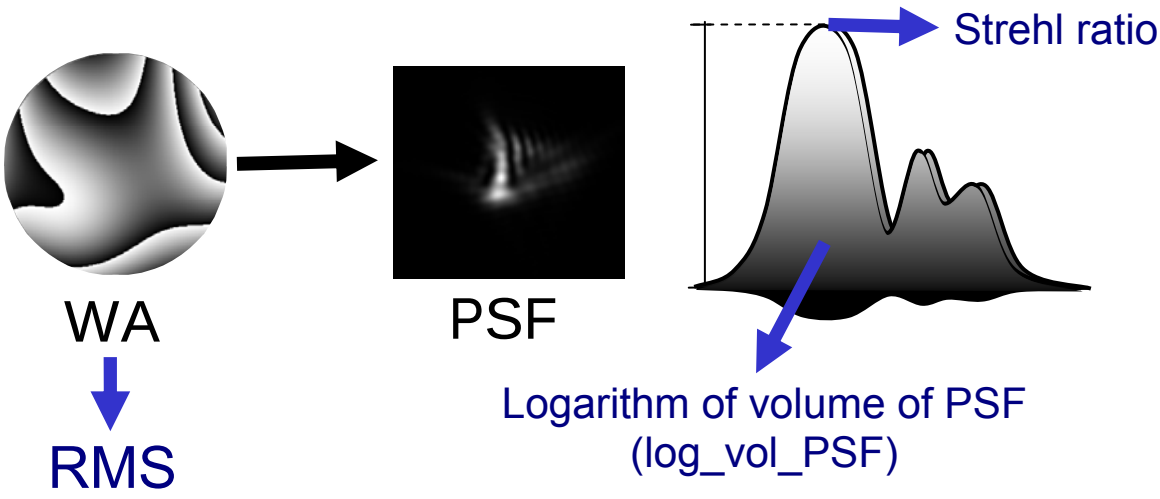

Figure 57. Schematic representation of optical parameters.

6.1.2 Optical quality across relevant zones of the PPL

In order to better understand the optical behavior in each case, the WA and PSF maps for the six tested zones of the PPL, the naked eyes and the zones of the lens plus eyes are shown in figure 58. PSF maps were calculated on the image plane where defocus was zero. In the locations of the corridor, C1 and C2, the ocular aberrations deteriorate the image quality significantly more than those of the lens. In zones of the PPL outside the corridor, astigmatism increases and becomes the dominant aberration. However, the small amount of coma produces a higher intensity at the bottom of the PSFs. For all locations, the different shapes of the WAs and PSFs depend on the aberrations coupling between eyes and PPL zones. For example, for eye JO at N1, the WA map shows a very aberrated system, but the PSF intensity is mainly concentrated in a small area. Figure 59 shows the Zernike values for the zones of the lens. We only show up to fourth order because for fifth order, the values of the coefficients were negligible. Small amounts of astigmatism (Zernike coefficients 3 and 5), coma (coefficients 7 and 8) and trefoil (coefficients 6 and 9), around 0.05 microns each one for 4.5-mm pupil diameter, were found in areas of the corridor of the PPL. In the other peripheral locations, astigmatism increases while coma and trefoil remained within the same small values as in the corridor. The other higher aberrations of the isolated PPL are negligible for every location. Zernike coefficients of the three eyes are presented in the same figure to be compared with those of the lens. The magnitude of coma and trefoil in the eyes is similar to those in the different zones of the lens. The higher aberrations are also nearly negligible, except the spherical aberration (coefficient 12) of subject JO. The ocular values of astigmatism are similar to those of the corridor and nearby zones of the PPL.

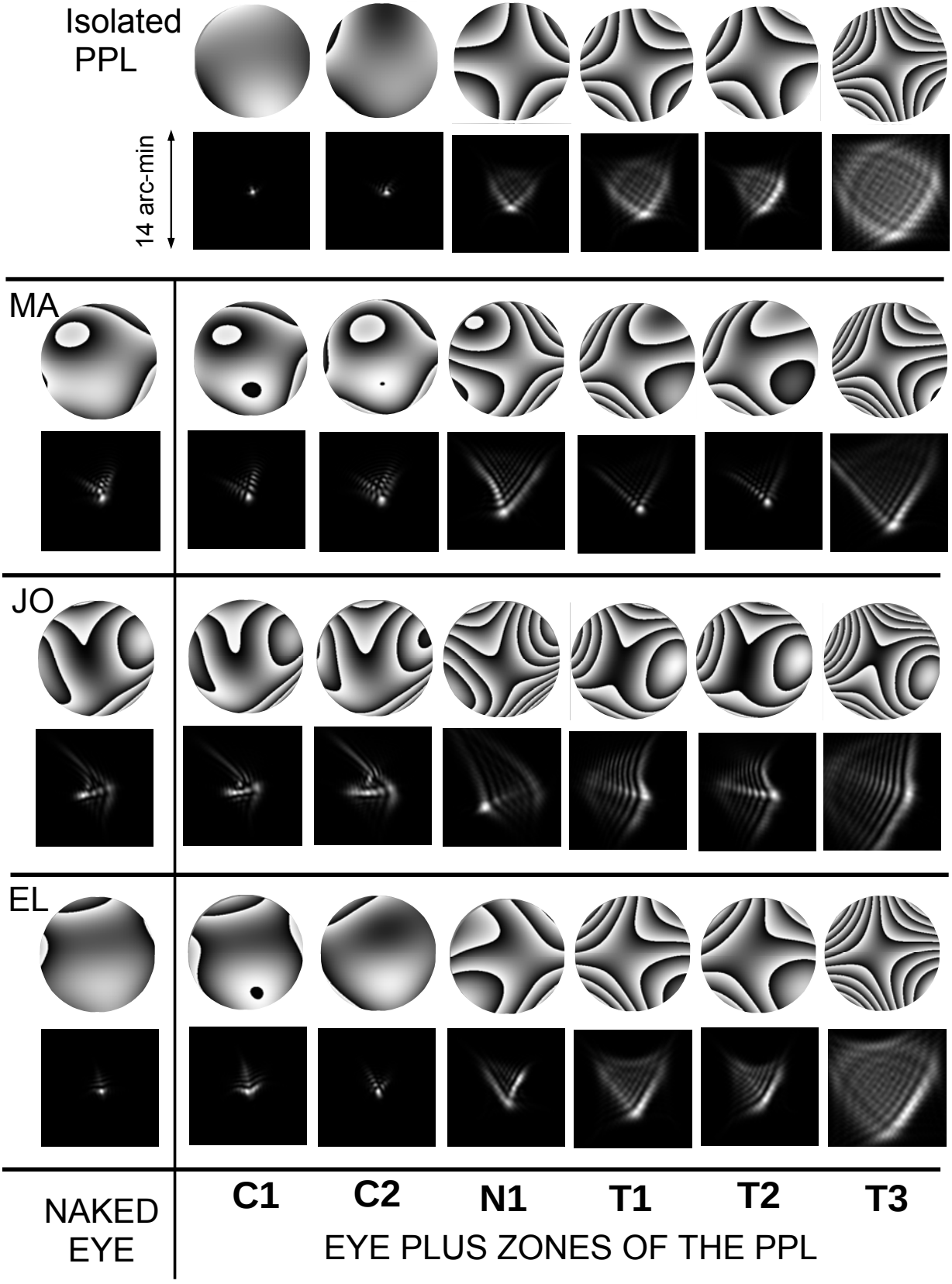

Figure 58. A modulus 2π representation of the WA and the associated PSFs of the naked eyes and the six tested zones of the PPL, measured independently and in combination by adding WAs. Defocus Zernike coefficient set to zero. 4.5-mm pupil diameter.

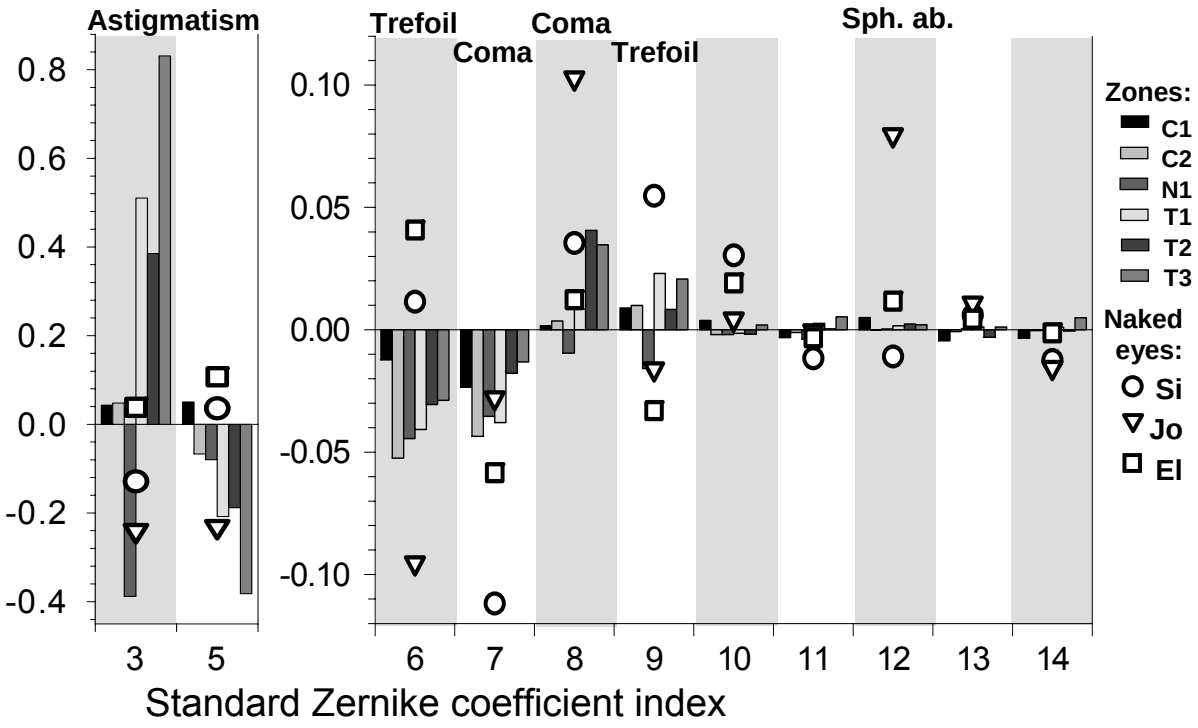

Figure 59. Zernikes coefficients of the naked eyes and the six zones of the isolated PPL, to be compared between them. 4.5-mm pupil diameter. The Seidel aberrations corresponding to Zernike coefficients are shown on top of the graph. The scale of astigmatism in microns can be transformed in diopters by multiplying by 1.94.

Figure 60 presents the optical metrics (RMS, Strehl ratio and Log_Vol_PSF) of the three eyes without lens and in combination with the six zones of the PPL, for 4.5-mm pupil diameter. For the small pupil, 3.0-mm diameter, the optical quality is better but the relative performance is similar to that shown for 4.5-mm pupil. The optical parameters have been calculated taking into account all aberrations (up to fifh order) except defocus (coefficient 4). Although, all metrics show that the optical quality is worse in peripheral locations of the lens mainly due to the increase of astigmatism, there are significant differences between the three metrics. For example, the optical quality of eye JO expressed by Log_Vol_PSF or by Strehl Ratio progressively decreases from naked eye to zone T3, while RMS shows an abrupt change in zone N1.

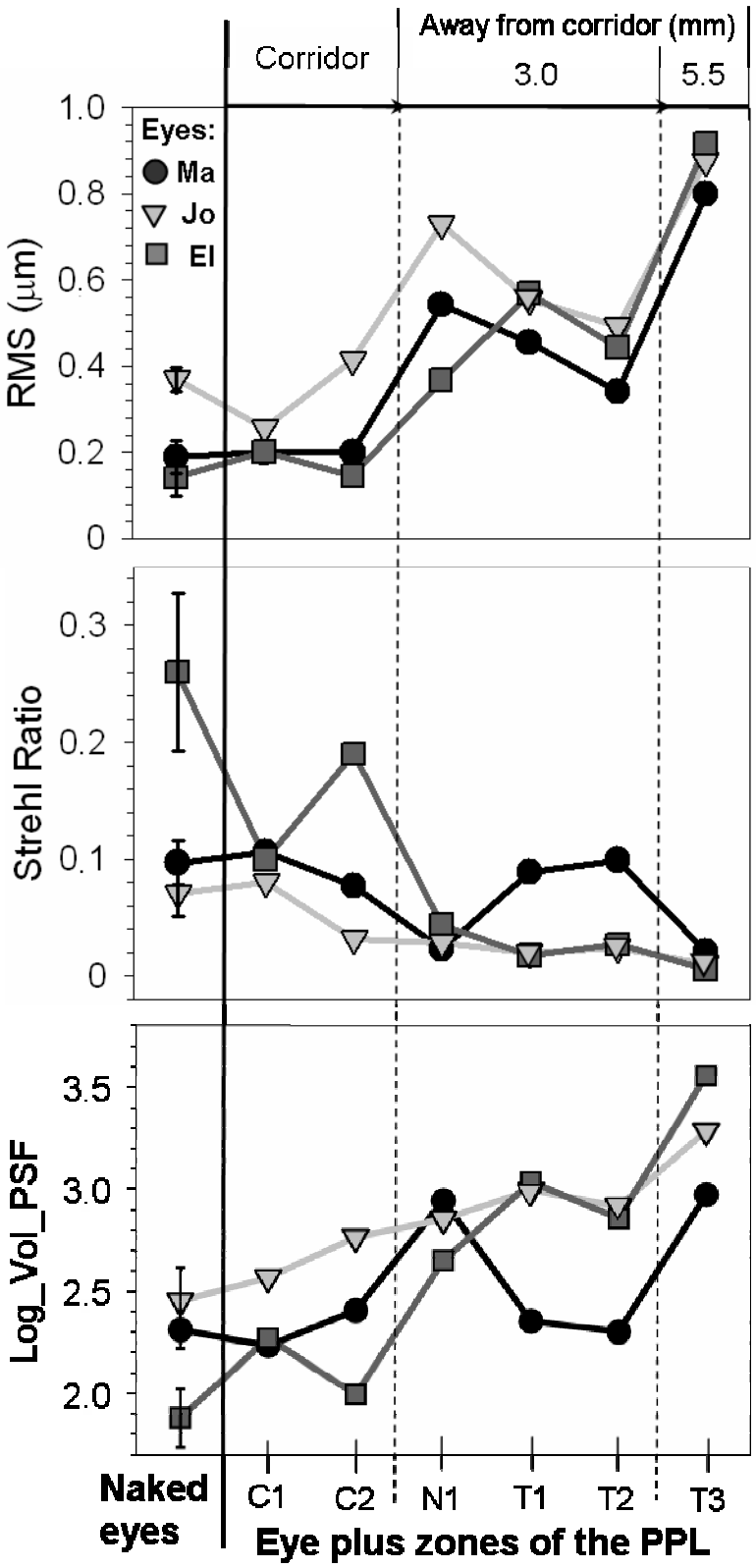

Figure 60. Optical parameters (RMS, Strehl ratio, Log_Vol_PSF) in the naked eyes and in combination with the six zones of the PPL. 4.5-mm pupil diameter.

As we will show in the section on correlations, the Log_Vol_PSF is the optical parameter that gives the highest correlation coefficient for the entire system eye plus lens, and in particular for 4.5-mm pupil size and 100% contrast VA (see figure 64). For this reason, we chose the metric Log_Vol_PSF for comparing the average optical quality of the eyes plus PPL with the lens alone and with the range of intersubject variability (standard deviation) of the naked eyes (figure 61). The optical quality of the isolated PPL decreases very fast from corridor to peripheral zones. However, the combination of the aberrations of the eye and the progressive lens reduces the relative differences of optical quality between central and eccentric zones. The aberration coupling reduces the optical quality in the corridor, while the peripheral areas remain the same or even improve with respect the PPL alone. The optical quality of the eyes through the zones of the corridor is in the range of variability of the eyes without lens. The corridor zones of the isolated PPL produce better optical quality than the naked eyes.

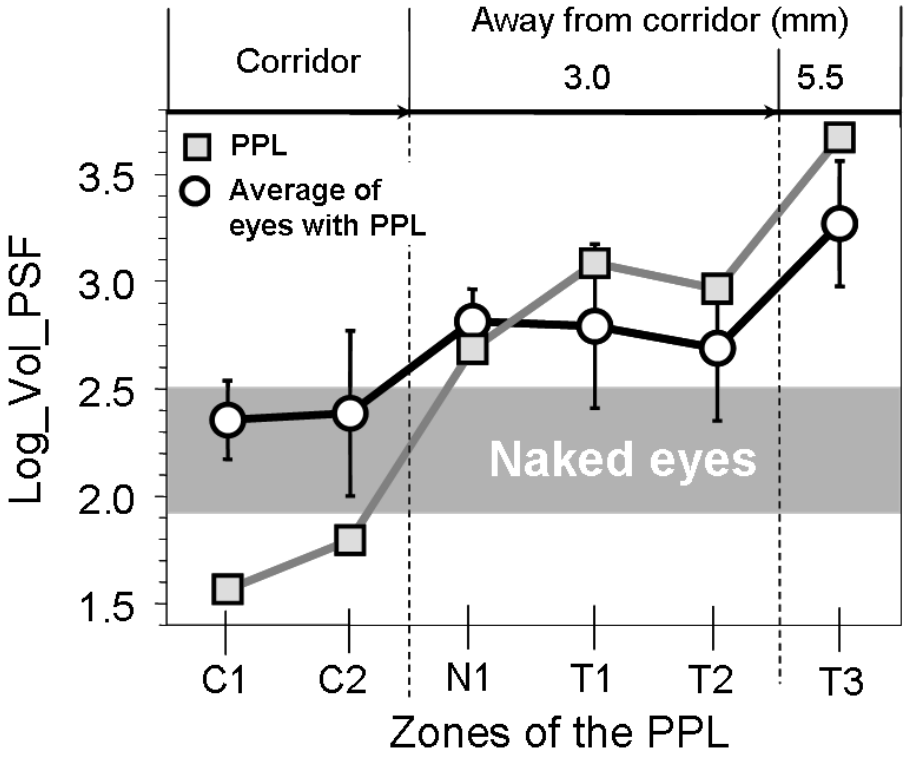

Figure 61. Optical quality expressed by Log_Vol_PSF of isolated PPL and average of the eyes with the PPL, in comparison with the range of intersubject variability (standard deviation) of the eyes without lens. 4.5-mm pupil diameter.

6.1.3 Relationship between optical parameters

Previously to study the correlations of optical metrics with VA, we analyze the relationship between optical parameters. Strehl ratio and RMS are commonly used to

evaluate the whole performance of optical systems. RMS and low Strehl ratio values denote a poor optical quality. But, only for small aberrations, several equations have been derived to express the relationship between both. [Mahajan 1982] proposed an exponential prediction of the Strehl ratio (SR) from RMS:

$$SR = \exp\left[-\left(\frac{2\pi}{\lambda} RMS\right)^2\right] \tag{16}$$

where λ is the wavelength. But, this equation gives the Strehl ratio with less than 10% error as long as Strehl ratio is equal or larger than 0.3, that means a RMS equal or lower than 0.1 μm. As alternative, for RMS between 0.1 and 0.2 μm, we propose a similar expression without the square:

$$SR = \exp\left[-\left(\frac{2\pi}{\lambda} RMS\right)\right] \tag{17}$$

Figure 62a shows the correlation of all our values of RMS and Strehl ratio, calculated in the isolated PPL and in combination with the three subjects, for both pupil sizes. The predictions from exponential equations 16 and 17 are also presented. As expected, the Strehl ratio values higher than 0.3 are well predicted by Mahajan equation. Lower values are better fit by equation (17) (R-squared values 0.92), but the prediction is worse for RMS values larger than 0.2 μm (Strehl ratio lower than around 0.15) because of the Strehl ratio values are randomly distributed. This behavior can be better seen when considering the natural logarithm of Strehl ratio in figure 62b. On the other hand, both optical parameters calculated from PSF, Ln_Strehl_R. and Log_Vol_PSF, are very nearly related. In the image plane, the intensity peak varies inversely proportional to the image spread. This means an inverse linear relationship between Strehl ratio and the volume of the PSF normalized to one, which results in a perfect linear correlation of Ln_Strehl_R. and Log_Vol_PSF values, figure 62c. These parameters are related by this expression:

$$\ln\_Strehl\_R. = 2.3(\log\_A - \log\_Vol\_PSF) \tag{18}$$

where A is the Vol_PSF when the Strehl ratio is 1. In our estimations, the value of A is 19.

Thus, the linear correlation coefficients of the visual acuities with Ln_Strehl_R. and Log_Vol_PSF values are equal. Thus, in the following sections we only use the Log_Vol_PSF.

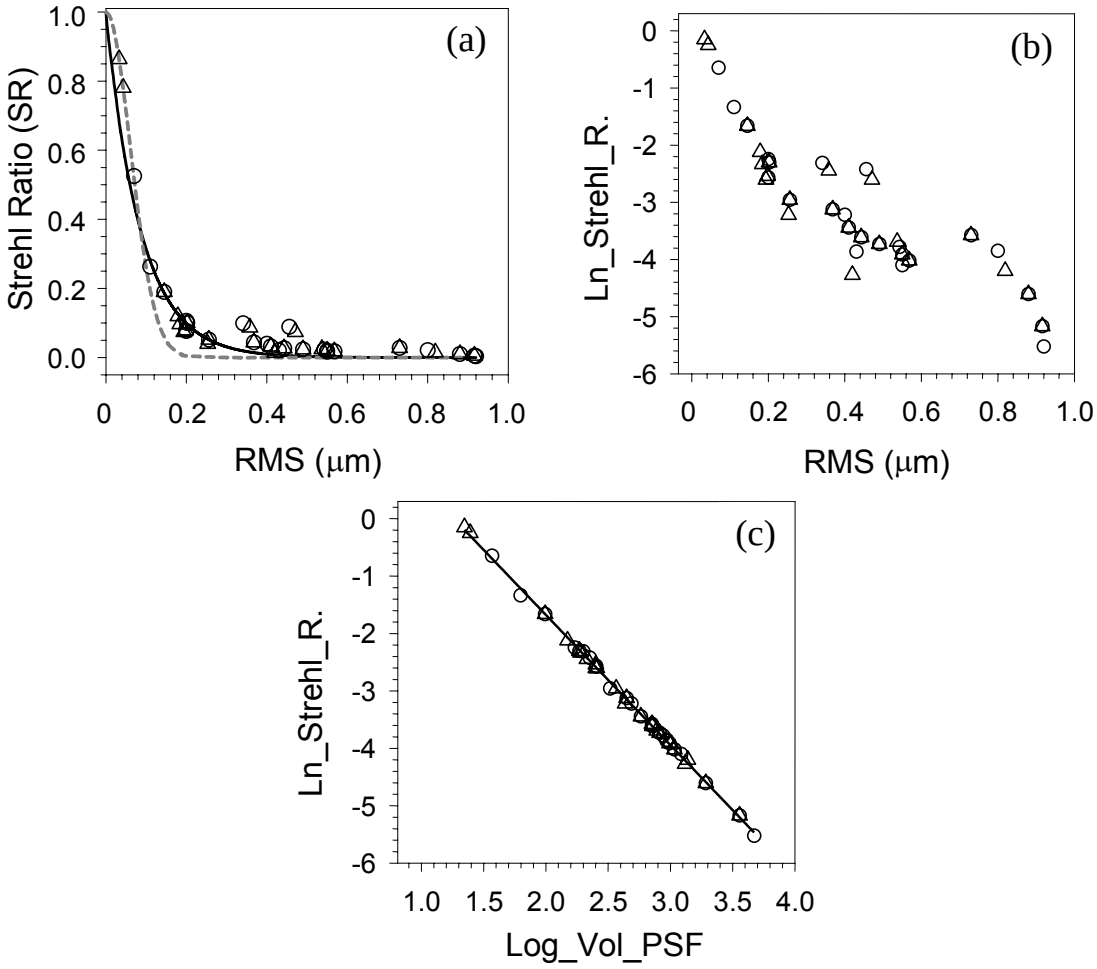

Figure 62. Relationship between optical parameters calculated for 3.0- (triangles) and 4.5-mm (circles) pupil diameters. Strehl Ratio versus RMS with predictions from Mahajan (dashed line) and our fitting (solid line) equations (a). Ln_Strehl_R. versus RMS (b). Perfect linear correlation of Ln_Strehl_R. and Log_Vol_PSF (c).

6.2 CORRELATION OF VISUAL ACUITY AND OPTICAL METRICS

The study of correlations between values of visual acuity and optical measurements allows to obtain the optical parameter which best predict visual performance. These relationships also would permit to analyze the visual tolerance to optical aberrations.

Figure 63 shows the relationship between VA, for both low and high contrast, and optical parameters (RMS, Strehl Ratio, Log_Vol_PSF and astigmatism) of the isolated PPL

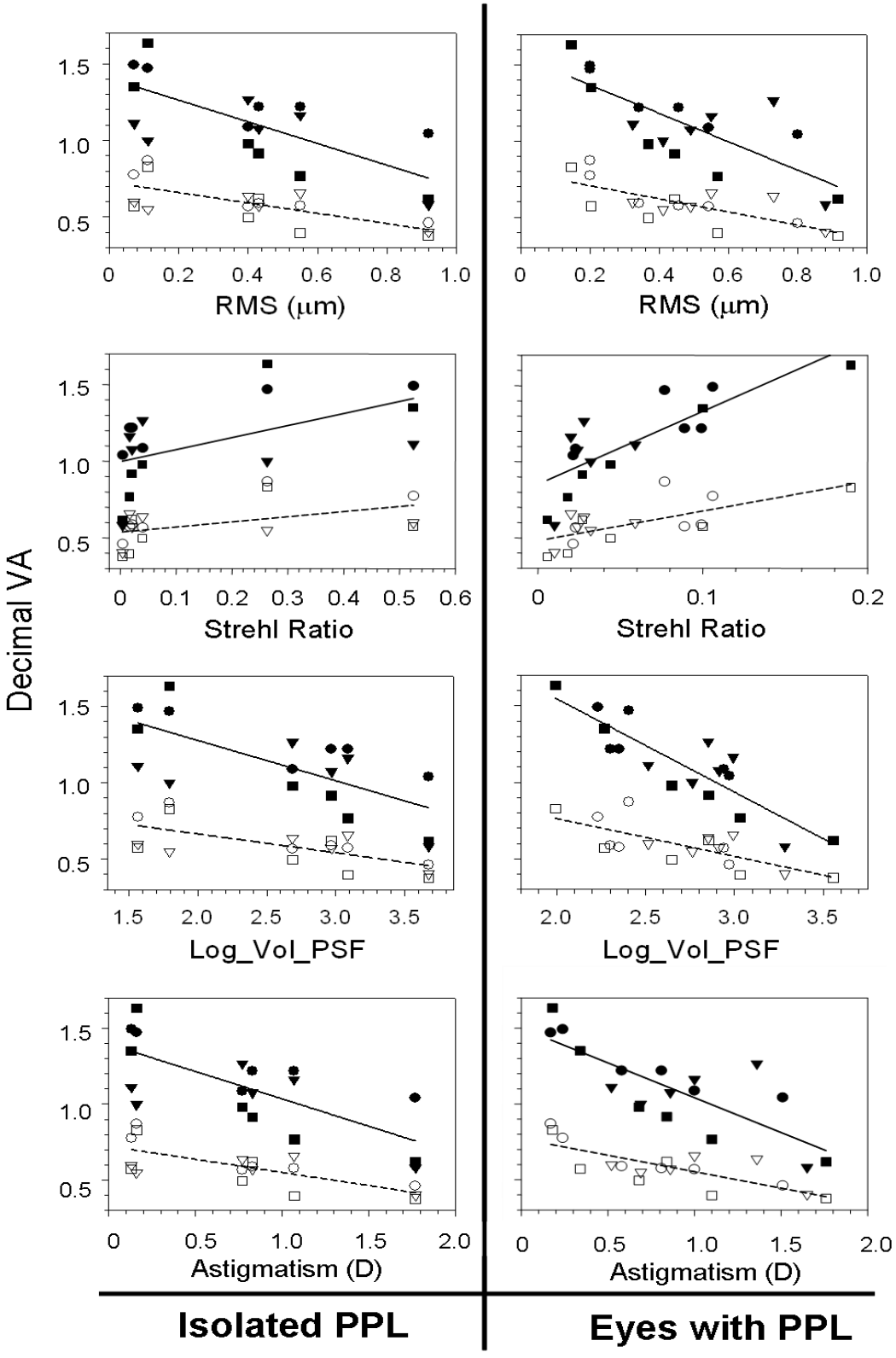

Figure 63. Correlation between optical parameters (RMS, Strehl ratio, Log_Vol_PSF and astigmatism) and all VA data of the subjects, eye MA (circles), eye JO (triangles) and eye EL (squares), taking into account only the WA of the PPL (Isolated PPL) and adding the WAs of the eyes and the lens (Eyes with PPL). VA and linear regression for both values of contrast: 100% (black symbols and solid lines) and 15% (white symbols and dashed lines). 4.5-mm pupil diameter.

and in situ (PPL plus eye), taking into account all results of the three subjects. These graphs are for 4.5-mm pupil diameter, since results of 3.0-mm pupil size show worse linear correlation coefficients. The solid lines are the linear fitting for 100% contrast VA and the dashed lines are the linear fitting for 15% contrast VA. The parameters RMS, Strehl Ratio and Log_Vol_PSF have been estimated from whole WA (except defocus). Linear correlations are better for the whole system eye with lens. VA versus Log_Vol_PSF shows all experimental values very close to the linear fitting.

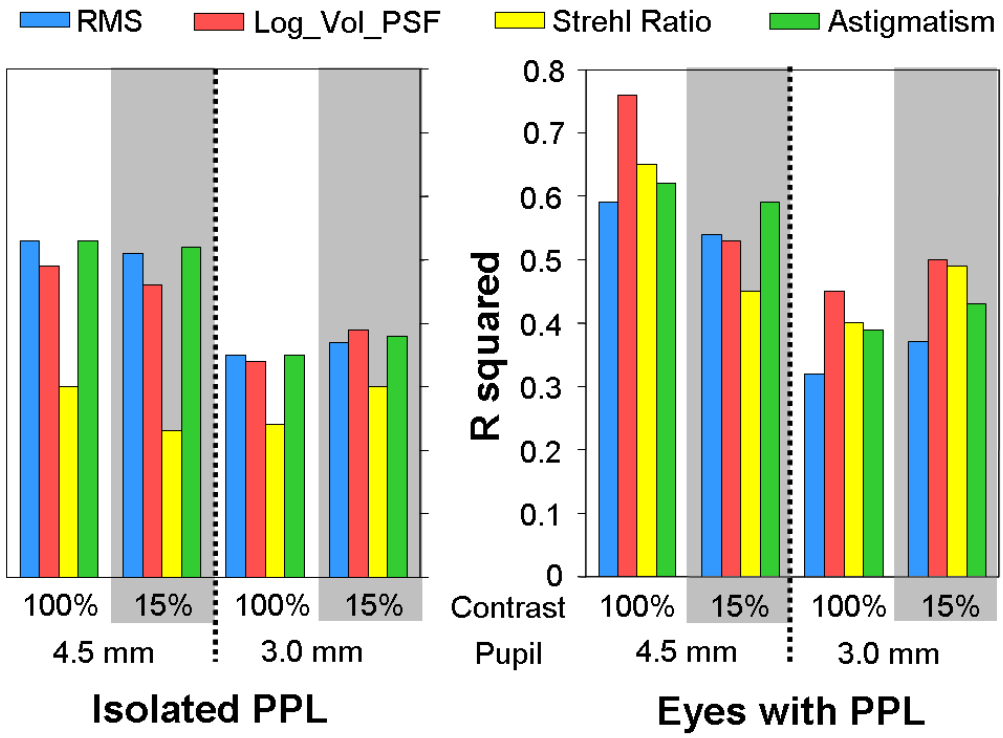

Figure 64. R-squared coefficients of the linear correlations between visual acuity data of the three subjects and optical metrics, considering only PPL and the complete system eyes plus PPL

In the statistical analysis, we calculated linear R-squared coefficients and p-values for all combinations of optical parameters and VA (figure 64). All optical metrics obtained from complete WA (with astigmatism and high order aberrations) are significantly correlated with VA ($p < 0.05$). However, there are important differences in the R-squared values. The parameters calculated from whole WA of the system eye plus lens correlate better than those of the lens alone. In general, when comparing results of both pupil diameters, better correlations are found for the larger pupil size. Considering only the PPL, Strehl Ratio presents the lowest correlation values (R-squared equal or lower than 0.3, $p > 0.02$). VA is relatively well correlated with RMS, Log_Vol_PSF and astigmatism of the isolated PPL (R-squared values around 0.5 for 4.5-mm pupil, $p < 0.002$). As expected, the majority of correlation values are higher when considering the entire system lens plus eye. In the cases

of 4.5-mm pupil and 100% contrast VA, all optical metrics have high values of correlation around 0.6 or higher ($p < 0.0002$), and in particular, the best correlation is produced by the parameter Log_Vol_PSF (R-squared equal to 0.76, $p < 0.0001$).

On the other hand, we have also studied the relationship of VA and Log_Vol_PSF taking into account only high order aberrations (astigmatism and defocus set to zero) for the entire system eye with the lens. But we have found any correlation between them, with linear R-squared coefficients below 0.2 for all cases, and p-values larger than 0.1.

6.3 PREDICTION OF VISUAL PERFORMANCE FROM OPTICAL PARAMETERS

In the process of designing a PPL, it is very advantageous to be able to predict visual performance from optical parameters. Thus, designers can a priori know the level of acceptance and satisfaction of the future users of the PPL. Many theoretical and empirical previous works have studied the optical quality and visual performance of progressive-power lenses. However, as far as we know, we have not found results on optical parameters that correlate better with psychophysical measurements in this kind of lenses for presbyopes. From our results of correlations between optical parameters and visual acuity, a main goal of our work has also been to find the optical parameter that better predicts the visual quality.

We have studied four optical parameters calculated from WA, two directly from WA (RMS and astigmatism) and two from PSF (Strehl Ratio and Log_Vol_PSF) for two pupil sizes, 4.5- and 3.0-mm diameters. In general, for the smaller pupil, the correlation values are worse, due to the reduction of the effect of aberrations. When considering the PPL alone, except Strehl Ratio, all optical parameters give similar values of correlation. It is well-known that Strehl Ratio is not a convenient image quality descriptor for high values of aberrations [Villegas *et al.* 2002]. Our results show good correlation values for the Strehl Ratio of the complete system eye plus lens, because the aberrations are not too high. However, as shown in figure 64, for the entire system PPL with the eye the parameter Log_Vol_PSF is the most adequate.

In summary, the logarithm of metrics directly related with image spread (Log_Vol_PSF, Ln_Strehl_R or equivalent) predicts slightly better VA than the RMS. This is in accordance with previous results [Villegas *et al.* 2002] that show a good linear correlation of the logarithm of the volume under the double-pass image normalized to one and VA measurements in presence of defocus. However, in addition to image spread, the shape of the image possibly also influences in the quality of vision [Applegate 2003, Fernandez 2002].

For instance, when eye JO is looking through the PPL, the Log_Vol_PSF is very similar in all zones, but in the zone N1 the PSF is very concentrated in a small circle (see figure 58). In this particular case, these optical conditions produce a high VA, 1.25 for high contrast and 4.5-mm pupil diameter.

6.4 VISUAL TOLERANCE TO OPTICAL ABERRATIONS

The effect of different wavefront aberrations on visual performance and the tolerance thresholds in visual ocular system is an important issue for researchers on visual optics. In particular, the tolerance limits of astigmatism and defocus have been widely studied for evaluating the visual quality and the acceptance of progressive-power lenses. However, the tolerance to other aberrations present in PPLs has still not been considered. In previous works, [Maitenaz 1967] regarded 0.3 D to be the tolerable limit of astigmatism, Davis assumed 0.5 D and Shinohara and Okazaki proposed values up to 1 D to be acceptable. In recent experiments done in our laboratory [Villegas *et al.* 2006, Villegas *et al.* 2008], in most subjects, visual acuity after correction of small amounts of astigmatism (lower than 0.5 D) did not improve. Sullivan and Fowler [Sullivan and Fowler 1989(b)] measured the grating VA eccentrically from a midpoint on the umbilical line of three PPL´s (2.00 D near addition), in a single subject. For all lenses, in eccentricities less than 10 degrees where the maximum astigmatism was around 1.5 D, VA was better than 1. Our results show a VA equal or better to 1 as long as total astigmatism (lens in combination with eye) is lower than 0.90 D (0.46-μm RMS). This value corresponds approximately to that in zones N1 and T1 (around 6 degrees of eccentricity).

In the works of Atchison [Atchison *et al.* 1997] and Marcos [Marcos *et al.* 1999] the values of tolerance to defocus (expressed as the half of whole range for which the target appears unchanged) were similar, around 0.50, 0.30 and 0.25 for 2-,4- and 6-mm pupil diameters. [Campbell 1957] suggested 0.215 D to be the limit of defocus for 3-mm pupil. In recent studies, [Atchison *et al.* 2005] reported a noticeable blur limit of 0.3 D for 4-mm pupil size and letter size of 1 arc-min. [Ciuffreda *et al.* 2006] also included presbyopes in their work, and they obtained a detectable blur threshold around 0.5 D for 5-mm pupil diameter and letter size of 2.5 arc-min. In our experiments, we estimated the defocus error as the difference between predicted from adding ocular refraction plus lens power and that measured directly by the focus corrector system with eye looking through the lens. Although there was a large variability in results (from 0.05 to 0.60 D), the average defocus error of

0.20 D (for 4.5-mm pupil diameter and smallest letter size that subject was able to read) is in concordance with previous outcomes.

Coma and trefoil are other aberrations also present in PPLs. In a recent work, Applegate [Applegate *et al.* 2003] showed that values of trefoil lower than 0.2 μm didn't decrease high contrast VA. In our study, the combination of similar amounts of coma, trefoil and astigmatism (total RMS around 0.1 μm) of the corridor of the PPL have a very small effect on visual performance independently of pupil size and letters contrast.

6.5 EFFECT OF FOCUS ERRORS ON OUR RESULTS

In our experiments, VA measurements were taken at best subjective focus, and the optical measurements were processed for defocus set to zero. Thus, we supposed a perfect response of the accommodation to changes in target vergence. In natural conditions, the high order aberrations, and in particular spherical aberration, may influence in the stimulus/response relationship [Plainis *et al.* 2005, Buehren and Collins 2006]. Furthermore, accommodation can produce small changes in the ocular aberrations, specially in the spherical aberration [Cheng *et al.* 2004, Artal *et al.* 2002(b), He *et al.* 2003]. The error in focus and the changes of high order aberrations increase progressively with the amount of accommodation. However, in the case of presbyopes, the small amounts of residual accommodation may only produce very small changes in defocus and in other aberrations.

On the other hand, it is commonly assumed that the optimum defocus that maximizes the optical quality should yield the best subjective focus [Thibos *et al.* 2004]. In our computing process, we also calculated the correlations of VA and the optical parameters on the image plane (Strehl Ratio and Log_Vol_PSF) where defocus maximized these parameters. The values of linear correlation coefficients were lower (0.44 for Strehl ratio, 0.51 for Log_Vol_PSF, with high contrast VA and 4.5-mm pupil diameter) than those obtained for defocus set to zero (0.65 and 0.76 respectively). This may be explained because, in some images, the maximum values were found in the plane of one of both Sturm foci or in nearby axial positions, far from the best subjective focus which was in or around the circle of least confusion.

Chapter 7

RESULTS (IV):

NEURAL ADAPTATION TO THE ABERRATIONS IN PPLS

Everybody talks about adaptation period to PPLs after dispensing. But what means adaptation? Adaptation could be defined as the adjustment to different conditions. PPLs are complex devices placed in front of the eyes which may change the visual behavior of subjects. The visual system undertakes several adjustments to optimize visual performance of PPLs. Two of these adjustments have been reported in former experiments: (1) the neural adaptation to distortion and (2) compensatory eye-head movements.

Due to the increment of power between far and near zones, the surface topography of PPLs change to achieve the correct blend between the different zones and it produces a distortion of extended objects [Jalie 2005]. During the first days of adaptation, the neural system seems to compensate this deformation. This adjustment is also produced in subjects with high myopia who are using spectacles. The negative lenses deform the extended objects in a barrel shape, but when a square grid is presented to a myopic subject corrected with spectacles, he perceives the grid perfectly square. This adaptation to the shape distortion was experimentally demonstrated by exposing subjects to photograhs of faces which appeared horizontally stretched by an arrangement of cylindrical lenses [O'Leary and McMahon 1991]. In another study, researchers showed that the adaptation to the three-dimensional distortion is caused by a change in the mapping between retinal disparity and perceived slant [Wendy *et al.* 2001]. In PPLs an additional problem to the distortion is the "swimming-effect", that is, when the subject moves body and head in normal viewing conditions, the movement of the distortion produces a swing of the field of view [Jalie 2005]. Although this effect is particularly troublesome when walking down stairs, subjects normally adapt to this problem during the first days or weeks wearing PPLs.

In relation to the eye and head movements, a study with 11 individuals showed different strategies depending on the lens used to read. For single vision lenses, subjects moved mainly the eyes, but for progressive lenses, the head movements were important, especially in a PPL with a narrower corridor [Han *et al.* 2003(a), Han *et al.* 2003(b)]. So, subjects adjust the eye and head movements to look through the optimal optical zone of the lens. To make easier the movements adaptation, in the last years, the main companies of ophthalmic lenses have commercialized PPLs with customized astigmatism distribution depending on eye and head movements before wearing lenses. For example, for turner eyes, the designs prioritize wider far and near areas [Jalie 2005].

As we have previously shown, PPLs present small amounts of coma and trefoil, in addition to astigmatism. The wavefront aberration varies spatially across the PPLs, and the wavefront of the entire system (eye plus lens) changes continuously due to the eye

movements to fixate objects. It is not clear whether the adaptation to PPLs also include the adaptation of the visual system to the optical aberrations of these lenses. Previous works [Mon-Williams *et al.* 1998, Villegas and Artal 2001] suggested a temporal adaptation to the continuous presence of defocus. Furthermore, other study proposed that the eye is adapted to its particular aberrations, because subjective blur when viewing a scene through one's own aberrations was less than that when the aberrations were rotated using an adaptive optics system [Artal *et al.* 2004]. These phenomena of neural adaptation might also play an role when patients adjust to PPLs. In this chapter, we address this problem by measuring visual acuity (VA) through different controlled areas of PPLs after subjects were adapted to the lenses during a period of up to one week.

7.1 SUBJECTS AND EXPERIMENTAL CONDITIONS

Four presbyopic subjects, who never previously had used PPLs participated in the study. Before beginning the experiments, the subjective refraction of every subject was determined. The "standard" times roman letters for testing the visual acuity in near vision [Duke 1993] was used to find the addition power for the reading distance. These are the refraction of both eyes and the age of every subject:

PA (43 years old): RE –1.50, LE –1.50, Ad 1.00 D
LS (47 years old): RE 0.00, LE 0.00, Ad 2.00 D
MO (50 years old): RE –0.50 –0.50 × 90, LE –1.50 –0.75 × 90, Ad 2.25 D
SP (51 years old): RE +0.50 –0.50 × 90, LE +0.25 –0.50 × 90 Ad 2.00 D

The PPLs were Varilux Panamic from Essilor (18-mm corridor length and 2.5-mm inset of the near vision) with the particular refraction and addition of each subject. We mounted the lenses in our workshop and the spectacles were dispensed assuming a pantoscopic tilt of 12º. For measuring the VA under controlled conditions, an identical lens for the left eyes was placed in our system (figure 30). VA of the left eyes was measured through three zones for intermediate vision of the PPL, all of them located 6-mm below the fitting cross. In figure 65, we can see the selected zones: within the corridor (C), 3 mm toward the nasal side (N), and 6 mm toward the temporal side (T). For three of the subjects (LS, MO, SP), VA was measured during the first week wearing the lenses: in the first day just before ever wearing the PPLs and after 2 and 7 hours, and 2, 4 and 7 days later. Measurements of subject PA were only taken during the first day.

VA for 100% contrast was measured using a force choice method described in the Methods chapter. Before beginning the measurements of VA, the best focus was determined subjectively with the Badal optometer, from a myopic position for minimizing the possible residual accommodation. Accommodation was not paralyzed and the pupil size was controlled with the CCD video camera. Every subject had around 4.5-mm pupil diameter.

The study followed the tenets of the Declaration of Helsinki, and signed informed consent was obtained from the subjects after the nature and all possible consequences of the study had been explained.

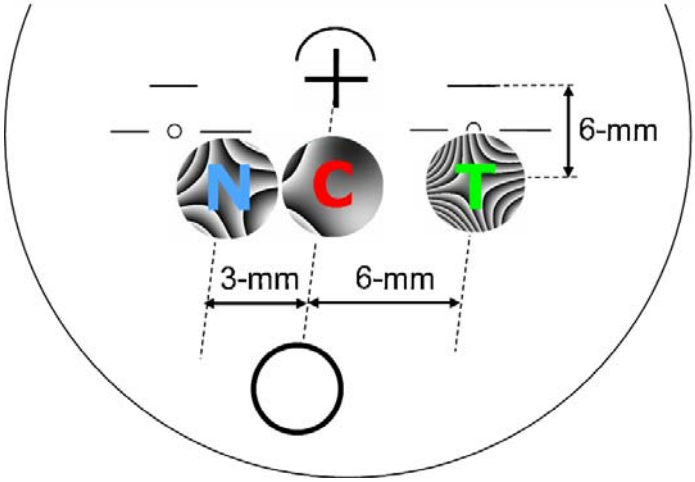

Figure 65. Selected zones to measure the neural adaptation to aberrations of PPLs with their corresponding WAs patterns for 4.5-mm pupil.

7.2 TEMPORAL EVOLUTION OF VA DURING A WEEK OF ADAPTATION TO PPLS

Figure 66 shows the VA of the left eyes of the subjects just before dispensing the PPLs (pre-adaptation measurement) and during the first week wearing the lenses. During the first day of adaptation, in three of the four subjects, far from improving the visual performance in time through the C, the VA decreases. In the zone N, the VA also decreases in two subjects and increases in the other two. And in the zone T, the VA goes up in all subjects except in one in whom it is stable. During the next days, in all subjects and for the

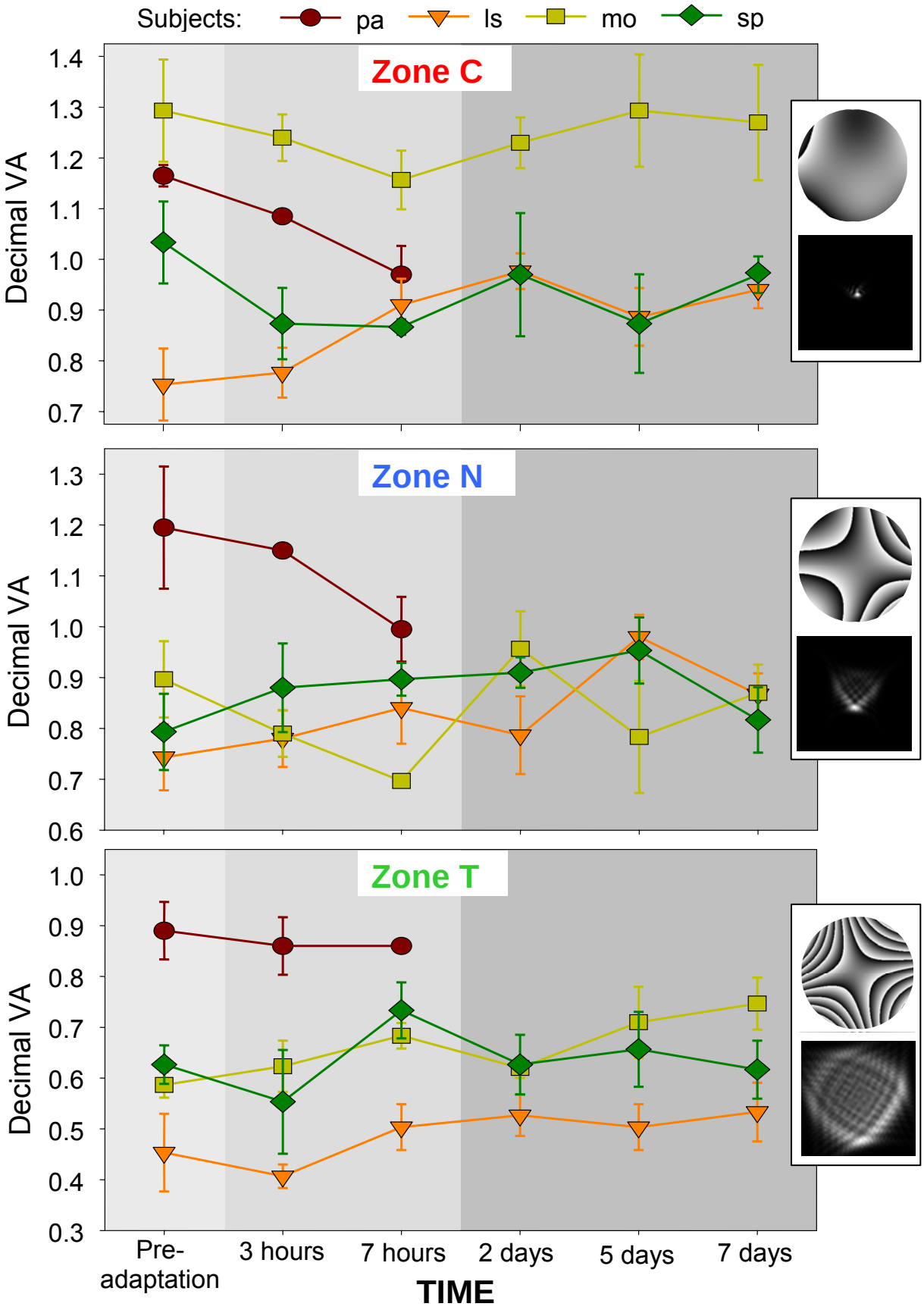

Figure 66. VA during the first week wearing PPLs, for the four subjects when looking through the three zones selected in figure 63, and the corresponding WA and associated PSF of the lens in these zones.

three zones, the evolution of the VA is stable or increases slightly. The most important improvement of VA in time is found for subject ls and zone C. In this case the VA varies from 0.75 in the pre-adaptation measurement to 0.95 after two days of adaptation. This result may be interpreted as a learning effect, since the values of VA in the first measurements (around 0.75) are too small to be a zone in the corridor of the PPL. In fact, all the other subjects have a higher VA in this zone. As expected, in zones N and T, the VA of subject PA is higher than in the other subjects due to the lower addition power of his PPL that produces smaller values of peripheral astigmatism.

The changes in VA are considered significant when the differences in VA are larger than the experimental errors, calculated as the sum of standard deviations. Table 3 shows the VA in pre-adaptation measurements and after 1 week, and the differences between them. The significant values of improvement are marked in black. Only in three of the nine cases, there is a considerable increase of VA during the first week. In other case, subject ls for zone T, the improvement of 0.08 is close to experimental error of 0.13. Thus, the main gain of VA during the week is produced looking through the zone T. As shown in figure 66, an important part of this increment is obtained during the first day of adaptation.

	Zone C			Zone N			Zone T		
Subject	ls	mo	sp	ls	mo	sp	ls	mo	sp
VA in pre-adaptation	0.75	1.29	1.03	0.74	0.90	0.79	0.45	0.59	0.63
VA after 1 week	0.94	1.27	0.97	0.87	0.87	0.82	0.53	0.75	0.62
Difference	**+0.19**	-0.02	-0.06	**+0.13**	-0.03	+0.03	+0.08	**+0.16**	-0.01
Experimental error	0.11	0.21	0.12	0.11	0.13	0.14	0.13	0.08	0.09

Table 3. VA values in pre-adaptation measurements and in seventh day. Positive differences note an improvement in VA. If these differences are higher than the experimental errors (sum of standard deviations), the improvement is significant (values in black).

We also calculated the intersubject average without considering the subject PA, since the addition power of his lenses are significantly lower than those of the other subjects. Theses results for each tested zone are shown in figure 67. The visual performance is better

in the zones where the astigmatism of the lenses is lower, that is, the VA is highest in the corridor (zone C) and it is lowest in the most peripheral location (zone T). VA is around 1.0, 0.8 and 0.6 in central, nasal and temporal zones where astigmatism values of the PPL are 0.15, 0.80 and 1.70 D respectively. In average, the VA is better after a week of adaptation, but through the central zone, the increment of 0.04 is not significant because it is much smaller than the average experimental errors of 0.12. In the 3-mm nasal zone, the highest increase of 0.07 is produced in the second day of adaptation, and then it is reduced to 0.04 after a week. The VA through the zone T mainly improves after seven hours of adaptation and this increment of 0.08 is maintained in the seventh day. This value is closer to the 0.12 of experimental error, but it is also not significant.

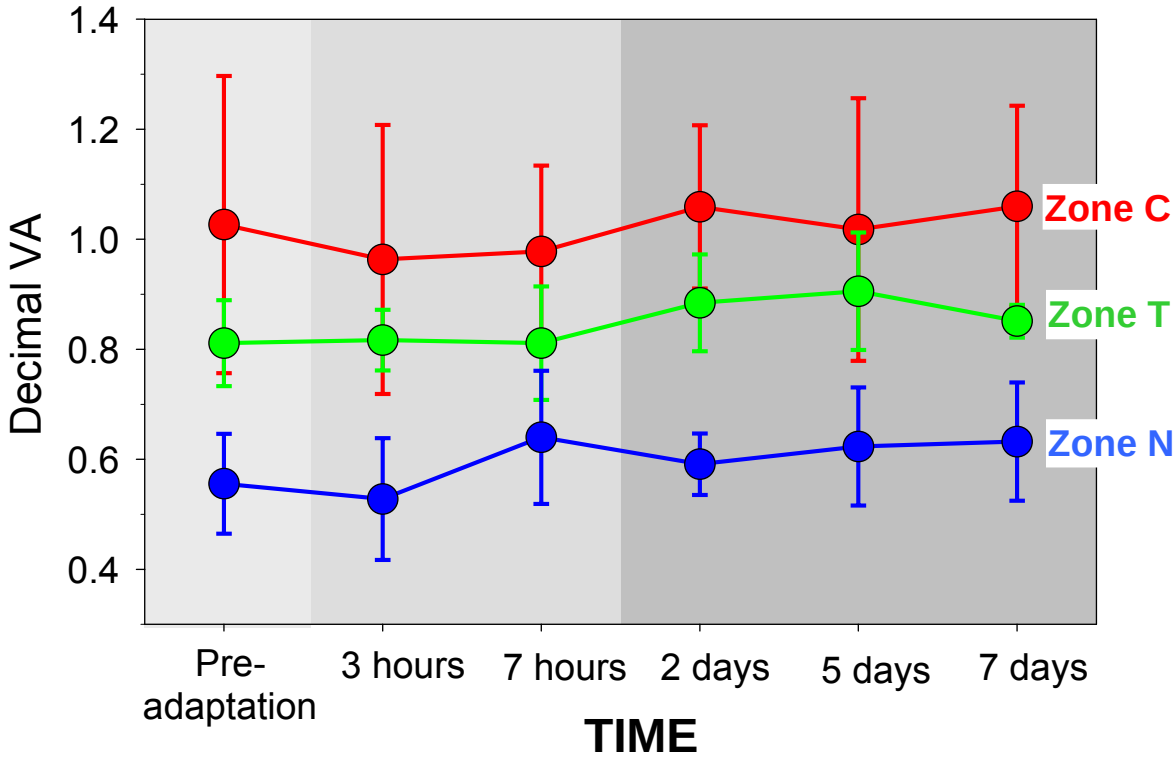

Figure 67. Intersubject average values (except subject PA) of VA for the three tested zones.

We find slight improvements of VA, but not significant, through the selected zones of the PPLs during the first week of adaptation to the new lenses. While a previous work [Artal *et al.* 2004] has clearly demonstrated neural adaptation to the eye's own aberrations, the adaptation to the wavefront aberrations of the PPLs seems more difficult, at least in the first week. This reduced ability of the visual system to adapt to the foveal image quality through the PPLs may be due to the exposure to a multiplicity of new aberration patterns, one for each direction of gaze. In the case of naked eye, during normal viewing, despite the optical

changes due to pupil diameter and accommodation, the retinal PSF preserves most of its shape features [Artal *et al.* 2003]. An example of this stability of PSF in an eye with different values of pupil diameters and accommodation is shown in figure 68. However, as shown in figure 69, in PPLs the wavefront aberration of the entire system, eye plus lens, and the retinal PSF is continuously changing because eye turns to fixate eccentric objects and looks through many zones of the PPLs with different wavefront patterns.

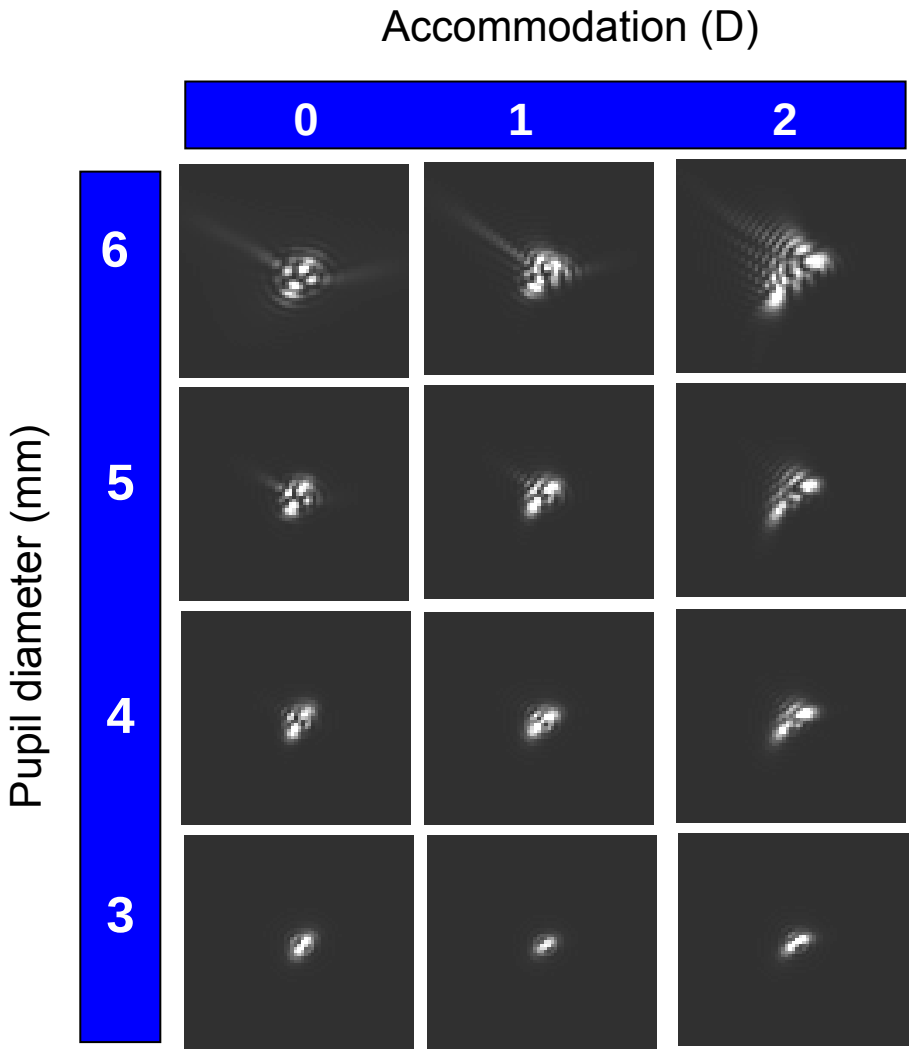

Figure 68. Example of the retinal PSF for different viewing conditions of accommodation and pupil size *[Artal et al. 2003]*

On the other hand, we have measured subjects only the first week wearing PPLs, but in the clinical practice, the adaptation period is longer, up to two weeks approximately. If we had extended the experiment one week more, perhaps the tendency of VA improvement may have followed.

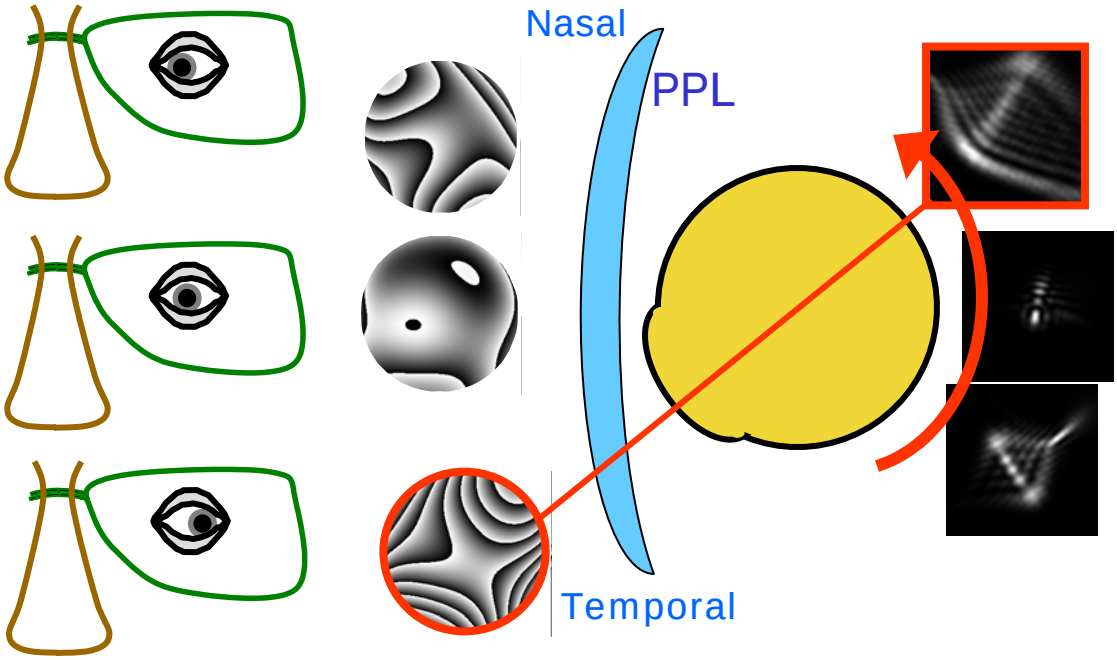

Figure 69. Example of the left eye of subject mo when is looking through the selected zones of the PPL. We show the movements of the eyes, the wavefront aberration of the entire system, eye plus zone of the lens, and the different shapes of PSF on retina.

These results suggest that the neural adaptation to aberrations probably plays a minor role in how patients adjust to PPLs, at least during the first week. In the first days of adaptation, this adjustment may be mainly driven by compensatory eye–head movements and perhaps gaze–contingent adaptation to the distortion rather than the blur introduced by the lenses.

Chapter 8

RESULTS (V):

OPTICAL COMPARISON BETWEEN CURRENT PPLS

In the chapter 4, we measured wave-aberrations at different locations of a particular PPL: Varilux Comfort (Essilor International, France). However, nowadays, numerical control lathe machines allow to generate many types of progressive surfaces with different optical characteristics depending on design criteria. Thus, every company markets their own designs of PPLs. The main goal of this chapter is to evaluate the optical quality of three current PPL designs and to show the differences among them.

We use our HS wavefront sytem (figure 30) in the configuration to measure isolated PPLs. From the HS images, WAs are reconstructed for 6-mm pupil size at the PPL plane. The aberrations are also computed for a smaller 4-mm pupil diameter by selecting the appropriate area, since higher pupil sizes are not very common in presbyopic eyes. Zernike coefficients and the RMS of the WA for every tested zone are obtained. The PSFs are also calculated from the WA.

8.1 DESCRIPTION OF THE PPLS AND THE TESTED ZONES

Since we have not commercial interest in any product, the lenses tested in this study are simply called A, B and C. The three lenses have in common the following characteristics: the progressive surface is on the front of the lens, glass material of refractive index 1.6, plano distance power, 2 D power addition; 18-mm corridor length (vertical measurement from the fitting cross to the center of the near circle) and 2.5-mm inset of the near portion.

For each of the three PPLs, the WA was measured in 20 zones spatially distributed as a 5×4 array of locations: a column along the corridor and at both sides (nasal and temporal) two columns 5 and 10 mm away from corridor. Figure 70 shows these locations of the measurement

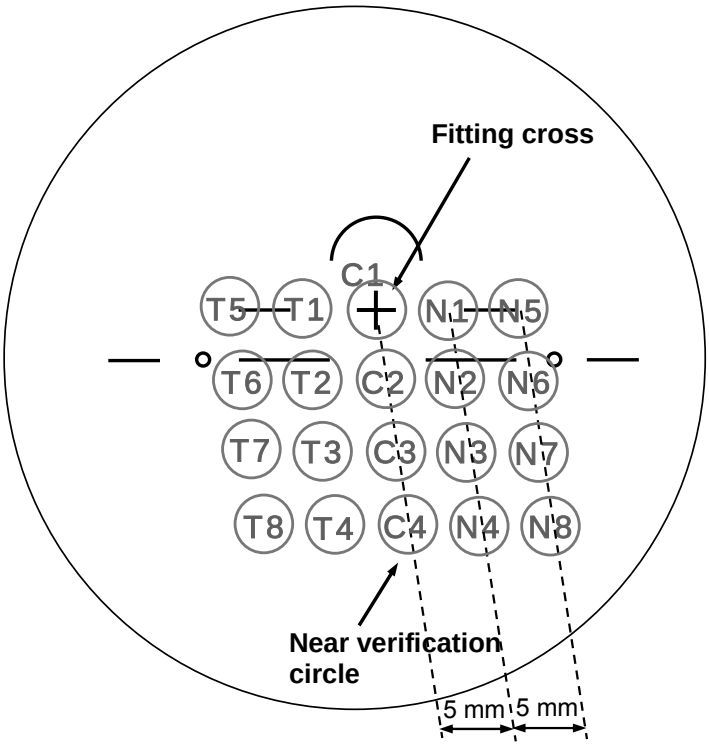

Figure 70. Measured zones with 4.0-mm in diameter in three current PPLs.

zones over the lens surface. Zones at the corridor are noted as C_i, and N_i, T_i those at the temporal and nasal side.

8.2 WA & PSF MAPS. ZERNIKE COEFFICIENTS

As an example of the differences we found between the three lenses in the WA and PSF, figure 71a shows this type of maps (with defocus set to zero) for three zones at intermediate vision (C_2 at the corridor, N_2 and T_2 at the nasal and temporal side 5-mm away from corridor) of the three tested PPLs for a 6-mm pupil diameter. For every lens, typical comatic shapes appear in the corridor zone. In the zones outside the corridor, astigmatism increases and becomes the dominant aberration, although the amount of astigmatism is different for each lens. Figure 71b shows the same results but without astigmatism; i.e, both defocus and astigmatism set to zero. This represents the impact of higher order aberrations. In addition to coma, small amounts of trefoil is also present in every case. It is interesting to note that the orientation of coma changes from vertical in the corridor to oblique direction in the peripheral zones, due to the defocus decrease outside the corridor.

The values of Zernike coefficients for all tested zones of the three PPLs are presented in figure 72. The evolution of defocus over the lenses is shown by coefficient 4. This coefficient and those corresponding to astigmatism (coefficients 3 and 5) are slightly different between the lenses. The magnitude and type of high order aberrations is similar for the three different lenses evaluated. The most important high order aberrations are coma (coefficients 7 and 8) and trefoil (coefficients 6 and 9). Other high order aberrations, including spherical aberration (coefficient 12), are nearly negligible in every PPL.

8.3 SPATIALLY RESOLVED OPTICAL PROPERTIES OF THE LENSES

In order to better show the spatially resolved optical properties of the lenses, mesh and contours plots for a rectangular area of the lenses were generated from interpolation of values of the 20 tested zones using an inverse distance method.

In any preliminary optical analysis of PPLs, it is essential to study the evolution of the addition over the lens. Figure 73 shows the filled contour plot with iso-power lines in the three lenses. The addition distribution is different in the three lenses. For lens A the addition progression begins above the fitting cross, in lens B the complete addition is reached further down, and lens C is an intermediate case. It is interesting to note that although in lens A the

spherical power increases faster from far to near zones than in lens B, lens A has a softer design. These differences between lenses are possible due to computer control lathe machines are able to generate any kind of surface design.

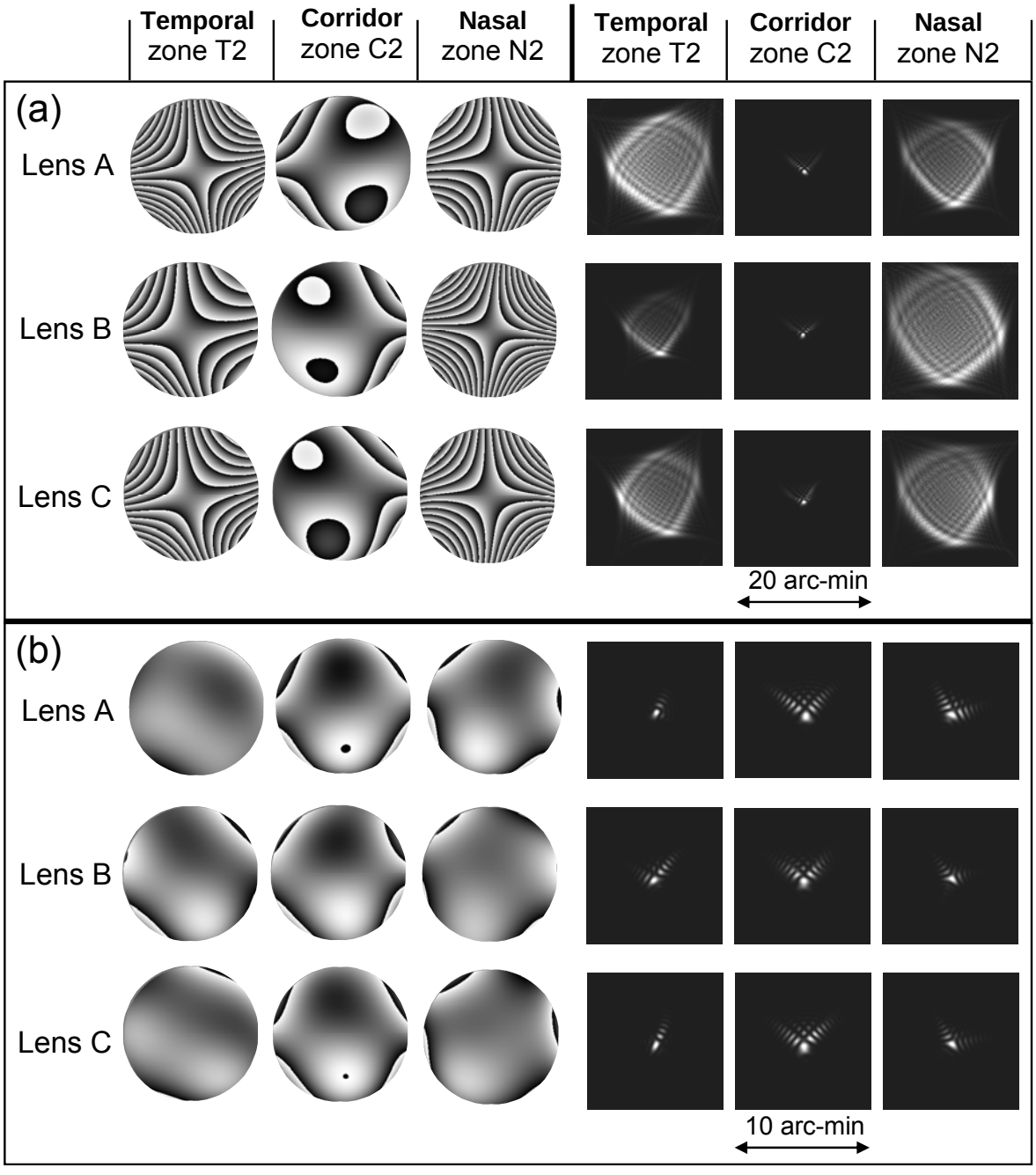

Figure 71. A modulus 2πrepresentation of the WA maps and the associated PSFs, at three intermediate zones (C2 at the corridor, N2 and T2 at the nasal and temporal side), as examples of the twenty tested zones, for each PPL. (a) Considering defocus zero. (b) Considering defocus and astigmatism zero. 6.0-mm pupil diameter.

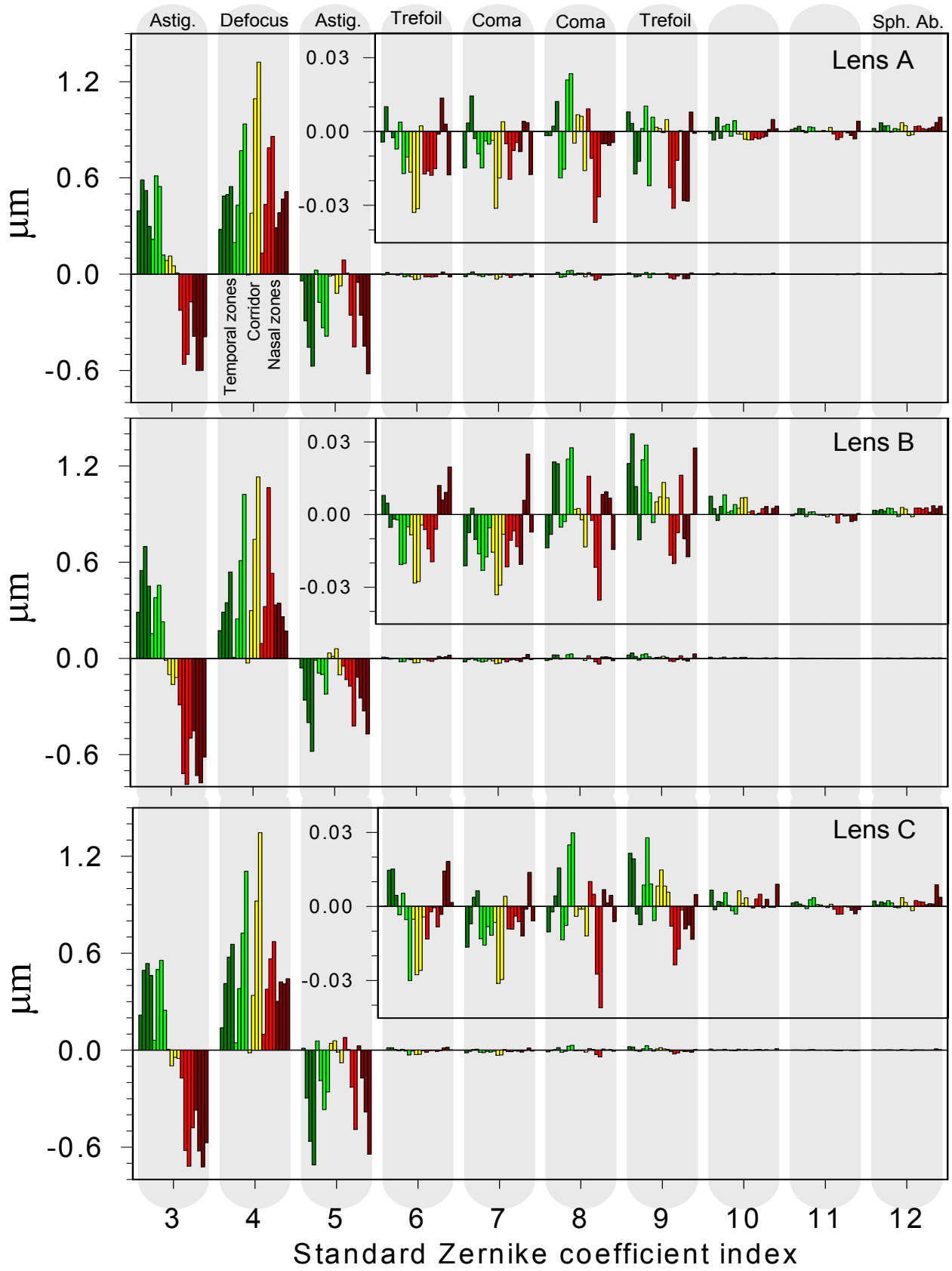

Figure 72. Zernike coefficients for the tested locations (for 4-mm-diameter zones) of the three progressive lenses: in the corridor (yellow bars), 5 mm away from corridor (green bars for temporal zones, red bars for nasal zones) and 10 mm from corridor (dark green bars for temporal zones, dark red bars for nasal zones). Bars from left to right correspond to zones from far to near. The high order coefficients (from coefficient 6 to 12) are also shown on a larger scale. The Seidel aberrations corresponding to Zernike coefficients are noted on top of the figure.

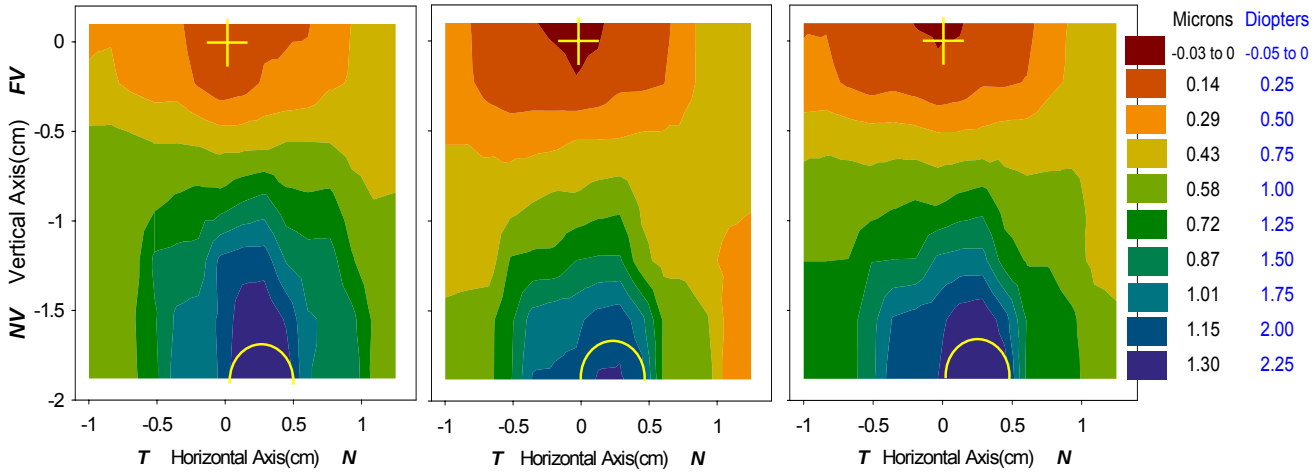

Figure 73. Filled contour plots of addition for 4.0-mm pupil diameter.

Figure 74 shows a 3D representation of the spatially resolved values of the RMS for the three lenses. All aberrations were included except defocus. The behavior is similar in every PPL, the lower values are in the corridor locations and the higher values in the intermediate peripheral zones. However, spatial differences in the aberration distribution are evident. Lens A shows a smoother change between central and peripheral zones than lenses B and C. Moreover, there are also differences between the nasal and temporal distribution. The amount of aberrations is similar at both sides of lens A, while the temporal side is clearly less aberrated in the other lenses, in particular for the lens B.

Figure 75 shows filled contour plots with iso-RMS lines for two different conditions: (a) only astigmatism and (b) only high order aberrations. Lens B has lower amount of astigmatism at the temporal side than at the nasal side, so it is what can be called an asymmetric design. In lens C, this difference is only observed in far and near vision, but not at the intermediate zones. Lens A is the most symmetric design, because there is only difference between nasal and temporal sides in the far vision area. In the three tested lenses, larger values of coma and trefoil are found in the corridor where the change of defocus is faster. In far and near areas and in the most peripheral zones, the amounts of these aberrations decrease to half the value in the corridor.

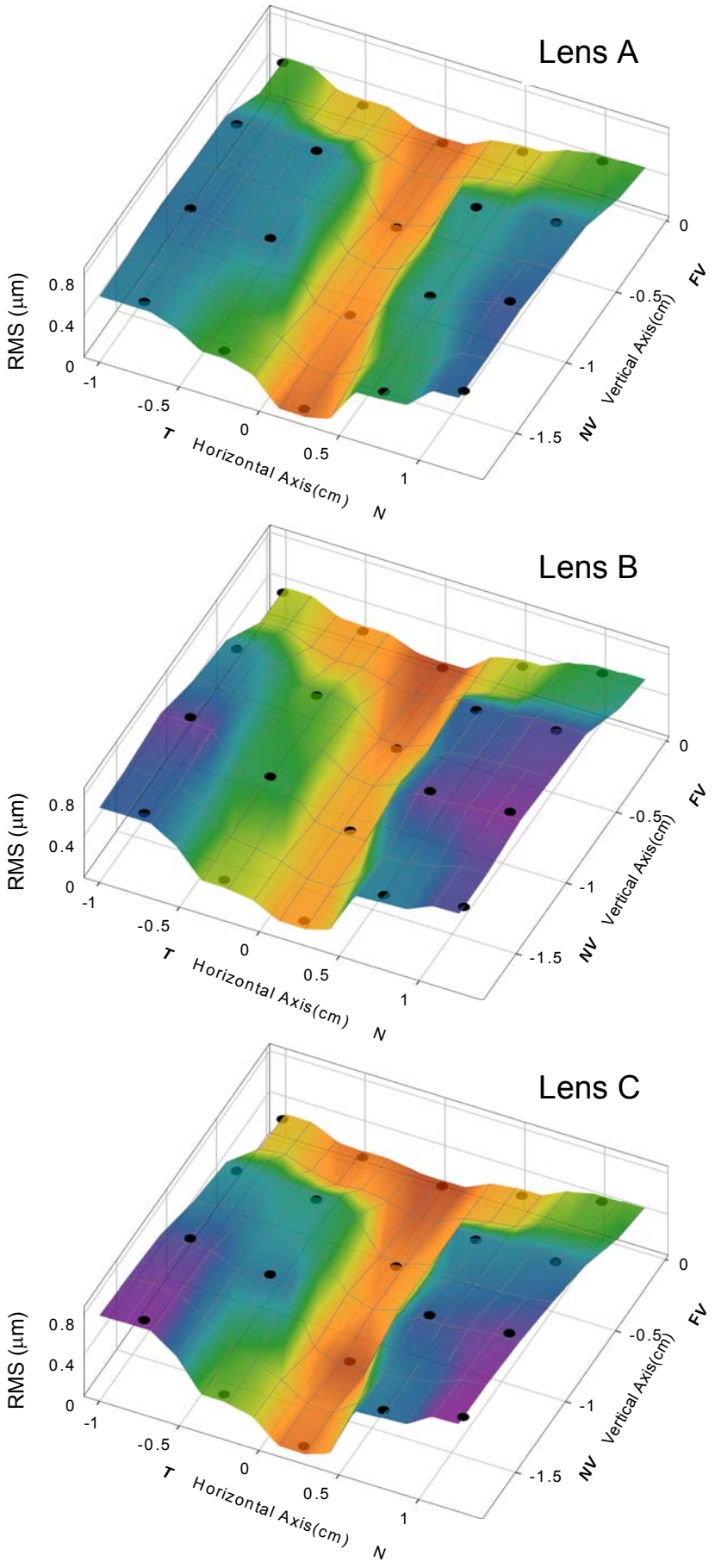

Figure 74. 3 D representation of the spatially resolved RMS for 4.0-mm pupil diameter, considering defocus zero.

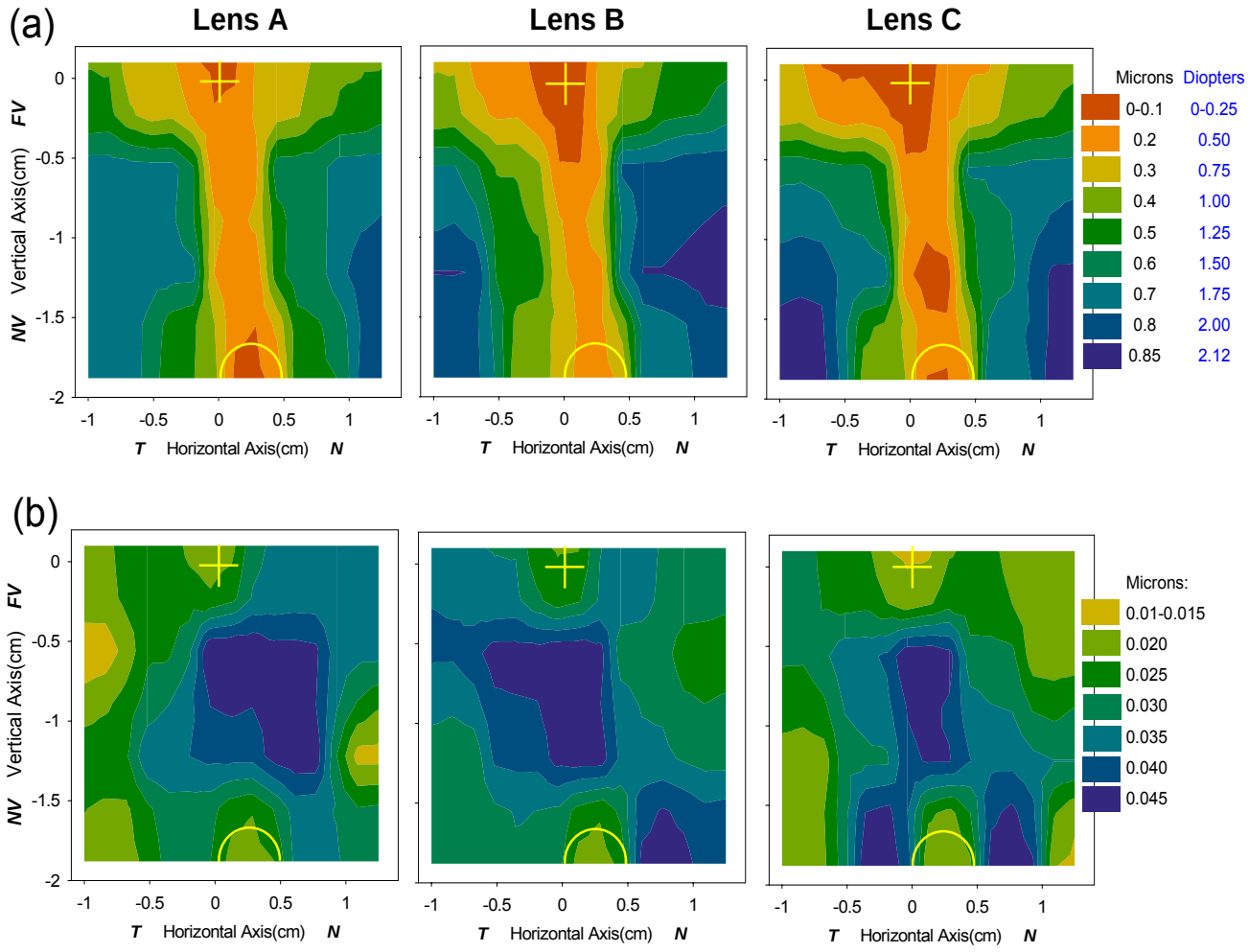

Figure 75. (a) Filled contour plots of RMS considering only astigmatism, with 4.0-mm pupil size. (b) For only high order aberrations, mainly coma and trefoil, since the other high aberrations are negligible.

8.4 AVERAGE RMS. HOW MUCH SOFT-HARD ARE THE DESIGNS?

In order to evaluate the amount of total aberration of the lenses, the average RMS values in the 20 zones were calculated for both (1) only astigmatism and (2) considering coma and trefoil. As we can see in figure 76, the average RMS is nearly the same in the three lenses, for both astigmatism and high order aberrations. In addition, standard deviations are also presented. Astigmatism reflects how either soft or hard a particular design is. Larger standard deviations denote more abrupt changes between central and peripheral zones. Lens A has the lowest value of standard deviation for astigmatism, 0.23 μm, in contrast to 0.27 μm and 0.29 μm of lenses B and C respectively. Following this

criterion, lens A is the softest design, while lens C is the hardest. In summary, the standard deviations of astigmatism denotes how much soft or hard is the design.

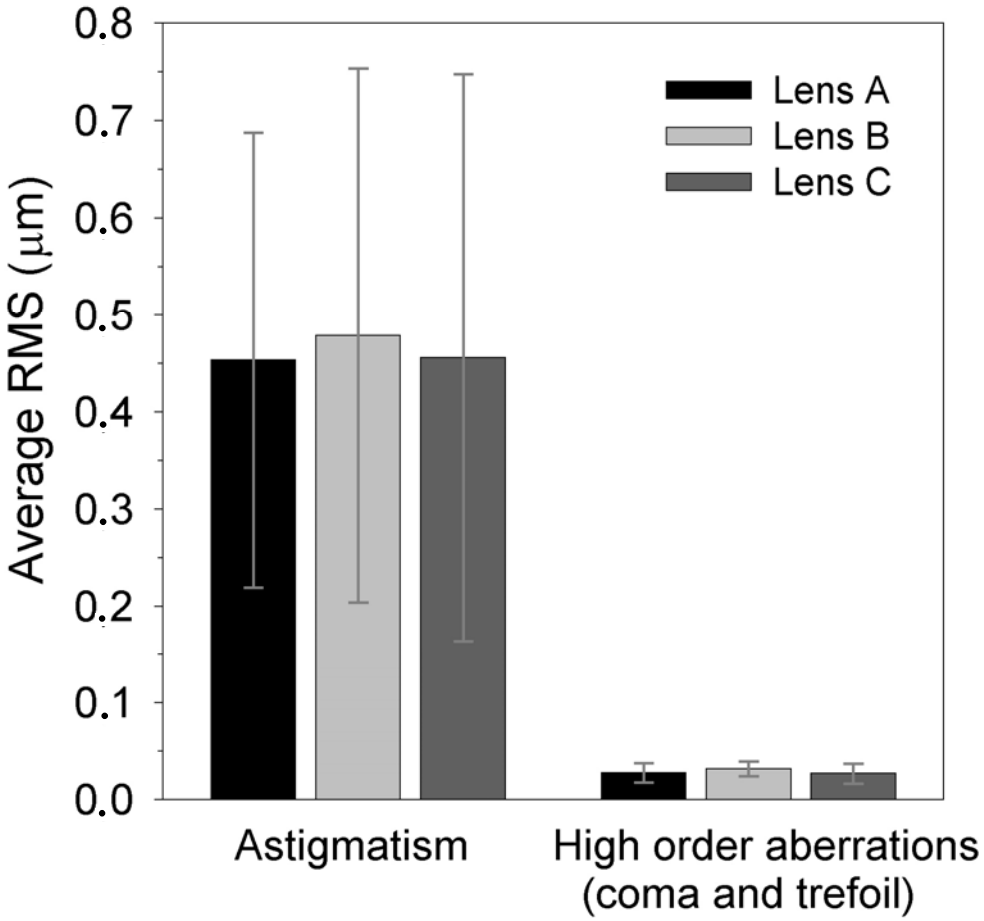

Figure 76. Average RMS of all tested zones of the lenses, for astigmatism and high order aberrations (coma and trefoil) with 4.0-mm pupil diameter. The error bars are the standard deviations.

8.5 PPLS LIKE A WATERBED

Although, in the last few years, newer designs of PPL can be produced by numerically controlled machines, our results show nearly equal average aberrations for both astigmatism and high order aberrations (coma and trefoil) in three different lenses. The small amounts of coma and trefoil are spatially distributed in a similar way on the three lenses. In the peripheral zones, high order aberrations decrease slightly and coma adopts an oblique orientation due to the distribution of addition. However, the distribution of astigmatism varies between the tested PPL designs. It depends on lens design philosophy, that is, what zones are considered for minimizing the astigmatic aberration. Peripheral vision has priority in the

softer designs, while binocular vision is taken more into account in asymmetrical designs. In this way, the tested PPLs perform like a waterbed, where the astigmatism is the water that can be moved but not eliminated.

The experimental data of the three PPLs of this chapter will be used to study the level of prediction of the analytical model proposed in the appendix to describe the WAs of PPLs.

CONCLUSIONS

1. We have developed a HS wavefront sensor capable of measuring the WA at different zones of any type of ophthalmic lens either alone or in combination with the eye. In particular, this system has been applied to study the spatially resolved optical performance at different locations under normal viewing conditions in progressive power lenses.

2. The expected on-eye performance of the lens may be accurately predicted from the measurement and addition of aberrations of a naked eye plus the lens.

3. In addition to astigmatism, coma and trefoil were found in the PPLs. In areas of the PPL outside the corridor, astigmatism increases, while third order aberrations slightly decrease from the umbilical line of power progression.

4. Some zones of the PPL have similar magnitude of coma and trefoil than in older eyes. These aberrations and small amounts of astigmatism of the presbyopic eyes could be coupled with those of the lens zones, modifying significantly the final retinal image quality.

5. In isolated PPLs, the optical quality decreases very fast from the corridor to the peripheral zones. However the aberration coupling with the eye tends to equalize the retinal image quality between central and outside zones of the progressive lenses.

6. The small amounts of astigmatism and higher order aberrations, coma and trefoil, that are present in the central areas (corridor, far and near zones) of progressive lenses appear to have a limited impact on VA.

8. In central and nearby locations, aberration coupling between eye and PPL can even yield slightly better VA than in the naked eye. At peripheral areas of the lens, larger amounts of astigmatism moderately reduce VA.

9. The Log_Vol_PSF, or equivalent, of the entire system eye plus PPL is the parameter that best predict the high contrast VA.

10. The VA measurements in PPLs provide a means to determine the tolerance range of the maximum permissible astigmatism and high order aberrations.

11. There is a slight improvement of VA, but not significant, through the peripheral zones of the PPLs during the first week of adaptation. This could be attributed to the difficulty

of the visual system to adapt to the multiplicity of new aberrations patters, one for each direction of gaze.

12. In current designs of PPLs with power progression in the first surface, there are differences in the spatial distribution of the aberrations but not in the average RMS over zones, indicating that current PPLs are somehow similar to a *waterbed*, with the aberrations being the water: they can be moved but they cannot be eliminated.

Appendix

ANALYTICAL ESTIMATIONS OF ABERRATIONS IN PPLS

An analytical model describing aberrations in PPLs [Blendowske *et al.* 2006] is studied in this section. The experimental data of the three PPLs of chapter 8 are used to study the level of prediction of this model. Thus, this simple analytical model could be useful for learning the optical principles of PPLs from the point of view of WAs.

A.1 ANALYTICAL MODEL OF PPL

We consider a simple analytical model of a progressive power surface extensively used in the (patent) literature [Alvarez 1967, Sheedy *et al.* 2005]. The surface sagitta is given by the following function:

$$f(x,y) = \frac{a}{6(n-1)}(y^3 + 3yx^2) \qquad \text{(A1)}$$

where n is the refraction index of the lens, a is the linear vertical increase in power. The coordinate y is considered along the centre of the corridor and coordinate x is perpendicular to the axis y (figure A1). A graphical representation of function (A1) is shown in figure A2 for n = 1.6 and a = 0.125 D/mm (that is, at 18-mm below the fitting cross the power addition is 2.25 D). This surface is symmetric to the umbilical line of the corridor (y axis). As expected, the sagitta values increase from far to near zones.

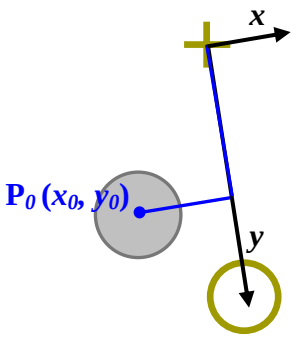

Figure A1. Coordinates in the analytical model of progressive surface.

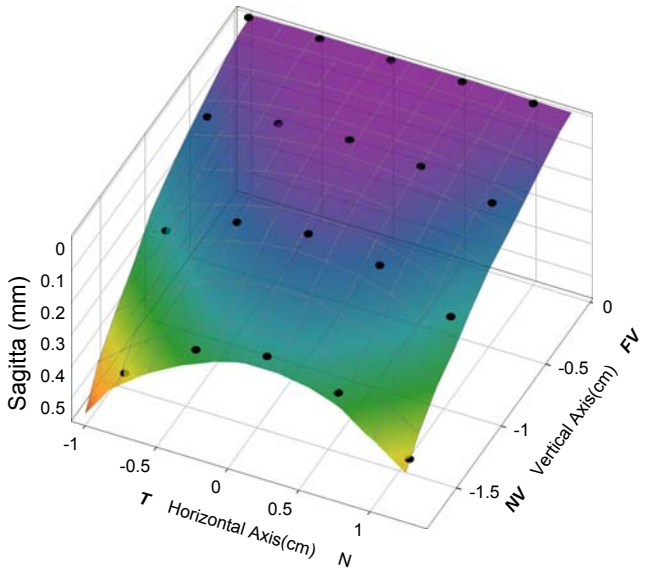

Figure A2. 3-D representation of the sagitta of a progressive power surface obtained from Eq. (A1), for refraction index 1.6 and vertical increase in power of 0.125 D/mm.

A Taylor expansion of the Eq. (A1) is used to describe the surface in a local zone with center in a point $P_0(x_0, y_0)$ (figure A1). Thus, we obtain an expression directly related with the wavefront:

$$W(x_0+x', y_0+y') = \frac{a}{6}\begin{cases} y_0^3 + 3y_0x_0^2 & \textit{Piston} \\ +6y_0x_0x' + 3(y_0^2+x_0^2)y' & \textit{Tilts} \\ +3y_0(x'^2+y'^2) & \textit{Defocus} \\ +6x_0x'y' & \textit{Astigmatism} \\ +y'^3+3x'^2y' & \textit{Trefoil and Coma} \end{cases} \quad \text{(A2)}$$

where the distances from P_0 are expressed by $x'=x-x_0$ and $y'=y-y_0$. In Eq. (A2), the aberration corresponding to each term is noted. The constant term (piston) is of no interest. We are not interested in prismatic effects (wavefront tilts) which are represented by linear terms. So, the rest of the terms belong to defocus, astigmatism, trefoil and coma.

In table A1, these Taylor terms are related to those of Zernike (Table 1) using polar coordinates. The radial coordinate (ρ) is normalized to 1 and the radius of the pupil is denoted by r_{max}. Constant and linear terms of Zernike polynomials are also neglected. In the case of astigmatism, the Taylor expansion only gives the polynomial corresponding to the

Zernike term with axis at ±45º. This approximation is not far from experimental results which give orientations around 55º for temporal zones and 125º for nasal zones. On the other hand, the coma and trefoil are expressed by a Taylor polynomial without terms proportional to cosθ or cos3θ, that means horizontal trefoil and coma are not represented. It is more or less in accordance with experimental values in the corridor and nearby zones.

Taylor polynomial	Zernike polynomial	Zernike coefficient	Aberrations
$(1/2)\,a\,\rho^2\,y_0\,r^2_{max}$	$\sqrt{3}\,2\rho^2$ *constant term (piston) is neglected*	C_4	Defocus
$(1/2)\,a\,\rho^2\,x_0\,r^2_{max}\sin2\theta$	$\sqrt{6}\,\rho^2\sin2\theta$	C_3	Astigmatism with axis at ±45º
$(1/12)\,a\,\rho^3\,r^3_{max}\,(\sin3\theta + 3\sin\theta)$	$\sqrt{8}\,(\rho^3\sin3\theta + 3\rho^3\sin\theta)$ *Term linear in ρ (tilt) is neglected*	C_6, C_7	Vertical trefoil and coma

Table A1. Relation between Zernike and Taylor polynomials with the corresponding aberration.

Making equal the Taylor and Zernike polynomials, we can calculate the Zernike coefficients from the data of the analytical surface expressed by equation (A1):

$$C_4 = \frac{\sqrt{3}}{12} a y_0 r_{\max}^2 \qquad C_3 = \frac{1}{2\sqrt{6}} a x_0 r_{\max}^2 \qquad C_6 = C_7 = \frac{1}{12\sqrt{8}} a r_{\max}^3 \tag{A3}$$

These coefficients are directly related to the linear progression in spherical power along the corridor (a). The astigmatism and defocus coefficients (C_3 and C_4) depend directly on the square of the pupil radius (r_{max}). If these coefficients are transformed in dioptres by using formulas (7), we obtain an expression according to the Minkwitz theorem:

$$Astigmatism = 2\frac{x_0}{y_0} Defocus \tag{A4}$$

that means that the increment of the lateral astigmatism is double that of the power (defocus) progression along the corridor.

The trefoil and coma coefficients (C_6 and C_7) are directly proportional to the third power of the pupil radius. For common pupil diameters in presbyopic eyes of 4 mm and a = 0.125 D/mm, these coefficients are 0.029 μm; but in eyes with higher pupil sizes, e.g. 6 mm,

the coma and trefoil values increase to 0.100 μm. Taking into account both coefficients (C_6 and C_7), the RMS values are 0.04 μm and 0.135 μm for 4 and 6-mm pupil size. The approximated values of Strehl ratio can be calculated by using Eq. (17). For 4-mm pupil diameter the Strehl ratio is 0.81 and for 6-mm pupil it is 0.21. Using equation (18), the corresponding values of Log_Vol_Psf are 1.4 and 2.0. In the figure 63 (for eyes with PPL), we can observe that these values of aberrations (RMS) and image quality (Strehl ratio, Log_Vol_Psf) have not a significant impact in visual quality.

A.2 COMPARISON OF THE ANALYTICAL MODEL WITH EXPERIMENTAL RESULTS

In order to know how much the analytical model resembles the performance of the current PPLs, we compare the experimental results of aberrations of the three PPLs studied in the chapter 8 with the predictions from the theoretical model.

Firstly, we need the parameter a for estimating every aberration from the model. In figure A3, we present a graph with the power profiles from the values of defocus in the tested zones of the corridor. For the three lenses, the values of a are calculated between each zone. A mean value for each PPL is estimated. Finally, the average between the three PPLs is 0.124 D/mm.

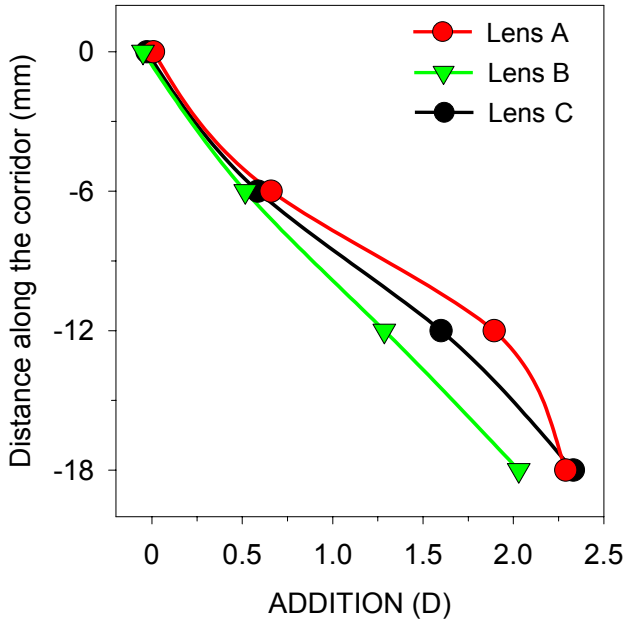

Value of *a* (D/mm)			
Interval	**Lens A**	**Lens B**	**Lens C**
C1-C2	0.110	0.094	0.103
C2-C3	0.206	0.128	0.169
C3-C4	0.066	0.124	0.122
Mean	**0.127**	**0.115**	**0.131**
Total mean = 0.124			

Figure A3. Power profile along the corridor of the three PPLs studied in chapter 8 and the values of parameter *a* calculated from the spherical power differences between the zones of the corridor.

Using this value of a, the value of astigmatism (C_3) is calculated from the corresponding Eq. (A3). Figure A4 shows the prediction of astigmatism in diopters. In comparison with experimental data of figure 75a, the model overestimates the astigmatism values in the most peripheral zones. The differences between the analytical and experimental data are shown in figure A5. Negative values means that the model gives amounts of astigmatism lower than the actual values. In the intermediate zones (from 5 to 15 mm under the fitting cross), the model predicts the astigmatism with an accuracy equal or better than 0.37 D, in temporal zones up to 5 mm away from corridor, and in nasal zones up to 8 mm away from corridor.

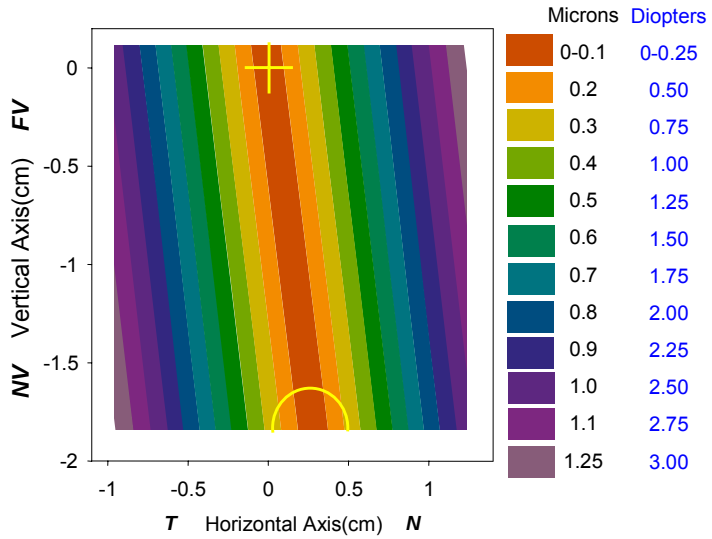

Figure A4. Filled contour plots of theoretical astigmatism estimated from the analytical model. 4-mm pupil diameter.

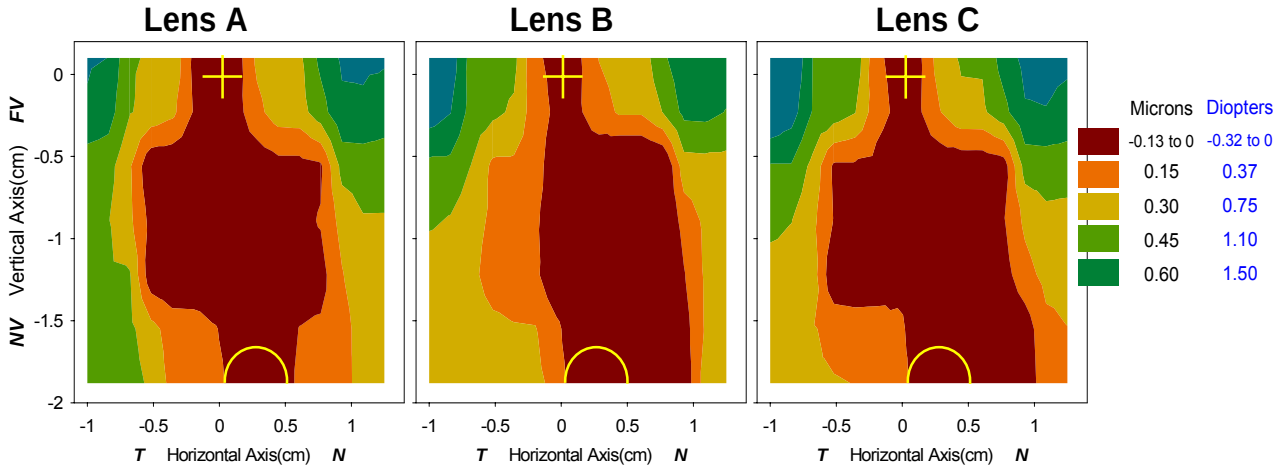

Figure A5. Differences in astigmatism between the analytical model and the experimental results (theoretical minus experimental results). 4-mm pupil diameter.

As we can see in the Eq. (A3), the theoretical values of vertical trefoil and coma (C_6 and C_7) don't depend on the position of the tested zone. So, for a = 0.124 D/mm and 4-mm pupil diameter, these aberrations have a value of 0.029 μm each one. The RMS contribution of coma and trefoil is 0.041 μm. This value is agreed with experimental data of intermediate zones of the corridor (figure 75b). Both aberrations are presented separately in figure A6. These graphs show the profile of the aberration along the corridor and in parallel lines from the experimental values, in comparison with the analytical amount of 0.029 μm. In general, the model only predicts with good accuracy in the zones of the corridor situated 6 and 12 mm under the fitting cross, where the spherical progression is maximum.

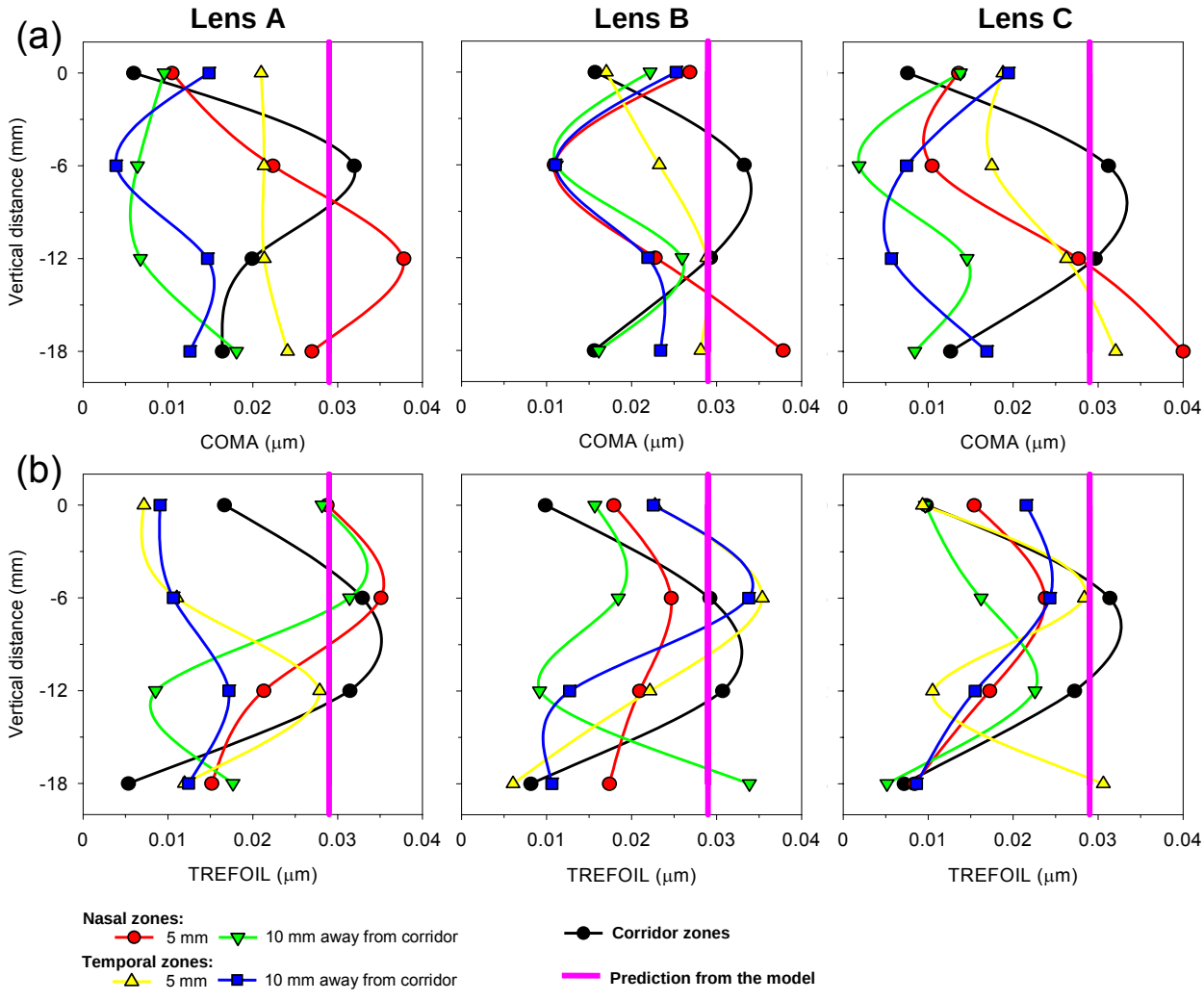

Figure A6. Profiles of coma (a) and trefoil (b) from experimental values along the different vertical lines (parallel to the corridor) in comparison with the predition from the analytical model. 4.0-mm pupil size.

The analytical model predicts mainly the aberrations of PPLs in the corridor and nearby zones. These results can be justified by the following reasons. The model is based in a spherical progressive surface. The marketed PPLs have three different areas. Two of them, used to far and near vision, are very similar to a spherical surface. The other is the corridor, where the spherical progression from far to near vision is produced and the model works very well. In the peripheral zones, the model overestimates the values of astigmatism, coma and trefoil. It is due to the fact that the model is too simple in comparison with the complex surfaces used in the manufacture of the actual PPLs.

BIBLIOGRAPHY

[Acosta *et al.* 2006] Acosta E, Chamadoira S, and Blendowske R. Modified point diffraction interferometer for inspection and evaluation of ophthalmic components. J Opt Soc Am A 2006; 23: 632-637.

[Alvarez 1967] Alvarez L W. Two-element variable-power spherical lens. United States patent 3305294.

[ANSI 1993] American National Standard for the Safe Use of Lasers ANSI Z136.1. (Laser Institute of America, Orlando, FL, 1993).

[Applegate *et al.* 2003] Applegate RA, Ballentine C, Gross H, Sarver EJ, Sarver CA. Visual acuity as a function of Zernike mode and level of root mean square error. Optom Vis Sci 2003; 80:97–105.

[Artal *et al.* 1995(a)] Artal P, Iglesias I, López-Gil N, Green DG. Double pass measurements of the retinal image quality with unequal entrance and exit pupil sizes and the reversibility of the eye's optical system. J Opt Soc Am A 1995; 12: 2358-2366.

[Artal *et al.* 1995(b)] Artal P, Marcos S, Navarro R, Miranda I, Ferro M. Through focus image quality of eyes implanted with monofocal and multifocal intraocular lenses. Optical Eng 1995; 34:772-779.

[Artal *et al.* 1999] Artal P, Guirao A, Villegas E, González C, Chateau N, Berrio E. Image quality in eyes with spherical aberration induced by soft contact lenses. In Vision Science and Its Applications, OSA Technical Digest (Optical Society of America, Washington DC, 1999): 232-235.

[Artal *et al.* 2001] Artal P, Guirao A, Berrio E, Williams DR. Compensation of corneal aberrations by internal optics in the human eye. Journal of Vision 2001; 1: 1-8.

[Artal *et al.* 2002(a)] Artal P, Berrio E, Guirao A, Piers P. Contribution of the cornea and internal surfaces to the change of ocular aberrations with age. J. Opt. Soc. Am. A 2002; 19: 137-143.

[Artal *et al.* 2002(b)] Artal P, Fernandez EJ, Manzanera S. Are optical aberrations during accommodation a significant problem for refractive surgery? J Refract Surg 2002; 18: S563–6.

[Artal *et al.* 2003] Artal P, Manzanera S, Williams DR. How stable is the shape of the ocular point spread function during normal viewing? Journal of Vision 2003; vol 3, abstract 30, page 30a.

[Artal *et al.* 2004] Artal P, Chen L, Fernández EJ, Singer B, Manzanera S, Williams DR. Neural adaptation for the eye's optical aberratins. J Vis 2004: 281-287.

[Atchison 1995] Atchison DA. Accommodation and presbyopia. Ophthal. Physiol. Opt. 1995; 15: 255-272.

[Atchison *et al.* 1997] Atchison DA, Charman WN, Woods RL. Subjective depth-of-focus of the eye. Optom Vis Sci 1997;74:511-520.

[Atchison *et al.* 2005] Atchison DA, Fisher SW, Pedersen CA, Ridall PG. Noticeable, troublesome and objectionable limits of blur. Vision Res 2005;45:1967–74.

[Bennett 2008] Bennett ES. Contact lens correction of presbyopia. Clin Exp Optom. 2008 Jan 14.

[Blendowske *et al.* 2006] Blendowske R, Villegas EA, Artal P. An analytical model describing aberrations in the progression corridor of progressive addition lenses. Optom Vis Sci 2006; 83: 666-671.

[Born and Wolf 1999] Born M, Wolf E. Principles of optics. 7th edition. Cambridge University Press, 1999.

[Boroyan *et al.* 1995] Boroyan HJ, Cho MH, Fuller BC, Krefman RA, McDougall JH, Sachaeffer JL, Tahran RL. Lined multifocal wearers prefer progressive addition lenses. J A Opto Assoc 1995; 66: 296-300.

[Bourdoncle *et al.* 1991] Bourdoncle B, Chauveau JP, Mercier JL. Ray tracing through progressive ophthalmic lenses. In: Lawrence E, ed. Proceedings of International Lens Design Conference, Monterey, CA, June 11–14, 1990.

[Bourdoncle *et al.* 1992] Bourdoncle G, Chauveau, Mercier JL. Traps in displaying optical performance of a progressive-addition lens. Appl Opt 1992; 31:3586-3593.

[Brandser *et al.* 1997] Brandser R, Haaskjold E, Drolsum L. Accuracy of IOL calculation in cataract surgery. Acta Ophthalmol Scand. 1997; 75:162-165.

[Brooks 1983] Brooks CW. Essentials for ophthalmic lens work. Fairchild Publications/Professional Press (Capital Cities Media). New York, 1983.

[Buehren and Collins 2006] Buehren T, Collins MJ. Accommodation stimulus-response function and retinal image quality. Vision Res 2006; 46:1633–45.

[Burns 1995] Burns D. Blur due to pupil area when using progressive addition spectacles. Ophthal. Physiol. Opt. 1995; 15: 273-279.

[Campbell and Green 1965] Campbell FW, Green DG. Optical and retinal factors affecting visual resolution. J Physiol 1965; 181:576-593.

[Campbell 1957] Campbell FW. The depth of field of the human eye. Opt Acta 1957;4:157-164.

[Canabal *et al.* 2001] Canabal H, Alonso J, Bernabeu E. Laser beam deflectometry based on a subpixel resolution algorithm. Opt Eng 2001; 40:2517-2523.

[Carretero *et al.* 1992] Carretero L, Fuentes R, Fimia A. Measurement of spherical aberration of intraocular lenses with the Ronchi test. Optom Vis Sci 1992; 69:190-192.

[Castejón-Monchón *et al.* 2002] Castejón-Mochón JF, López-Gil N, Benito A and Artal P. Ocular wavefront statistics in a normal young population. Vis Res 2002; 42: 1611-1617.

[Castellini *et al.* 1994] Castellini C, Francini F, Tiribilli B. Hartmann test modification for measuring ophthalmic progressive lenses. Appl Opt 1994; 33:4120-4124.

[Charman and Jennings 1976] Charman WN, Jennings JAM. The optical quality of the monochromatic retinal image as a function of focus. Br J Physiol Opt 1976; 31:119-134.

[Chateau *et al.* 1996] Chateau N, De Brabander J, Bouchard F, Molenaar H. Infrared pupillometry in presbyopes fitted with soft contact lenses. Optom Vis Sci 1996; 73: 733-741.

[Cheng *et al.* 2004] Cheng H, Barnett JK, Vilupuru AS, Marsack JD, Kasthurirangan S, Applegate RA, Roorda A. A population study on changes in wave aberrations with accommodation. J Vis 2004; 4: 272–80.

[Chiam *et al.* 2007] Chiam PJ, Chan JH, Haider SI, Karia N, Kasaby H, Aggarwal RK. Functional vision with bilateral ReZoom and ReSTOR intraocular lenses 6 months alter cataract surgery. J Cataract Refract Surg. 2007; 33: 2057-61.

[Ciuffreda *et al.* 2006] Ciuffreda KJ, Selenow A, Wang B, Vasudevan B, Zikos G, Ali SR. 'Bothersome blur': a functional unit of blur perception. Vision Res 2006;46: 895–901.

[DeFranco 2008] DeFranco L. Multifocal contact lenses. allaboutvision.com/over40/. January 2008.

[Diepes and Tameling 1988] Diepes H, Tameling A. Comparative investigations of progressive lenses. Am J Optom Physiol Opt 1988; 65: 571-579.

[Doane and Jackson 2007] Doane JF, Jackson RT. Accommodative intraocular lenses: considerations on use, function and design. Curr Opin Ophthalmol. 2007; 18: 318-24.

[Duke 1993] Duke-Elder's Practice of Refraction (revised by D. Abrams).10th edition. Churchill Livingstone. 1993

[Elliot *et al.* 1995] Elliot DB, Yang KCH, Whitaker D. Visual acuity changes throughout adulthood in normal, healthy eyes: seeing beyond 6/6. Optom Vis Sci 1995; 72: 186-191.

[Fauquier *et al.* 1995] Fauquier C, Bonnin T, Miege C, Roland E. Influence of combined power error and astigmatism on visual acuity. In Vision Science and Its Applications, OSA (Optical Society of America, Washington DC, 1995): 151-154.

[Fernández *et al.* 2001] Fernandez EJ, Iglesias I and Artal P. Closed-loop adaptive optics in the human eye. Opt. Lett. 2001; 26: 746-748.

[Fernandez 2002] Fernandez EJ, Manzanera S, Piers P, Artal P. Adaptive optics visual simulator. J Refract Surg 2002;18:S634–8.

[Fowler and Sullivan 1989] Fowler CW, Sullivan CM. A comparison of three methods for the measurement of progressive addition lenses. Ophthal. Physiol. Opt. 1989; 9: 81-86.

[Fuerst 2006] Fuerst RF. Understanding multifocal intraocular lenses and their importance to your practice. Review of Optometry (on line). October 2006.

[González *et al.* 1997] Gonzalez C, Villegas ER, Carretero L, Fimia A. Ronchi test for testing the powers of bifocal intraocular lenses. Ophthalmic Physiol Opt 1997; 17:161-163.

[Grosvernor 2002] Grosvernor T. Primary care optometry. 4th ed. Butterworth-Heinemann, USA 2002.

[Guirao *et al.* 1999] Guirao A, Gonzalez C, Redondo M., Geraghty E, Norrby S, Artal P. Average optical performance of the human eye as a function of age in a normal population. Inv Ophth Vis Sci 1999; 40: 203-213.

[Han *et al.* 2003(a)] Han Y, Ciuffreda KJ, Selenow A, Bauer E, Ali SR, Spencer W. Static aspects of eye and head movements during reading in a simulated computer-based environment with single-vision and progressive lenses. Invest Ophthalmol Visual Sci 2003; 44: 145-153.

[Han *et al.* 2003(b)] Han Y, Ciuffreda KJ, Selenow A and Ali SR. Dynamic interactions of eye and head movements when reading with single-vision and progressive lenses in a simulated computer-based environment. Invest Ophthal Vis Sci 2003; 44: 1534-1545.

[Harbers *et al.* 1996] Harbers G, Kunst PJ, Leibbrandt GWR. Analysis of lateral shearing interferograms by use of Zernike polynomials. Appl Opt 1996; 35:6162-6172.

[Hartmann 1900] Hartmann J. Bemerkungen uber den Bau und di Justirung von Spektrographen. Zt Instrumentenkd 1900; 20:47.

[Hartmann 1904] Hartmann J. Objektuvuntersuchungen. Zt Instrumentenkd 1904; 24:1.

[Hayashi *et al.* 2001] Hayashi K, Hayashi H, Nakao F, Hayashi F. Correlation between pupillary size and intraocular lens decentration and visual acuity of a zonal-progressive multifocal lens and a monofocal lens. Ophthalmology 2001; 108: 2011-7.

[He *et al.* 2003] He JC, Gwiazda J, Thorn F, Held R, Huang W. Change in corneal shape and corneal wavefront aberrations with accommodation. J Vis 2003; 3: 456–63.

[Hong *et al.* 2001] Hong X, Himegaugh N, Thibos LN. On-eye evaluation of optical performance of rigid and soft contact lenses. Optom Vis Sci 2001; 78: 872-880.

[Howland and Howland 1977] Howland HC and Howland B. A subjective method for the measurement of monochromatic aberrations of the eye. J Opt Soc Am 1977; 67:1508-1518.

[Hunter *et al.* 2006] Hunter JJ, Campbell MC and Geraghty E. Optical analysis of an accommodating intraocular lents. J Cataract Refract Surg. 2006; 32: 269–78.

[Iglesias *et al.* 1998] Iglesias I, Berrio E and Artal P. Estimates of the ocular wave aberration from pairs of double pass retinal images. J Opt Soc Am A. 1998; 15: 2466-2476.

[Jalie 1994] Jalie M. The Principles of Ophthalmic Lenses. ABDO, 4ª ed., London 1994.

[Jalie 2000] Jalie M. Ophthalmic lenses and dispensing. BH Optician, Oxford 2000.

[Jalie 2005] Jalie M. Progressive lenses, part 2. Optometry today 2005; 17:35-45

[Kaufman and Alm 2003(a)] Kaufman PL, Alm A. Adler's physiology of the eye, clinical application. 10th ed. St. Louis (Missouri): Mosby (Elsevier Science), 2003. Section 11 (Central Visual Pathways) by Matsubara JA.

[Kaufman and Alm 2003(b)] Kaufman PL, Alm A. Adler's physiology of the eye, clinical application. 10th ed. St. Louis (Missouri): Mosby (Elsevier Science), 2003. Chapter 7 (Accommodation and Presbyopia) by Glasser A. and Kaufman PL.

[Keeney *et al.* 1995] Keeney AH, Hagman RE, Cosmo JF. Dictionary of ophthalmic optics. National Academy of Opticianry. Butterworth-Heinemann, USA 1995.

[Kent 2005] Kent D. Multifocal Corneas: Coming Soon? Review of Ophthalmology on line. 2005. Vol. No. 12:07 Issue:7/15/2005.

[Koeppl *et al.* 2005] Koeppl D, Findl O, Menapace R, Kriechbaum K, Wirtitsch M, Buehl W, Sacu D, Drexler W. Pilocarpine-induced shift of an accommodating intraocular lens: AT-45 Crystalens. J Cataract Refract Surg 2005; 31: 1290-1297.

[Kris 1999] Kris MJ. Practitioner trial of SOLA Percepta progressive lenses. Clin Exp Optom 1999; 82: 187-190.

[Lavin 2001] Lavin M. Multifocal intraocular lenses: Part 1. Optometry Today. May 4, 2001.

[Legge *et al.* 1987] Legge GE, Mullen KT, George CW, Campbell FW. Tolerance to visual defocus. J Opt Soc Am A 1987; 4:851-863.

[Le Grand 1964] Le Grand Y. Optique Physiologique, vol 1 : La Dioptrique de l'œil et sa Conection. Editions de la Revue d'Optique, Paris, France.

[Leibbrandt *et al.* 1996] Leibbrandt GWR, Harbers G, Kunst PJ. Wavefront analysis with high accuracy by use of a double-grating lateral shearing interferometer. Appl Opt 1996; 35: 6151-6161.

[Lesiewska-Junk and Kaluzny 2000] Lesiewska-Junk H, Kaluzny J. Intraocular lens movement and accommodation in young patients. J. Cataract Refract. Surg. 2000; 26: 562-565.

[Liang *et al.* 1994] Liang J, Grimm B, Goelz S, Bille JF. Objective measurement of wave aberrations of the human eye with the use of a Hartmann-Shack wavefront sensor. J Opt Soc Am A 1994; 11: 1949-1957.

[Liang and Williams 1997] Liang J, Williams DR. Aberrations and retinal image quality of the normal human eye. J Opt Soc Am A 1997; 14: 2873-2883.

[Liang *et al.* 1997] Liang J, Williams DR and Miller DT. Supernormal vision and high-resolution retinal imaging through adaptive optics. J Opt Soc Am A 1997; 14: 2884-2892.

[Mahajan 1982] Mahajan VN. Strehl ratio for primary aberrations: some analytical results for circular and annular pupils. J Opt Soc Am A 1982; 72: 1258-1266.

[Mahajan 2001] Mahajan VN. Optical imaging and aberrations. Part II: Wave diffraction optics. SPIE (International Society for Optical Engineering) Bellingham, Washington, 2001.

[Maitenaz 1967] Maitenaz B. Image retienne donnée par une verre correcteur de puissance progressive. Revue d'Optique 1967; 46: 233-241.

[Malacara 1992] Malacara D. Optical Shop Testing. 2nd ed. New York: Wiley, 1992.

[Malacara and Malacara 1992] Malacara D and Malacara Z. Testing and centering of lenses by means of a Hartmann test with four holes. Opt Eng 1992; 31:1551-1555.

[Marchini *et al.* 2004] Marchini G, Pedrotti E, Sartori P and Tosi R. Ultrasound biomicroscopic changes during accommodation in eyes with accommodating intraocular lenses; pilot study and hypothesis for the mechanism of accommodation. J Cataract Refract Surg. 2004; 30: 2476–2482.

[Marcos *et al.* 1999] Marcos S, Moreno E, Navarro R. The depth-of-field of the human eye from objective and subjective measurements. Vision Res 1999;39:2039-2049.

[Marsack *et al.* 2004] Marsack JD, Thibos LN, Applegate RA. Metrics of optical quality derived from wave aberrations predict visual performance. J Vis 2004; 4:322-328.

[Meeteren 1974] Meeteren van A. Calculations on the optical modulation transfer function of the human eye for white light. Optica Acta 1974; 21:395-412.

[Mejía-Barbosa and Malacara-Hernández 2001] Mejía-Barbosa Y, Malacara-Hernández D. A Review of Methods for Measuring Corneal Topography. Optom Vis Sci 2001;78:240-253.

[Meslin 2007] Meslin D. Varilux University. Essilor, Paris, June 2007.

[Miller *et al.* 1997] Miller AD, Kris MJ, Griffiths AC. Effect of small focal errors on vision. Optom Vis Sci 1997;74:521-526.

[Minkwitz 1963] Minkwitz G. Über den Flächenastigmatisms bei gewissen symmetrischen Aspharen. Optica Acta 1963; 10:223–227.

[Mon-Williams *et al.* 1998] Mon-Williams M, Tresilian JR, Strang NC, Kochhar P, Wann JP. Improving vision: neural compensation for optical defocus. Proc R Soc Lond B Biol Sci 1998; 265: 71-77.

[Morales and Malacara 1983] Morales A, Malacara D. Geometrical parameters in the Hartmann test of aspherical mirrors. Appl Opt 1983; 22:3957.

[Moreno-Barriuso *et al*. 2001] Moreno-Barriuso E, Marcos S, Navarro R and Burns S. Comparing laser ray tracing, the spatially resolved refractometer, and the Hartmann-Shack senor to measure the ocular wave aberration. Optom Vis Sci 2001; 78: 152-156.

[Mouroulis and Zhang 1992] Mouroulis P, Zhang H. Visual instrument image quality metrics and the effect of coma and astigmatism. J Opt Soc Am A 1992; 9: 34-42.

[Murphy 2003] Murphy J. Surgery for 'Short Arm Syndrome'. Several surgical procedures for presbyopia-some more successful than others-may soon be FDA approved. Review of Optometry on line. 2003; Vol. No. 140:12 Issue:12/15/03.

[Navarro *et al.* 1993] Navarro R, Ferro M, Artal P, Miranda I. Modulation transfer functions of eyes implanted with intraocular lenses. Appl Opt 1993; 32:6359-6357.

[Noll 1976] Noll RJ. Zernike polynomials and atmospheric turbulence. J Opt Soc Am 1976; 66: 207-211.

[O'Leary and McMahon 1991] O'Leary A, McMahon M. Adaptation to form distortion of a familiar shape. Percept Psycholphys 1991; 49: 328-332.

[Olsen 2007] Olsen T. Improved accuracy of intraocular lens power calculation with the Zeiss IOL Master. Acta Ophthalmol Scand. 2007; 85:84-87.

[Oshika *et al.* 2002] Oshika T, Mimura T, Tanaka S, Amano S, Fukuyama M, Yoshitomi F, Maeda N, Fujikado T, Hirohara Y, Mihashi T. Apparent accommodation and corneal wavefront aberration in pseudophakic eyes. Invest Ophthalmol Vis Sci. 2002; 43:2882-6.

[Ossma *et al.* 2007] Ossma IL, Galvis A, Vargas LG, Trager MJ, Vagefi MR, McLeod SD. Synchrony dual-optic accommodating intraocular lens. Part 2: pilot clinical evaluation. J Cataract Refract Surg. 2007; 33: 47-52.

[Piers *et al.* 2000] Piers T, Hull CC. Optical Fourier filtering for whole lens assessment of progressive power lenses. Ophthal. Physiol. Opt. 2000; 20: 281-289.

[Plainis *et al.* 2005] Plainis S, Ginis HS, Pallikaris A. The effect of ocular aberrations on steady-state errors of accommodative response. J Vis 2005; 5 :466–77.

[Platt and Shack 2001] Platt BC and Shack R. History and Principles of Shack-Hartmann wavefront sensing. J Refract Surg 2001; 17: s573-s577.

[Porter *et al.* 2001] Porter J, Guirao A, Cox IG and Williams DR. Monochromatic aberrations of the human eye in a large population. J Opt Soc Am A 2001; 18: 1793-1803.

[Prieto *et al.* 2000] Prieto PM, Vargas-Martín F, Goeltz S, Artal P. Analysis of the performance of the Hartmann–Shack sensor in the human eye. J Opt Soc Am A 2000; 17:1388-1398.

[Rottenkolber and Podbielska 1996] Rottenkolber M, Podbielska H. Measuring ophthalmologic surfaces by means of moiré deflectometry. Opt Eng 1996; 35:1124-1133.

[Sandstedt *et al.* 2006] Sandstedt CA, Chang SH, Grubbs RH, Schwartz DM. Light-adjustable lens: customizing correction for multifocality and higher-order aberrations. Trans Am Opthalmol Soc. 2006; 104: 29-39.

[Santamaría *et al.* 1987] Santamaria J, Artal P, Bescós J. Determination of the point-spread function of the human eye using a hidrid optical-digital method. J Opt Soc Am A 1987; 4:1109-1114.

[Schwartz 2003] Schwartz DM. Light-adjustable lens. Trans Am Ophthalmol Soc. 2003; 101:417-36.

[Selenow *et al.* 2002] Selenow A, Bauer EA, Ali SR, Spencer LW, Ciuffreda KJ. Assessing visual performance with progressive addition lenses. Optom Vis Sci 2002; 79: 502-505.

[Shack and Platt 1971] Shack RV and Platt BC. Production and use of a lenticular Hartmann screen. J Opt Soc Am 1971; 61:656.

[Sheedy *et al.* 1987] Sheedy JE, Buri M, Bailey IL, Azus J and Borish IM. Optics of progressive addition lenses. Am J Optom Physiol Opt 1987; 64: 90-99.

[Sheedy *et al.* 2005] Sheedy JE, Campbell C, King-Smith E and Hayes JR. Progressive powered lenses: the Minkwitz theorem. Optom Vis Sci 2005; 82: 916-22.

[Smirnov 1961] Smirnov MS. Measurement of the wave aberration of the human eye. Biophysics 1961; 6:776-794.

[Spiers and Hull 2000] Spiers T, Hull CC. Optical Fourier filtering for whole lens assessment of progressive power lenses. Ophthal. Physiol. Opt. 2000; 20: 281-289.

[Sullivan and Fowler 1988] Sullivan CM, Fowler CW. Progressive addition and variable focus lenses: A review. Ophthal Physiol Opt 1988; 8:402-414.

[Sullivan and Fowler 1989(a)] Sullivan CM, Fowler CW. Analysis of a progressive addition lens population. Ophthal Physiol Opt 1989; 9: 163-70.

[Sullivan and Fowler 1989(b)] Sullivan CM, Fowler CW. Grating visual acuity testing as a means of psychophysical assessment of progressive addition lenses. Optom Vis Sci 1989; 66: 565-572.

[Thibos 2000] Thibos LN. Principles of Hartmann-Shack aberrometry. In Vision Science and Its Applications, OSA Trends in Optics and Photonics Series (Optical Society of America, Washington DC, 2000): 163-169.

[Thibos *et al.* 2000] Thibos LN, Applegate RA, Schwiegerling JT, Webb R. and VSIA Standards Taskforce Members. Standards for reporting the optical aberrations of eyes. In Vision Science and Its Applications, OSA Trends in Optics and Photonics Series (Optical Society of America, Washington DC, 2000): 232-244.

[Thibos *et al.* 2004] Thibos LN, Hong X, Bradley A, Applegate RA. Accuracy and precision of objective refraction from wavefront aberrations. J Vis 2004; 4: 329–51.

[Tucker and Charman 1975] Tucker J, Charman WN. The depth of focus of the human eye for Snellen letters. Am J Optom Physiol Opt 1975;52:3-21.

[Tunnacliffe 1993] Tunnacliffe A H. Introduction to Visual Optics. Association of British Dispensing Opticians (ABDO), London 1993.

[Tunnacliffe 1995] Tunnacliffe A H. Essentials of dispensing. ABDO, London 1995.

[Villegas and Artal 2001] Villegas EA, Artal P. Neural transfer function for different optical defocus. Invest Ophthalmol Vis Sci 2001; 42(4): 873 Suppl. S MAR 15 2001.

[Villegas *et al.* 2002] Villegas EA, González C, Bourdoncle B, Bonnin T, Artal P. Correlation between optical and psychophysical parameters as a function of defocus. Optom Vis Sci 2002; 79: 60-67.

[Villegas *et al.* 2006] Villegas EA, Alcon E, Artal P. The effect of correcting small astigmatisms on visual acuity. Invest Ophthalmol Vis Sci 2006;47:E-abstract 1173.

[Villegas *et al.* 2008] Villegas EA, Alcon E, Artal P. Optical quality of the eye in subjects with normal and excellent visual acuity. Invest Ophthalmol Vis Sci 2008; 49(10): 4688-96.

[Vingolo *et al.* 2007] Vingolo EM, Grenga P, Iacobelli L, Grenga R. Visual acuity and contrast sensitivity: AcrySof ReSTOR apodized diffractive versus AcrySof SA60AT monofocal intraocular lenses. J Cataract Refract Surg. 2007; 33: 1244-7.

[Volk and Weinberg 1962] Volk D, Weinberg J. The omnifocal lens for presbyopia. Arch. Ophthal 1962; 68:776-785.

[Walsh *et al.* 1984] Walsh G, Charman WN and Howland HC. Objective technique for the determination of monochromatic aberrations of the human eye. J Opt Soc Am A 1984; 1: 987-992.

[Wendy *et al.* 2001] Wendy JA, Martin SB, Raymond van E. Adaptation to three-dimensional distortions in human vision. Nature Neuroscience 2001; 4: 1063-1064.

[Woods *et al.* 1996] Woods RL, Bradley A, Atchison DA. Monocular diplopia caused by ocular aberrations and hyperopic defocus. Vision Res 1996; 36:3597-3606.

[Wyant and Creath 1992] Wyant J, Creath K. Basic wavefront aberration theory for optical metrology. Applied Optics and Optical Engineering, vol. XI. Academic Press Inc., Boston 1992.

[Wyant and Smith 1975] Wyant JC, Smith FD. Interferometer for measuring power distribution of ophthalmic lenses. Appl Opt 1975; 14:1607-1612.

ABSTRACTS OF PUBLISHED PAPERS

1040-5488/03/8002-0106/0 VOL. 80, NO. 2, PP. 106–114
OPTOMETRY AND VISION SCIENCE

ORIGINAL ARTICLE

Spatially Resolved Wavefront Aberrations of Ophthalmic Progressive-Power Lenses in Normal Viewing Conditions

ELOY A. VILLEGAS, BscOptom and PABLO ARTAL, PhD

Laboratorio de Optica, Dept. de Física, Universidad de Murcia, Campus de Espinardo, Murcia, Spain

ABSTRACT: *Purpose.* To measure the wavefront aberration at different locations in progressive-power lenses (PPL's) isolated and *in situ* (PPL's plus eye). *Methods.* A Hartmann-Shack wavefront sensor was used to measure progressive-power lenses and human eyes either independently or in combination. In each selected zone, the lens was placed and tilted accordingly to simulate natural viewing conditions. We measured 21 relevant locations across an isolated PPL (plano lens of power addition of 2 D). In six of the locations, the wavefront aberration of the eye plus PPL were obtained in two ways: (1) by direct measurement of the system and (2) by adding the individual wavefront aberrations of the eye and the lens for each appropriate zone. In every case, we obtained the wavefront aberration as Zernike polynomials expansions, the root mean square error, the point-spread function, and the Strehl ratio. *Results.* Along the corridor of the PPL, third-order coma and trefoil, and astigmatism were the dominant aberrations. In areas of the PPL outside the corridor, astigmatism increased, whereas other aberrations remained similar to the lens center. Small differences were found between the direct and calculated methods used to obtain the wavefront aberration of the eye with the lens, and the possible sources of errors were discussed. In some lenses zones, the aberrations of the lens may be compensated by the particular aberrations of the eye, yielding improved optical performance over that present in the lens alone. *Conclusions.* We designed and built a wavefront sensor to perform spatially resolved aberration measurements in ophthalmic lenses, in particular in PPL's, either isolated or in combination with the eye. The aberrations appearing in the PPL were compared with those in normal aged eyes. (Optom Vis Sci 2003;80:106–114)

Key Words: progressive-power lenses, wavefront aberration, ocular aberration, Hartman-Shack sensor, ophthalmic lenses

Ophthal. Physiol. Opt. 2004 **24:** 419–426

Comparison of aberrations in different types of progressive power lenses

Eloy A. Villegas and Pablo Artal

Laboratorio de Optica, Departamento de Física, Universidad de Murcia, Campus de Espinardo (Edificio C), Murcia, Spain

Abstract

Recently, computer numerically controlled machines have permitted the manufacture of progressive power lenses (PPLs) with different designs. However, the possible differences in optical performance among lens designs are not yet well established. In this work, the spatially resolved aberrations, at 20 relevant locations, of three PPLs with different designs were measured with a Hartmann–Shack wavefront sensor. The wavefront aberration (WA), its root mean square error (RMS) and the point-spread function were obtained. Spatially resolved plots are shown for all aberrations, astigmatism alone, and for higher order aberrations. The average RMS of all zones is also compared, and the standard deviation is used as a parameter to evaluate the level of hard-soft design. We find differences in the spatial distribution of the aberrations but not in the global RMS, indicating that current PPLs are rather similar to a waterbed, with the aberrations being the water: they can be moved but they cannot be eliminated.

Keywords: current designs, Hartmann-Shack sensor, optical performance, progressive addition lenses, progressive power lenses, wavefront aberration

1040-5488/06/8309-0672/0 VOL. 83, NO. 9, PP. 672–681
OPTOMETRY AND VISION SCIENCE

ORIGINAL ARTICLE

Visual Acuity and Optical Parameters in Progressive-Power Lenses

ELOY A. VILLEGAS, OD, and PABLO ARTAL, PhD

Laboratorio de Optica, Department de Física, Universidad de Murcia, Murcia, Spain

ABSTRACT

Purposes. The purposes of this study are to explore the effect of astigmatism and high-order aberrations of progressive-power lenses (PPLs) on visual acuity (VA) and to find a good optical metric for evaluating visual performance of PPLs.

Methods. A Hartmann-Shack (HS) wavefront sensor was used to measure PPLs and human eyes either independently or in combination. An additional channel permits the measurement of VA under the same optical conditions. Measurements were taken in six relevant locations of a PPL and in three eyes of different normal subjects. In every case, we obtained the wavefront aberration as Zernike polynomials expansions, the root mean square (RMS) error, and two metrics on point spread function (PSF): Strehl ratio and the common logarithm of the volume under the PSF normalized to one (Log_Vol_PSF).

Results. Aberration coupling of the PPL with the eye tends to equalize the retinal image quality between central and peripheral zones of the progressive lenses. In the corridor of the PPL, the combination of small amounts of coma, trefoil, and astigmatism (total RMS 0.1 μm) does not significantly affect VA. The continuous increase of astigmatism from corridor to outside zones reduces moderately the quality of vision. The highest correlations between optical metrics and VA were found for Log_Vol_PSF of the entire system eye plus PPL.

Conclusions. Ocular aberrations reduce optical quality difference between corridor and peripheral zones of PPLs. In the same way, VA through the corridor is similar to that of eyes without a lens and it decreases slowly toward peripheral locations. VA through PPLs is well predicted by the logarithm of metrics directly related with image spread (Log_Vol_PSF or equivalent) of the complete system of the eye with the lens.

(Optom Vis Sci 2006;83:672–681)

Key Words: progressive-power lenses, visual acuity, wavefront aberrations, optical metrics, correlations

1040-5488/06/8309-0666/0 VOL. 83, NO. 9, PP. 666–671
OPTOMETRY AND VISION SCIENCE

ORIGINAL ARTICLE

An Analytical Model Describing Aberrations in the Progression Corridor of Progressive Addition Lenses

RALF BLENDOWSKE, PhD, ELOY A. VILLEGAS, OD, and PABLO ARTAL, PhD

Laboratorio de Optica, Universidad de Murcia, Murcia, Spain

ABSTRACT

Purpose. In the progression corridor of a typical progressive addition lens (PAL) with an addition of 2.5 D, the power changes by roughly 1/8 D/mm. This renders a power difference of some 0.5 D across a typical pupil diameter of 4 mm. Contrary to this fact, PALs do work well in the progression zone. To explain why, we apply a simple model to derive wavefront characteristics in the progression zone and compare it with recent experimental data.

Methods. We consider a simple analytic function to describe the progression zone of a PAL, which has been introduced by Alvarez and other authors. They considered the power change and astigmatism, which are second-order wavefront aberrations. We include third-order aberrations and compare them with spatially resolved wavefront data from Hartmann-Shack-sensor measurements.

Results. The higher-order aberrations coma and trefoil are the dominant aberrations besides astigmatism as given by experimental data. According to our model, the third-order aberrations in the transition zone are strongly coupled to the power change and the cubic power of the pupil radius. Their overall contribution according to experimental data is nicely reproduced by our model. The numeric contribution of higher-order aberrations is small and, for practical purposes, the wavefront can be described locally by the second-order components of sphere and astigmatism only.

Conclusions. We propose a simple analytical model to understand the optics in the progression corridor and nearby zones of a PAL. Our model confirms that for typical pupil sizes, all higher-order aberrations, including the dominant modes of coma and trefoil, are small enough to render an undisturbed vision in the progression zone. Therefore, higher-order aberrations have a minimal impact on the optical performance of these lenses.

(Optom Vis Sci 2006;83:666–671)

Key Words: progressive addition lens, progression zone, Alvarez lens, higher-order aberrations, coma, trefoil, Hartmann-Shack-wavefront sensor